POLITECNICO DI TORINO

Dipartimento di Ingegneria Meccanica e Aerospaziale

Corso di Laurea Magistrale in Ingegneria Meccanica

Master's Degree Thesis

Simulation of the Dynamic Response of Aeronautical Gears Equipped with Damper Rings

Supervisors:

Prof. Carlo Rosso

……

Ing. Edoardo Peradotto

……

Candidate:

Alessandro Durastante

……

March 2018

Sommario

L'insorgere di fenomeni vibratori su componenti in esercizio può condurre al cedimento ad alto numero di cicli. In buona parte dei casi una corretta progettazione permette di desintonizzare i componenti nel loro campo operativo, facendo cioè in modo che le frequenze proprie del sistema non ricadano all'interno di questo intervallo. I vincoli di progetto imposti in ambito aeronautico, tuttavia, non rendono sempre applicabile questa procedura. Si presenta quindi la necessità di ridurre l'entità delle vibrazioni per prevenirne gli eventuali effetti dannosi. La soluzione analizzata nel corso di questo lavoro di tesi prevede l'installazione di anelli smorzatori (damper rings), realizzati in acciaio, all'interno di un'apposita cava ricavata all'interno della cartella dell'ingranaggio. Questa soluzione è la più utilizzata in ambito industriale, principalmente perché comporta bassi costi di realizzazione degli anelli e semplicità di installazione.

Nasce pertanto l'esigenza di simulare l'interazione tra l'ingranaggio e l'anello smorzatore, in modo da prevederne gli effetti al variare di alcuni parametri operativi caratteristici. Questo tipo di contatto comporta notevoli difficoltà di simulazione, a causa dei fenomeni fortemente non lineari che si sviluppano all'interfaccia tra i due componenti. A questo scopo è stato sviluppato da Avio Aero, in collaborazione con il Politecnico di Torino, un software in-house in grado di riprodurre con sufficiente accuratezza il contatto.

Nel corso della presente tesi è stata seguita la parte finale dello sviluppo del software; si è quindi provveduto alla finalizzazione del codice ma soprattutto alla validazione dei risultati prodotti. Nel seguito è dunque descritta la struttura generale del programma ed è illustrata la procedura di validazione seguita, con il confronto tra i risultati ottenuti e i rilievi sperimentali. Sono inoltre riportate delle analisi volte a determinare i limiti di applicabilità dei modelli implementati e la sensibilità dei risultati rispetto alcuni parametri ritenuti critici ai fini della simulazione. Queste analisi sono fondamentali ai fini di una corretta progettazione del sistema considerato, ma anche per ottenere una migliore comprensione dei fenomeni dinamici che si sviluppano dall'ingranamento tra ruote dentate in generale.

Abstract

The raise of vibrating phenomena on operating components can lead to failure due to high cycle fatigue. In most cases, a correct design procedure allows to off-tune the components in their operating range, ensuring therefore that resonance frequencies aren't in this range. Design constraints in the aeronautical industry, anyway, make this procedure not always applicable. It is thus essential to damp the vibrations entity, in order to prevent possible harmful effects. The solution studied during this thesis work is the installation of damper rings, made of steel, inside a specific groove obtained inside the gear web. This is the most used solution in industry, mainly because of its cost-effectiveness and simplicity of application.

It is then important to simulate the interaction between the gear and the damper ring, in order to foresee the damping effect varying some operating characteristic parameters. This kind of contact implies significant simulating difficulties, because of the strongly non-linear phenomena developed on the interface between the two components. A specific in-house software has been realized in cooperation by Avio Aero and Politecnico di Torino, in order to perform the contact simulation with sufficient accuracy.

During the present master thesis work, the final part of the tool development has been performed; the activity was related to code finalization and most importantly to results validation. In the following, the tool basic structure is described and the validation procedure is explained, along with comparison between simulations results and experimental data. Specific analyses have been furthermore performed, in order to determine the feasibility of the implemented models and the sensitivity of the results with respect to some parameters, that have been found to be critical for the simulation correctness. These analyses are essential to design a damped gear system, but also to get a better comprehension of the general dynamic phenomena developed by the mesh process between gears.

Contents

1 Introduction

The core topic of the present master thesis work is the simulation of the dynamic vibrations related to the mesh between two rotating gears. More specifically, simulations are about forced vibrations, due to the external load produced by the power transmission and the contact interaction between the gear and the damper ring. Given the periodicity of the involved phenomena, the system response is investigated in the frequency domain by using classic dynamic analysis techniques. In the following paragraphs a general overview of the simulated components is given, along with some basics of dynamic analysis, that have been found to be useful for the comprehension of the next chapters.

1.1 Gear fundamentals

The tool used during the present work is designed to simulate the damping produced by the installation of a damper ring on a generic cyclic symmetric component; in the industrial reality, however, the most important intended use of damper rings is the reduction of gears resonance peaks amplitude. In fact, as stated in the summary, it is not always possible to avoid the occurrence of resonances in the operating speed range, because of the extreme weight constraints imposed in the aeronautical industry. Several gear geometries are supported for the analysis, and are briefly described in the following.

1.1.1 Spur gears

Spur gears are the most common kind of gears that can be found in mechanical transmission. They exchange power between two parallel shafts. Teeth are usually shaped using an involute profile, in order to obtain a better load distribution and avoid sudden impacts, dangerous for the component structure. Spur gears have several advantage, that make them widely used in industry; the most important are:

- Their structure guarantees a considerably high stiffness, making spur gears suitable for the transmission of large power;
- Since teeth are radially oriented, there is no axial load on structural supports (bearings). This is only a theoretical property, of course, but the real axial push is very low if compared to other kind of gears.

The main disadvantages of spur gears are the noise and vibrations generated during the mesh process; this particular feature makes them more suitable for large, static applications than for transportations. An example of spur gear is shown in Figure 1-1.

Figure 1-1: Spur gear

1.1.2 Helical gears

Helical gears are the natural evolution of spur gears. The tooth profile is usually involute shaped once again, but teeth edges are not parallel to the rotation axis; instead it determines an angle, called helix angle, constant along the face width. The transmission connects two parallel shafts. In order to correctly mesh, two helical gears must have the same helical angle (as well as the same pressure angle). Compared with spur ones, these gears show the following advantages:

- They allow a higher efficiency, due to the better load distribution during the pitch;
- The produced noise is significantly lower, due to the smoothness of the contact.

These traits make helical gears more suitable for applications where noise and vibration control is essential, and for high speed applications. An example of helical gear is shown in Figure 1-2.

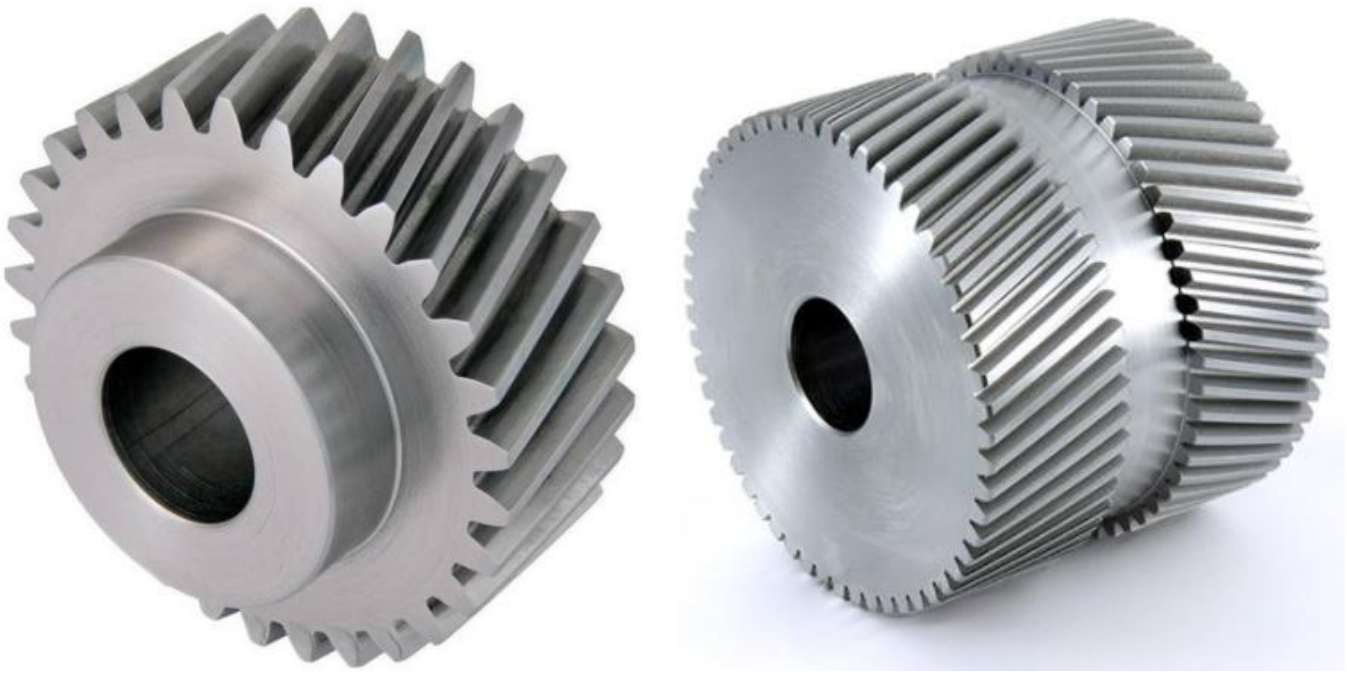

Figure 1-2: Helical and double helical gears

The main disadvantage is a direct consequence of the teeth shape: in fact in this case an axial load is induced on supports, that must be properly chosen. In order to balance the axial push, double helical gears are often used. They are assembled by two helical gears mirrored with respect to the front plane. In such a configuration, the axial load produced by a helix is balanced by the reaction produced by the other (if helixes are not correctly aligned, anyway, instability could occur). Between the two helixes there could be a groove or not; in the second case the gear is called a herringbone gear. An example is given in Figure 1-2.

1.1.3 Bevel gears

Bevel gears are used to connect two non-parallel axes. They are not generated from cylinders, like the previous gears, but their primitive geometry is a cone instead. The primitive cones of two meshing bevel gears must have the same vertex. Teeth can be straight or helical, according to the load conditions. Given the previous considerations, in aeronautical gearboxes the great majority of bevel gears also have helical teeth, given the strict operating conditions which these transmissions are subject to. An example of bevel gear is given in Figure 1-3.

Figure 1-3: Bevel gear

1.1.4 Typical turbofan power transmission chain

The majority of the simulated components equip turbofan engines. It has therefore found useful to provide a basic description of the kinematic chain that allows the extraction of mechanical power from the main engine shaft. The structure of the transmission is reported in Figure 1-4.

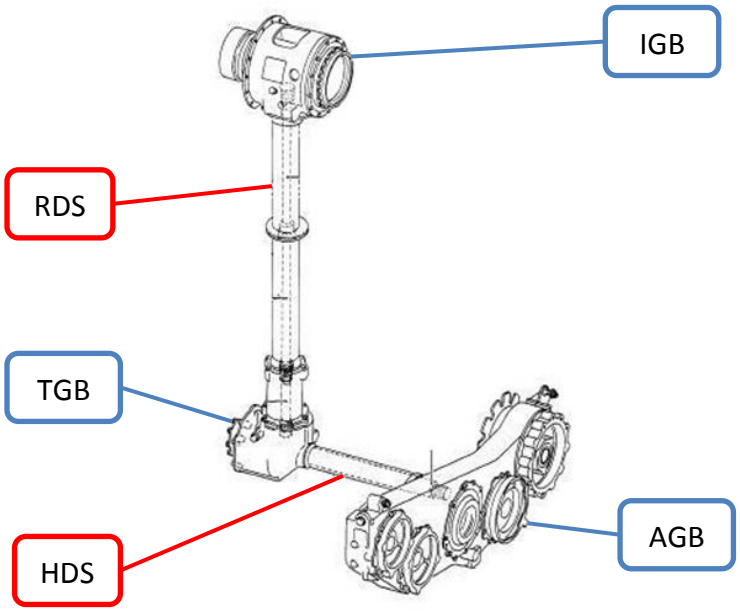

Figure 1-4: Typical turbofan transmission

In the figure, three gearboxes can be recognized (blue mark):

- Inlet Gearbox (IGB), connecting the engine shaft and the radial drive shaft (RDS); IGB gears are bevel ones, because they need to connect shafts which form a $90°$ angle;
- Transmission Gearbox (TGB), connecting RDS and HDS (horizontal drive shaft); this gearbox connects the power stage of the engine to the rest, and is composed of bevel gears again;
- Auxiliary Gearbox (AGB), which transmits the power extracted from the engine to the aircraft utilities. In this case the involved shafts are parallel, so there is no need of bevel gears.

In the present work, gears from IGB and IGB have been simulated; these gearboxes are located directly downstream the power generator (the engine shaft) and are subject to the whole power extracted. Gears belonging to these gearboxes work therefore in extreme conditions, and their functioning is crucial for the engine operation. Potential failures in this part of the transmission would force to land an entire aircraft fleet, so it is very important have economic and efficient means to fix and avoid breakdown.

1.2 System overview

The system simulated during the present work is made of a principal rotating component (in most cases a gear) and a damper ring. The latter is placed inside a groove obtained on the gear web; the position of the groove depends on the specific mode to damp, so it could be anywhere located according to the specific case. An example of such a system is shown in Figure 1-5.

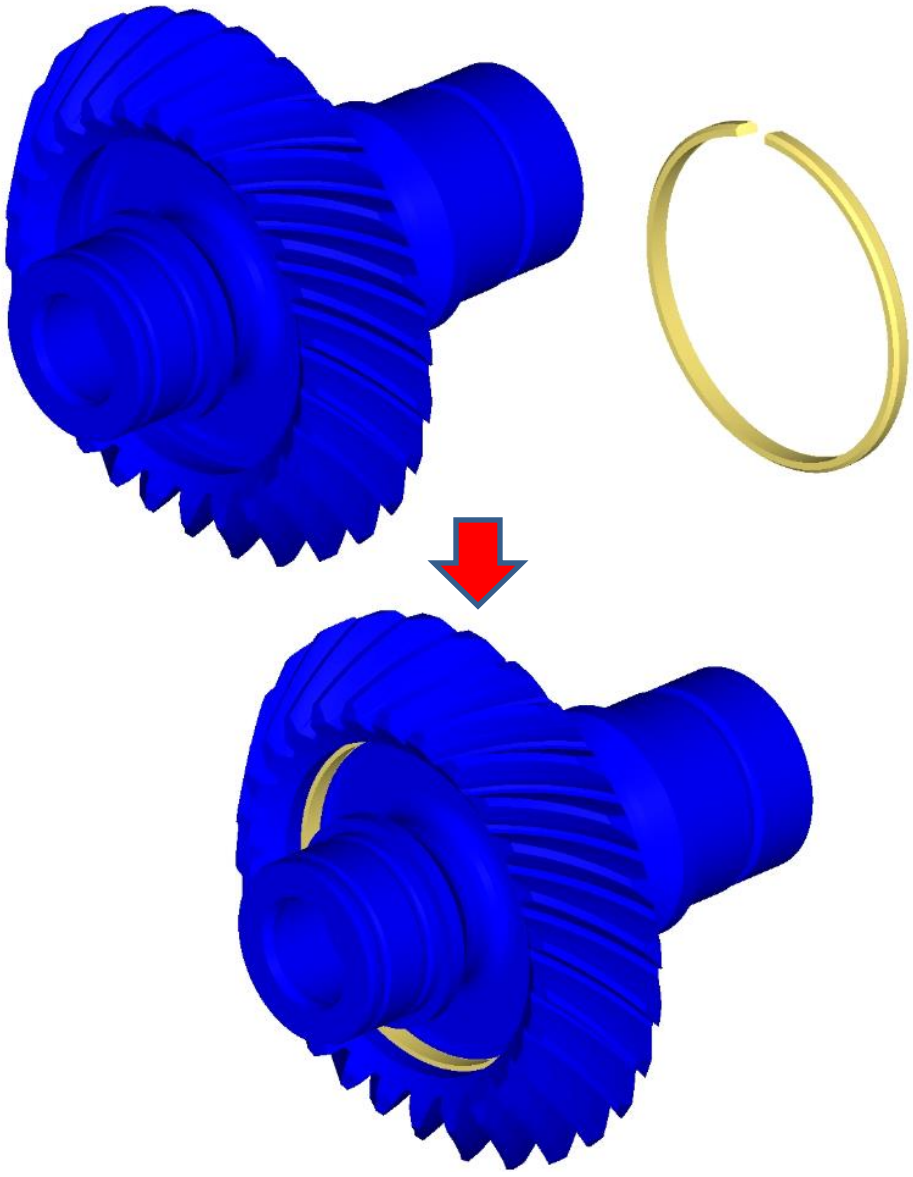

Figure 1-5: Simulated system

By observing the previous figure, it is possible to notice a lateral cut in the damper ring geometry; this feature allows the damper to be deformed and therefore equipped. In operating conditions,

centrifugal load forces contact between gear and ring, generating slithering relative motion. A certain amount of energy is dissipated this way and resonance peaks are softened.

The particular geometry of gears allows one of the most important simplifications of the entire work: in fact a gear is made of z identical sectors repeated on a complete $360°$ revolution, where z is the number of teeth. This is called a cyclic symmetric geometry and its main advantage is that it is possible to study one single cyclic sector instead of the entire structure, applying then specific boundary condition (drastically reducing computation time). This hypothesis is applied to the damper ring, which is not properly cyclic symmetric, due to the lateral cut presence; a first approximation is therefore introduced in the model, and will be thoroughly discussed in the following. In Figure 1-6 it is possible to observe the extraction of the cyclic sector from the full model.

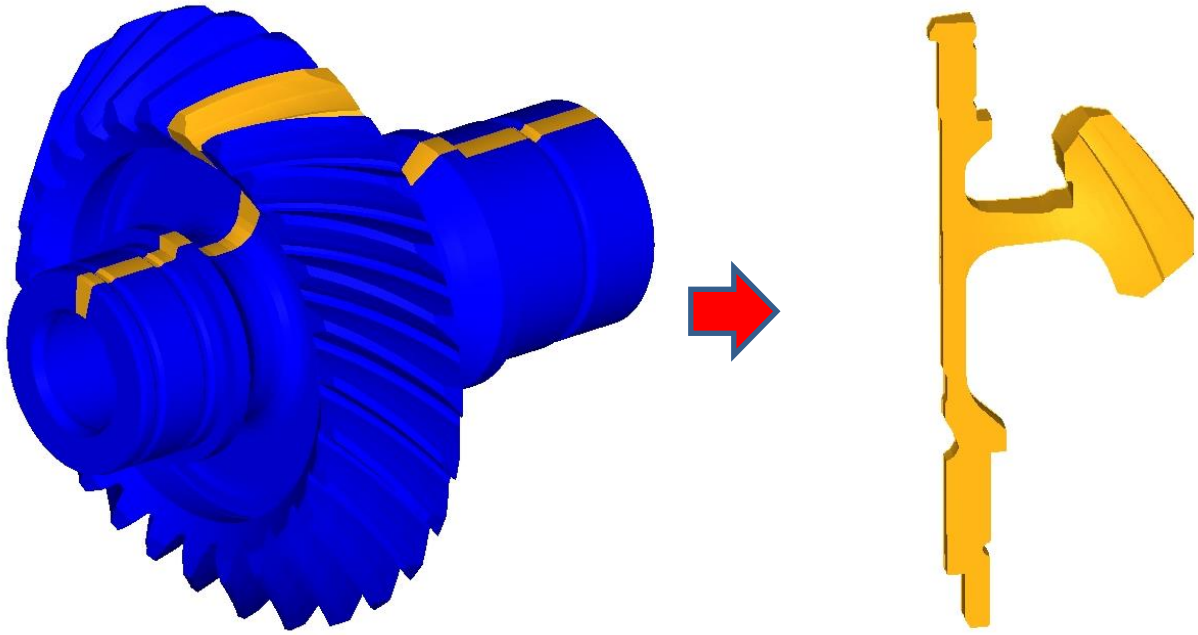

Figure 1-6: Cyclic sector extraction

1.3 Mechanical vibrations analysis fundamentals

1.3.1 Multiple degree of freedom systems

Simulated components are modeled by using finite elements (FE) techniques. Continue bodies are therefore reduced to a finite set of nodes and elements. Each node has three degrees of freedom (the displacements in the three space directions), and the interaction between nodes is simulated using springs and dampers. A multiple degrees of freedom system has been therefore obtained, and its response is computed by modal analysis techniques. The graphic representation of a simple, non-damped system is reported in Figure 1-7.

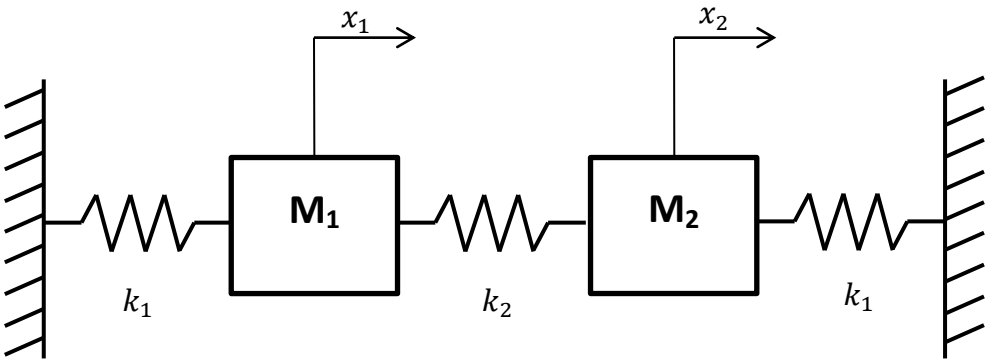

Figure 1-7: Two DoF vibrating system

The present system clearly has two degrees of freedom, represented by the two masses displacements. Motion equations are therefore:

$$\begin{cases} m_1 \cdot \ddot{x}_1 + k_1 \cdot x_1 - k_2 \cdot (x_2 - x_1) = 0 \\ m_2 \cdot \ddot{x}_2 + k_1 \cdot x_2 + k_2 \cdot (x_2 - x_1) = 0 \end{cases}$$

The previous equations can be written in matrix form:

$$[M] \cdot \{\ddot{x}\} + [K] \cdot \{x\} = \{0\}$$

Being:

$$\begin{cases} [M] = \begin{bmatrix} m_1 & 0 \\ 0 & m_2 \end{bmatrix} \\ [K] = \begin{bmatrix} k_1 + k_2 & -k_2 \\ -k_2 & k_1 + k_2 \end{bmatrix} \end{cases}$$

In this case the system is not subject to an external excitation. The system response is computed by considering a displacement vector such as:

$$\{x\} = \{X\} \cdot \cos(\omega \cdot t + \phi)$$

Where X is a time constant vector. By substituting the previous expression in the motion equation, it is possible to determine the natural frequencies of the non-damped system by solving the following eigenvalues problem:

$$det([K] - \omega^2 \cdot [M]) = 0$$

The problem has n eigenvalues, where n is the number of degrees of freedom of the system. The associated eigenvectors ($\{\Psi_1\}$ and $\{\Psi_2\}$ in this case) are called mode shapes of the system, and define how the structure vibrates at a certain natural frequency.

Once the natural frequencies and the mode shapes have been determined, it is possible to define the modal mass and stiffness matrices:

$$\begin{cases} [M_m] = [\Psi]^T \cdot [M] \cdot [\Psi] \\ [K_m] = [\Psi]^T \cdot [K] \cdot [\Psi] \end{cases}$$

It is possible to prove that these matrices are diagonal. These property is called mode orthogonality, and it is very important when damping is introduced in the system. In the present simulations, in fact, proportional damping is used, because it allows a simpler but accurate implementation. Under this hypothesis the damping matrix is determined as a linear combination of mass and stiffness ones. Using these proportionality factors, it is possible to determine a damping ratio for each specific mode. The modal damping matrix is therefore diagonal and the mode shapes of the damped system are those computed previously without further modifications. Damping causes a shift in resonance frequencies, according to the following expression:

$$\omega_{d,i} = \omega_{n,i} \cdot \sqrt{1 - {\zeta_i}^2}$$

Where:

- $\omega_{d,i}$ is the natural frequency of the damped system at the i_{th} mode;
- $\omega_{n,i}$ is the natural frequency of the un-damped system at the i_{th} mode;
- ζ_i is the damping ratio at the i_{th} mode.

If the present work an external load is applied on the structure. Given a force amplitude in the frequency domain, called $\{F\}$, the simulation determines the displacements magnitude $\{X\}$, by applying the expression:

$$\{X\} = [A(\omega)] \cdot \{F\}$$

Where $A(\omega)$ is the receptance matrix, defined as the inverse of the dynamic stiffness matrix. According to the previous notation, $A(\omega) \in \mathbb{C}^{n,n}$, and its elements are defined as:

$$a_{j,k}(\omega) = \sum_{r=1}^{n} \frac{\psi_{j,r} \cdot \psi_{k,r}}{k_r - m_r \cdot \omega^2 + i \cdot \omega \cdot c_r}$$

Where i is the imaginary unit.

1.3.2 Rotor dynamics basics

In order to understand how the external exciting force is computed, it is important to highlight some basic concepts about dynamics in rotating bodies. When vibrating at a certain frequency, cyclic symmetric components show nodal diameters; these are non-deformed lines passing through the rotation axis. Each mode exhibits a certain number of nodal diameters. Increasing frequency, a certain

number of nodal diameters (for example 2) are observed more than one time: for each nodal diameter there are infinite natural frequencies (and therefore mode shapes). It is possible to group the dynamic behavior of a cyclic structure in modal sets. Each set contains one frequency for each nodal diameter. It is important to notice that for a specific cyclic structure, the maximum number of nodal diameters that can be observed is equal the half of the number of cyclic sectors z. In Figure 1-8 it is possible to see the modal deformed for $ND = \{1,2,3,4\}$.

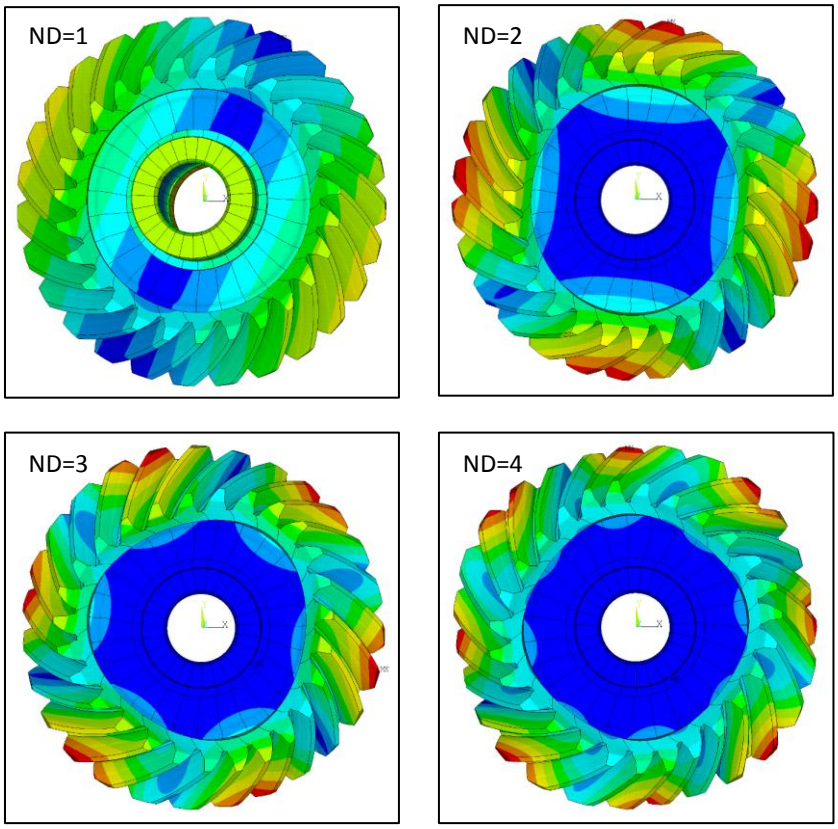

Figure 1-8: Modal analysis results

1.3.3 Dynamic force

The main external load that excites the system is due to the mesh process. This force trend in the time domain is given by a lot of different factors. A specific model for the precise exchanged force computation is currently implemented in POLIGear. Its features will be furtherly investigated in the following chapters. In this introduction, anyway, the attention is focused on the harmonic nature of the force, so any other variability factor has been neglected. Under this hypothesis and considering a cylindrical reference system centered on the rotation axis, the transmitted load can be seen as an harmonic function of time:

$$\begin{cases} f(t) = F_0 \cdot \cos(z \cdot \Omega \cdot t) & , \ \theta = \theta_0 \\ f(t) = 0 & , \ \theta \cong \theta_0 \end{cases}$$

Where:

- F_0 is the static load, computed by the transmitted torque;
- z is the number of teeth;
- Ω is the rotational speed of the gear;
- θ_0 is the angular position in which the external load is applied.

The mesh force can be expanded in its Fourier series along the $360°$

$$f(t) = \frac{F_0}{\pi}\sum_{n=0}^{\infty}\cos\big(n\cdot(\theta-\theta_0)\big)\cdot\cos(\omega\cdot t)$$

Where:

- n is the generic harmonic;
- $\omega = z\cdot\Omega$.

Simulation is performed in a reference system that rotates along with the gear. The angular coordinate in this system is:

$$\theta_R = \theta - \Omega\cdot t$$

By substituting the previous expression in the Fourier expansion, it is possible to obtain:

$$f_R(t) = \frac{F_0}{2\pi}\sum_{n=0}^{\infty}\{\cos[(\omega - n\cdot\Omega)\cdot t]\cdot\cos(n\cdot\theta_R) + \sin[(\omega - n\cdot\Omega)\cdot t]\cdot\sin(n\cdot\theta_R) + \\ + \cos[(\omega + n\cdot\Omega)\cdot t]\cdot\cos(n\cdot\theta_R) - \sin[(\omega + n\cdot\Omega)\cdot t]\cdot\sin(n\cdot\theta_R)\}$$

Two contributions are then recognized. The mesh force has two rotating components: one concordant and one discordant with the rotational speed; these are called forward and backward components. Considering the harmonic n, the harmonic force has therefore pulsation equal to:

$$\omega_{b/f} = \omega \pm n\cdot\Omega = \Omega\cdot(z\pm n) = \Omega\cdot EO_{b/f}$$

$$\begin{cases} EO_b = z + n \\ EO_f = z - n \end{cases}$$

Where the engine orders of the forward and backward force components have been defined. The physical meaning of the engine order is the following: given an arbitrary harmonic, the corresponding force component will have two different pulsations, equal to EO_b and EO_f times the rotational speed. It is clear that a specific harmonic shall be selected according to the mode simulated. It is therefore essential to correctly choose the component. Considering the rotating reference system, each nodal diameter virtually determines infinite natural frequencies, represented as horizontal lines on the Campbell diagram (Figure 1-9, black lines). The excitation line (which is approximately a straight line) splits in two components, backward and forward in fact (orange lines), whose slope is determined by

the specific harmonic considered, that determines two engine order values. As it is possible to notice in the figure, theoretically infinite intersections are determined. Experimental evidence, anyway, proves that not all these intersections are critical. It is in fact possible to demonstrate that a certain mode, distinguished by a number of nodal diameters ND, is excited by the harmonic which index n is equal to ND. The same mode is furthermore excited by the harmonic which engine order is equal to ND, because in this case the force has exactly the same shape as the modal deformed for that specific mode. All the previous considerations can be summarized by the following expression:

$$EO_{b/f} = k \cdot z \pm ND \quad , \quad k \in \mathbb{N}$$

Where:

- $EO_{b/f}$ are the backward and forward engine orders to extract from the complete dynamic force;
- ND is the number of nodal diameters that characterizes the mode of interest.

In the present work only $k = 1$ cases have been considered, being the only ones in typical operating range.

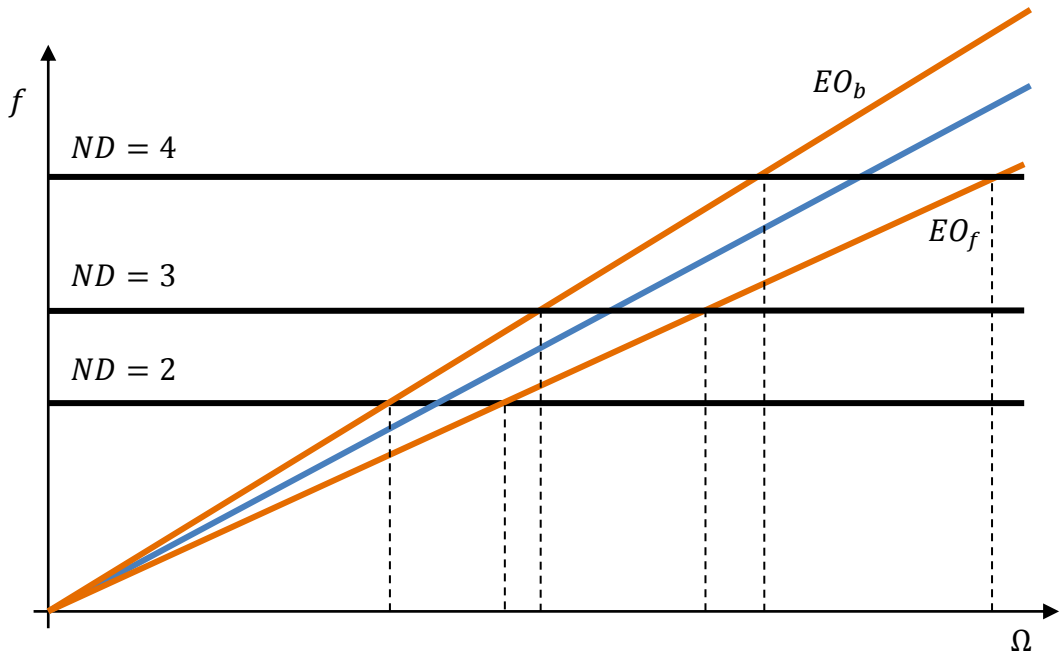

Figure 1-9: Campbell diagram

2 Numerical model

The starting point for the analysis is the system mathematical modeling. As previously described, the system is made up of a main component (typically a gear, a turbine disk or a seal) and a damper ring, anyway shaped. For each component a finite element model is built. Since matrices so obtained are too heavy to be processed by the tool in reasonable time, some reduction techniques will be performed; these processes allow to drastically reduce computation time and at the same time to preserve the dynamic behavior of the structure. The external load to be applied is computed by using a dedicated model, proposed by Parker and will be deeply investigated in the following.

2.1 Equilibrium equations

Once the finite element mesh is realized, the degrees of freedom of the structure (infinite for a continuous system) will be reduced to the ones related to the nodes defined. These degrees of freedom can be regrouped in two vectors $\{q_G\}$ and $\{q_D\}$, respectively for the main component and for the damper ring. According with this notation, equilibrium equations for the system are:

$$[M_G] \cdot \{\ddot{q}_G\} + [C_G] \cdot \{\dot{q}_G\} + [K_G] \cdot \{q_G\} = \{F_{G,TOT}\}$$

$$[M_D] \cdot \{\ddot{q}_D\} + [C_D] \cdot \{\dot{q}_D\} + [K_D] \cdot \{q_D\} = \{F_{D,TOT}\}$$

In the previous equations, the load vectors are given by:

$$\{F_{G,TOT}\} = \{F_G\} + \{F_{CF,G}\} + \{F_{NL}\}$$

$$\{F_{D,TOT}\} = \{F_{CF,D}\} - \{F_{NL}\}$$

In which:

- $\{F_G\}$ is the external load, produced by the meshing between the two gears (or by the pressure load for a turbine disk);
- $\{F_{CF}\}$ is the centrifugal load caused by the rotation;
- $\{F_{NL}\}$ contains the forces exchanged on the interface between the main component and the damper ring; as will be explained in the following, these forces are produced by the friction, and non-linearity are so introduced in the system.

The solution of such a system requires too much time to be performed, because it requires the explicit integration of the equations. Since just the steady state solution is required, it is possible to pass to the frequency domain and to apply the harmonic balance method. By this method, an arbitrary function in the time domain is expressed as a series of harmonic terms:

$$X(t) = X^{(0)} + \sum_{n=1}^{N} X^{(n)} \cdot e^{in\omega t}$$

The system becomes so:

$$[K_G]^{(0)} \cdot \{q_G\}^{(0)} = \left\{F_{G,TOT}\right\}^{(0)} \qquad [D_G]^{(n)} \cdot \{q_G\}^{(n)} = \left\{F_{G,TOT}\right\}^{(n)}$$

$$[K_D]^{(0)} \cdot \{q_D\}^{(0)} = \left\{F_{D,TOT}\right\}^{(0)} \qquad [D_D]^{(n)} \cdot \{q_D\}^{(n)} = \left\{F_{D,TOT}\right\}^{(n)}$$

Dynamic stiffness matrices are defined by:

$$D = -(n \cdot \omega)^2 \cdot [M] + i \cdot (n \cdot \omega) \cdot [C] + [K]$$

Where i is the imaginary unit and n is the considered harmonic number. In this tool the single harmonic balance method (SHBM) is implemented, so the previous expressions can be simplified to their final form:

$$[D_G]^{(1)} \cdot \{q_G\}^{(1)} = \left\{F_{G,TOT}\right\}^{(1)}$$

$$[D_D]^{(1)} \cdot \{q_D\}^{(1)} = \left\{F_{D,TOT}\right\}^{(1)}$$

It is so required to apply an external load obtained extracting just one harmonic term from the meshing force series expansion. The term is the one that excites the specific simulated mode, and it is extracted following the procedure explained in the introduction on vibratory systems.

2.2 Matrix reduction

The equations previously described involve very large matrices, and cannot be efficiently solved by a not commercial tool. It is anyway noticed that the simulated structures are composed by z identical sectors (where z is the number of teeth if the component is a gear). This remark allows to apply the cyclic symmetry hypothesis: instead of producing an entire component's FEM model, only one sector mesh is created, meaningfully reducing the matrices dimension. It is interesting to notice that this is an approximation, because the external load is not cyclic symmetric. Since the computation still requires too much time, three reductions are sequentially performed in order to build the final matrices.

2.2.1 CMS reduction

This is the first step in the reduction of the matrices. Since the process is very heavy, for the main component it is performed by an optimized FEM solver (supported commercial software are ANSYS and NASTRAN). To use this reduction technique it is required to divide nodes in two groups, called master and slaves; at the end of the reduction, the slave nodes will be replaced with an arbitrary

number of modal degrees of freedom. Of course the reduced matrix eigenvalues will be as similar to the original ones as the number of slave modes grows. The master modes are:

- Nodes belonging to the sector's right and left interfaces, because they will be essential for the application of the cyclic symmetry;
- Nodes where the external load will be applied;
- Nodes of interest, where for example a proximity sensor is located;
- Nodes belonging to the contact interface between the main component and the damper ring;
- Nodes to be constrained (by applying bearings for example).

The degrees of freedom previously listed are grouped into the $\{q_m\}$ vector, the others into the $\{q_s\}$ one. The differential system is then reordered:

$$\begin{bmatrix} M_{mm} & M_{ms} \\ M_{sm} & M_{ss} \end{bmatrix} \cdot \begin{Bmatrix} \ddot{q}_m \\ \ddot{q}_s \end{Bmatrix} + \begin{bmatrix} C_{mm} & C_{ms} \\ C_{sm} & C_{ss} \end{bmatrix} \cdot \begin{Bmatrix} \dot{q}_m \\ \dot{q}_s \end{Bmatrix} + \begin{bmatrix} K_{mm} & K_{ms} \\ K_{sm} & K_{ss} \end{bmatrix} \cdot \begin{Bmatrix} q_m \\ q_s \end{Bmatrix} = \begin{Bmatrix} F_m \\ F_s \end{Bmatrix}$$

The CMS transformation matrix is:

$$\begin{Bmatrix} q_m \\ q_s \end{Bmatrix} = \begin{bmatrix} I & 0 \\ \phi_m & \phi_s \end{bmatrix} \cdot \begin{Bmatrix} q_m \\ \eta_s \end{Bmatrix} = [T_{CMS}] \cdot \begin{Bmatrix} q_m \\ q_s \end{Bmatrix}$$

Where η_s is the vector of the modal degrees of freedom and the ϕ_m and ϕ_s matrices are computed by:

$$[\phi_m] = -[K_{ss}]^{-1} \cdot [K_{sm}]$$

$$\{[K_{ss}] - \omega^2 \cdot [M_{ss}]\} \cdot [\phi_s] = 0$$

By applying the reduction, the system can be expressed as:

$$\begin{bmatrix} M_{BB} & M_{Bl} \\ M_{lB} & M_{ll} \end{bmatrix} \cdot \begin{Bmatrix} \ddot{q}_m \\ \ddot{\eta}_s \end{Bmatrix} + \begin{bmatrix} C_{BB} & C_{Bl} \\ C_{lB} & C_{ll} \end{bmatrix} \cdot \begin{Bmatrix} \dot{q}_m \\ \dot{\eta}_s \end{Bmatrix} + \begin{bmatrix} K_{BB} & K_{Bl} \\ K_{lB} & K_{ll} \end{bmatrix} \cdot \begin{Bmatrix} q_m \\ \eta_s \end{Bmatrix} = \begin{bmatrix} I & \phi_m \\ 0 & \phi_s \end{bmatrix} \cdot \begin{Bmatrix} F_m \\ F_s \end{Bmatrix}$$

Where the mass (and stiffness) matrix components are so defined:

$$[M_{BB}] = [M_{mm}] + [M_{ms}] \cdot [\phi_m] + [\phi_m]^T \cdot [M_{sm}] + [\phi_m]^T \cdot [M_{ss}] \cdot [\phi_m]$$

$$[M_{Bl}] = ([M_{ms}] + [\phi_m]^T \cdot [M_{ss}]) \cdot [\phi_s]$$

$$[M_{lB}] = [\phi_s]^T \cdot ([M_{sm}] + [M_{ss}] \cdot [\phi_m])$$

$$[M_{ll}] = [\phi_s]^T \cdot [M_{ss}] \cdot [\phi_s]$$

The matrix $[M_{ll}]$ is a diagonal one, and it is equal to the identity matrix if a particular normalization approach is chosen; in this case, the matrix $[K_{ll}]$ (which is diagonal too) has the square natural frequencies on its diagonal.

A particular case of CMS reduction is the Guyan reduction, which matrices are obtained by substituting $[\phi_m] = -[K_{ss}]^{-1} \cdot [K_{sm}]$ into the previous equations. This reduction technique is implied in the explanation because it is performed as a part of the Tran reduction. In fact reducing a dynamic problem matrices by Guyan is not correct, because the slave degrees of freedom are completely neglected, along with their dynamic behavior

2.2.2 Cyclic symmetry

As explained before, only one sector is used to build the final finite elements model. Since components are made of repeated identical sectors. It is reasonable to think that each sector interface (right or left) will show the same displacement as the other and a phase shift related to the rotation verse and the nodal diameter. In mathematical terms it is expressed as:

$$\{q_r\} = \{q_l\} \cdot e^{-i\varphi} \quad , \quad \varphi = \frac{2\pi}{z} \cdot ND$$

Where z is the number of cyclic sectors and ND is the number of nodal diameters of interest. It is possible to write the constraint matrix, used to translate the sector's matrices into the full 360˚ ones:

$$[T] = \begin{bmatrix} I & I \\ I \cdot e^{-i\varphi} & I \end{bmatrix}$$

$$[M_{TOT}] = [T]^T \cdot [M_{SECT}] \cdot [T] \quad , \quad [K_{TOT}] = [T]^T \cdot [K_{SECT}] \cdot [T]$$

It is immediately clear the main cyclic symmetry disadvantage: the phase shift is related to one single engine order; by this approach is so possible to simulate only one mode shape by one.

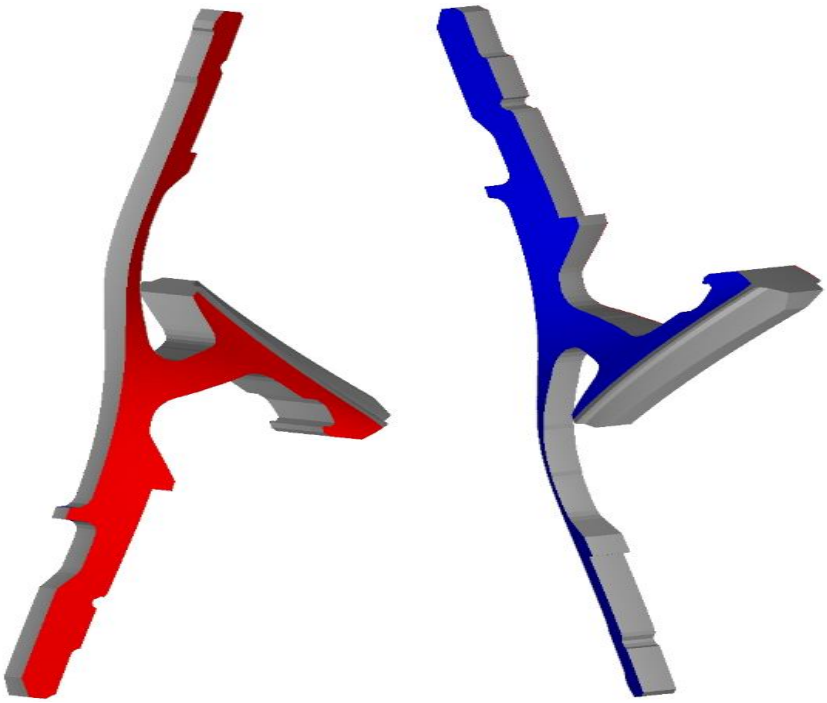

Figure 2-1: Left and right cyclic sector interface

2.2.3 Tran reduction

Left and right interface nodes are kept as master nodes during the CMS reduction, due to the application of the cyclic constraints. Because of this, CMS reduced matrices dimension is too high to be processed by MATLAB, and a further step is required. This is the Tran reduction: basically the interface nodes are reduced to a certain number of interface modes. This modes are defined as the eigenvectors of the eigenproblem:

$$[K_L] \cdot [\Psi] = [M_L] \cdot [\Psi] \cdot \omega^2$$

Where the $[M_L]$ and $[K_L]$ are the Guyan reduced matrices obtained considering only the interface nodes as master. Once the eigenvectors are computed, only the first ones are selected. A trade-off between accuracy and computation speed must be found: the interface modes are so chosen as one third of the CMS modes. It is essential anyway to not choose a number of interface modes lesser than six, because rigid displacements of the structure wouldn't be considered, producing a significant mismatch between the natural frequencies of the reduced matrices and the original ones. The reduction gives:

$$\begin{Bmatrix} q_r \\ q_l \end{Bmatrix} = \begin{bmatrix} \Psi \cdot e^{-i\varphi} \\ \Psi \end{bmatrix} \cdot \{\eta_l\}$$

2.2.4 Final reduced matrix

When the eigenvalues matrix $[\Psi]$ is computed, it Is possible to determine the final reduction matrix combining all the relations explained above. The CMS master nodes vector $\{q_m\}$ is so composed;

- $\{q_c\}$: main component / damper ring contact interface nodes;
- $\{q_f\}$: nodes where the external load is applied;
- $\{q_a\}$: nodes of interest (for any reason);
- $\{q_l\}$ and $\{q_l\}$: left and right sector's interface nodes, respectively;
- $\{\eta_s\}$: slave modes produced by the CMS reduction.

On the basis of the previous considerations, the reduction matrix is defined as:

$$[\Gamma] = \begin{bmatrix} I & 0 & 0 \\ 0 & \Psi \cdot e^{-i\varphi} & 0 \\ 0 & \Psi & 0 \\ 0 & 0 & I \end{bmatrix}$$

$$\begin{Bmatrix} q_c \\ q_f \\ q_a \\ q_r \\ q_l \\ \eta_s \end{Bmatrix} = [\Gamma] \cdot \begin{Bmatrix} q_c \\ q_f \\ q_a \\ \eta_I \\ \eta_s \end{Bmatrix}$$

And the final mass and stiffness matrices are computed:

$$[M_{FIN}] = [\Gamma]^T \cdot [M_{CMS}] \cdot [\Gamma] \quad , \quad [K_{FIN}] = [\Gamma]^T \cdot [K_{CMS}] \cdot [\Gamma]$$

The described procedures are repeated for the damper ring sector, which is always lighter than the main component one. This allows to perform the entire reduction procedure inside the MATLAB environment.

2.3 Differential system assembling

When the matrices are reduced, the last step before solving the equations system is building the damping matrix $[C_{FIN}]$ and sequentially the dynamic stiffness matrix $[D]$. This operation requires to estimate a damping ratio ζ. The same result is achieved by imposing a quality factor Q, since the two parameters are related by the expression:

$$\zeta = \frac{1}{2 \cdot Q}$$

Usually it is convenient to use the Q-factor, because approximate values for various materials can be found in literature. During this work an automatic Q-factor estimation has been implemented into the code. The procedure followed will be explained in the following.

2.3.1 Q-factor estimation

When experimental data are available, it is possible to directly estimate their quality factor; the found value is then passed to the tool and applied to the solution. There are several methods used in the quality factor estimation, often based on energetic consideration, since the information provided by

the parameter regards the energy dissipation ratio. A single degree of freedom generic frequency response is shown in Figure 2-2. The half power method is chosen to perform the estimation. As graphically described, the method determines the frequency bandwidth in which the FRF is greater than the root mean square of the maximum amplitude. The Q-factor is then computed by the following expression:

$$Q = \frac{f_0}{(f_2 - f_1)}$$

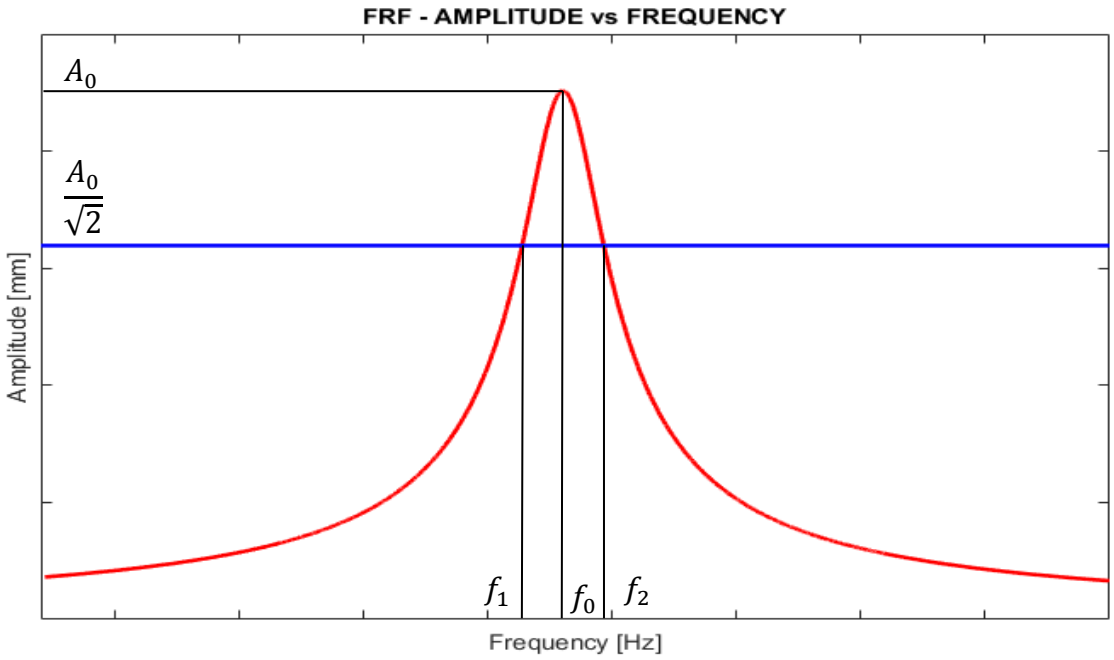

Figure 2-2: Half power Q-factor

It is important to notice that the half power method is analytically defined in the case of Gaussian curves. If experimental data are broken up (for example because of bad sampling) or significantly asymmetric the estimation could not be accurate; in this case the exact determination of the Q-factor requires energetic techniques.

2.3.2 Damping matrix

It is in the following described the procedure used to determine the damping matrix. Such a procedure could be directly performed during the finite element mesh creation; it has been chosen anyway to keep the damping as a free parameter, easily adjustable even when the first stage of the reduction has been performed. This is also the correct choice taking into account the computation time required to produce and export an overabundant CMS reduced matrix on which apply the whole procedure. The damping matrix is given by the expressions:

$$[C_{TOT}] = [\Phi_r]^{-1} \cdot \left[C_{diag}\right] \cdot [\Phi_r]$$

$$c_{diag,i,j} = \begin{cases} 2 \cdot \zeta \cdot \omega_{0,i} & , \ i = j \\ 0 & , \ i \neq j \end{cases} \quad , \quad \{\Phi_{r,k}\} = \frac{\{\Phi_k\}}{\sqrt{m_k}}$$

Where $[\Phi]$ and ω_0 are the eigenvectors of the following problem and m_k are the mass participation factors.

$$([K_{TOT}] - {\omega_0}^2 \cdot [M_{TOT}]) \cdot [\Phi] = 0$$

It is in the end possible to build the dynamic stiffness matrix and solve the differential system.

3 Meshing dynamic force

As explained in the introduction, the tool simulates one mode shape by one. Each mode shape is determined by one precise engine order, and corresponds with an intersection on the Campbell diagram. The meshing force is the main vibration source, and must be computed to determine the linear response (that is the frequency response of the gear without any damper ring), the starting point for the damped response. In an approximate model one could think to use the static force transmitted between mating gears (simply computable from the torque and a significant radius); known the force, it is necessary to filter it, because of its rotatory nature. The last step is the extraction of the correct harmonic component, then used to excite the specified mode. This approach doesn't take in account the dynamic overload of the force. The real dynamic force will present a fluctuating trend around its static value. This phenomenon considerably changes the frequency series expansion, leading to different results. A more accurate model has been therefore preferred. This is the one proposed by Parker [7].

3.1 Transmission error

The transmission error is commonly recognized as the main vibration and noise reason in gears meshing. This error is always present in motion transmission, and consists in the fact that the output speed (linear or rotational) will be slightly different from the theoretical one, expressed by $\omega_{out} = \omega_{in} \cdot \tau$, where τ is the gear ratio. The reasons of the transmission error presence are multiple:

- Gear geometry: of course the real component's geometry will not be perfectly identical to the designed one; one main error cause can so identified in the components manufacturing, that inevitably causes imperfections and surface roughness;
- Transmission components stiffness: analytical relations are often derived considering an infinite stiffness for gears, bearings and every other component into the mechanical transmission; this stiffness, combined with the components masses, determines inertial effects on the system, causing dynamic forces.

The implemented model uses the static transmission error (that is due to the components elasticity at lower load conditions) as source of time variant meshing stiffness; by the model the dynamic force is computed in the time domain.

The static transmission error is estimated by Transmission3D, a commercial software that simulates in detail the meshing zone. The result is a transmission error function for each of the main directions (radial, tangential and axial); these functions are referred to the single mesh cycle. Only the tangential component is chosen, because it is the one in the torque transmission direction and so the most relevant through all. Static transmission error is given in radians and is the same for both the meshing gears. Since a linear displacement is required for the Parker model, anyway, data must be multiplied for a length factor (a radius, since studying rotating bodies); the selected parameters is the base

radius of the equivalent spur gear (to which the system is reduced). The base radius is chosen above the pitch radius because the dynamic model is referred to the contact line. By this scaling, the specific gear transmission error is computed.

3.2 Dynamic force

The computation is performed by reducing the meshing gears to the equivalent model shown in Figure 3-1.

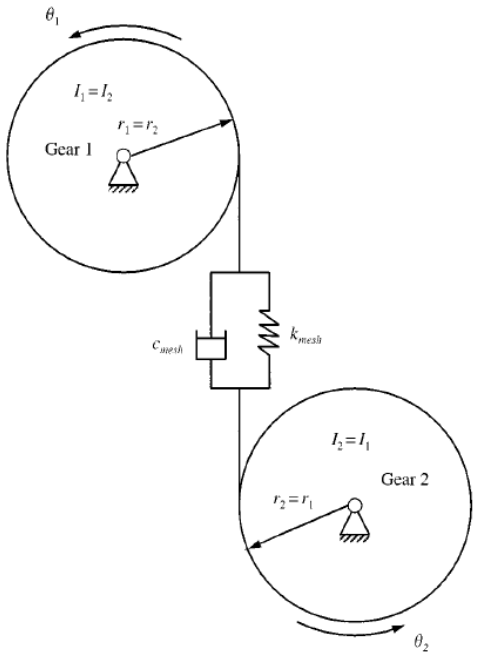

Figure 3-1: Equivalent model

As can be seen, the whole mesh is outlined as a lumped parameters system, composed by a mass, a spring and a viscous damper. Radius shown in the figure are the real base radius if the simulated component is a spur gear or an helical gear. Usually, anyway, simulation deal with bevel gears, so equivalent spur gear parameters must be computed. Since the gear module is often given referring to the outer diameter in the drawings, it is necessary to calculate the mid face width module, from which the searched base radius is obtained. This is expressed by the expression:

$$m_{mf} = m \cdot \frac{(PX - TX/2)}{PX}$$

Where:

- m and m_{mf} are the gear modules at the outer diameter and at the mid face width respectively;
- PX is the outer cone distance;
- TX is the face width.

The base radius is then computed just like any spur gear.

The next step of the process is the dynamic transmission error computation, since it is the direct cause of the vibrations. It is so integrated the following differential equation:

$$m \cdot \ddot{x} + c \cdot \dot{x} + F(t) = F_s \quad , \quad F_s = \frac{T}{R_b}$$

$$F(t) = \begin{cases} k(t) \cdot x & , \ x \geq 0 \\ 0 & , \ x < 0 \end{cases}$$

Where:

- x is the dynamic transmission error;
- m is the system's equivalent mass, determined from base radius and polar inertias as:
$$m = \frac{J_1 \cdot J_2}{J_1 \cdot {R_{b2}}^2 + J_2 \cdot {R_{b1}}^2}$$
- $k(t)$ is the meshing stiffness, time variant because of the transmission error presence. It is mathematically derived from torque T, base radius and static transmission error STE as:
$$k(t) = \frac{T}{R_b \cdot STE(t)}$$
- c is the viscous damping is assumed constant with a damping ratio $\zeta = 0{,}08$ and expressed as:

$$c = 2 \cdot \zeta \cdot \sqrt{m \cdot \bar{k}} \quad , \quad \bar{k} = mean\big(k(t)\big)$$

- F_s is the static force transmitted during the mesh.

The particular feature of the model is the form given to the elastic mesh force $F(t)$; it is in fact taken in account the contact loss prospect, in which case there is no dynamic force exchanged between the meshing gears.

The differential system is explicitly integrated on the time range required to complete an arbitrary number N of revolution of the gear (in this case five revolutions were used, to allow the solver to reach convergence). The static transmission error is given for a single mesh cycle, so it will be periodically repeated for $z \cdot N$ times, because this is the number of mesh cycles along all the revolutions.

When the system is solved, the time trend of the dynamic transmission error $x(t)$ is known, and the dynamic force is computable by applying the following expression:

$$F_{DYN}(t) = c \cdot \dot{x}(t) + k(t) \cdot x(t)$$

It is important to notice that the differential equation is solved for each rotational speed in the simulated range. This is useful because it helps to recognize a possible meshing frequency. An

example of typical dynamic force trend is shown in Figure 3-2. In the first section the force substantially, indicating that the solver still is in the transient phase (in fact this part of the solution will be discarded). On the right the stationary trend is shown, with fluctuations around the static force value as pronounced as the STE is variable into the mesh cycle.

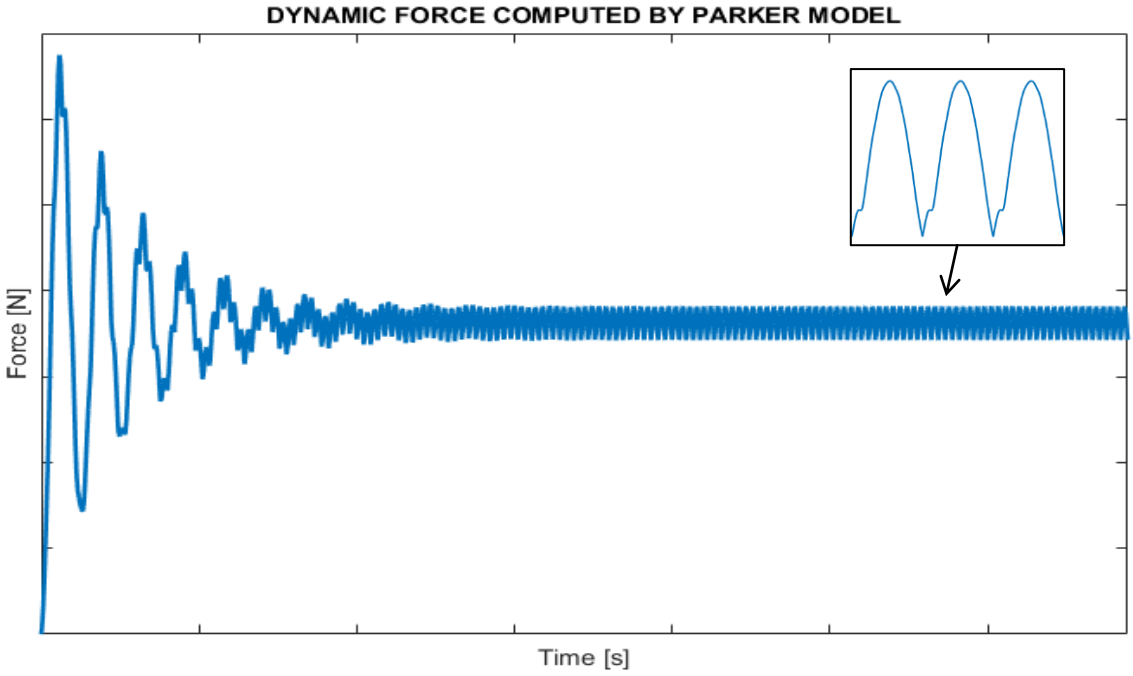

Figure 3-2: Dynamic force vs time

3.3 Harmonic component

The Parker model output is the time trend of the dynamic force exchanged during the mesh. What is needed, anyway, is the force which a single tooth is subject to. It is necessary to move into another reference system which is co-rotating with the gear. In order to pass into this new system, a filter must be applied to the dynamic force; the filter contains the information about the number of teeth in contact at every instant. The parameter that summarizes this information is the contact ratio. This is a load dependent number which estimation is very difficult for bevel gears. The model, anyway, is about equivalent spur gears, so a simplified relation is given by:

$$CR = \frac{\sqrt{{R_{a1}}^2 - {R_{b1}}^2} + \sqrt{{R_{a2}}^2 - {R_{b2}}^2} - I \cdot \sin\alpha}{\pi \cdot m \cdot \cos\alpha}$$

Where:

- R_a is the outside radius;
- R_b is the base radius;
- I is the gears wheelbase;

- α is the pressure angle;
- m is the gears module.

If only one tooth were in contact at each moment of time, the filter window would have the trend shown in Figure 3-3, since the tooth exchanges force just for the duration of a single pitch. The filtered force will be thus given by:

$$F_{WIN}(t) = F_{DYN}(t) \cdot W(t)$$

Being $W(t)$ the window function.

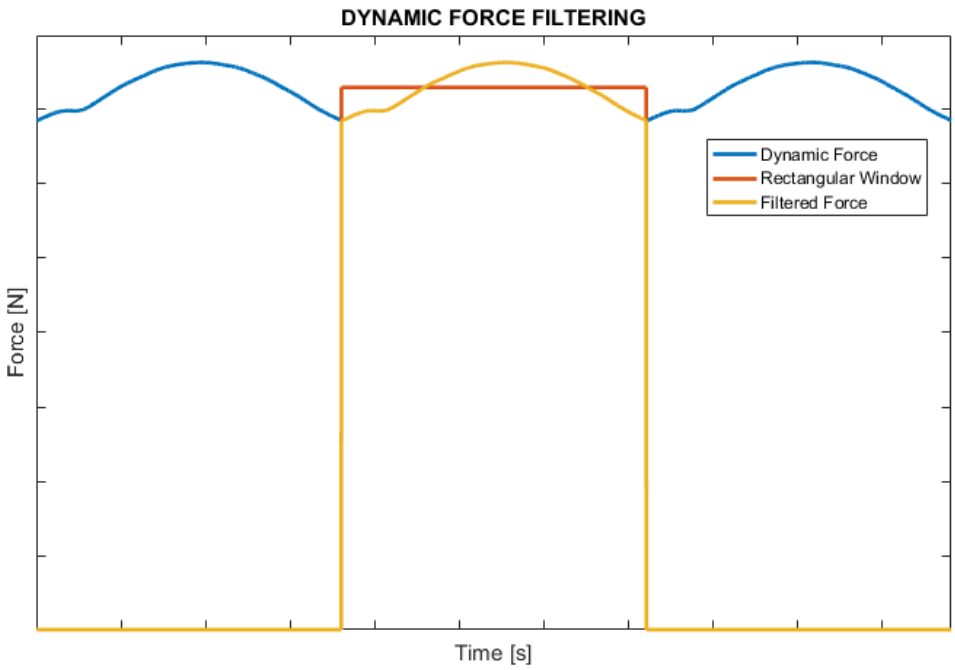

Figure 3-3: Force filtering, rectangular window

Of course in physical systems there always is more than a single tooth in contact. Bevel gears in particular are specifically designed to better distribute the load among the teeth, so they always keep at least two or three teeth in contact. The dynamic force computed from the model is anyway related to a spur gear, and so must be the contact ratio selected, in order to avoid a wrong estimation of the filtered force. Extensive analysis on the contact ratio variation was performed and is presented in the following. It is also important to correctly position the window function inside the time domain, because the harmonic decomposition should be performed on the real force which the tooth is subjected to during its pitch. The response is extremely sensitive to the window shifting, and also a slight bad positioning could lead to not negligible mismatches. The filter window function is therefore built after determining the exact time required for one pitch and interpolating dynamic force in this range.

The final step in the external load computation is the harmonic decomposition. As explained previously the analysis is performed on a cyclic sector, which symmetric boundaries are applied to. When solving the differential system in the frequency domain, then not all the dynamic load provided by the Parker model must be applied to the tooth; only the correct component is extracted. This component is defined by the engine order of the problem (a parameter referring to the modes opening in the Campbell diagram). The extraction operation is particularly simple in the MATLAB environment, because the harmonic decomposition is performed by the fast Fourier transform (fft) algorithm, that directly processes a time (or angle) domain function into its discrete Fourier transform (its spectrum), that is its series expansion in the frequency domain:

$$f_k(t) \xrightarrow{FFT} F_k(\omega) = \sum_{i=1}^{n} f_j(t) \cdot W_n^{(i-1)\cdot(k-1)} \quad , \quad W_n = e^{(-2\cdot n\cdot j)/n} \qquad k = 1,2,\dots,n$$

Since the engine order is given by:

$$EO = z \pm ND$$

Where:

- z is the number of cyclic sectors;
- ND is the number of nodal diameters;
- $\pm$ is referred to the particular mode shape: for a backward a $+$ is used, for a forward a $-$.

Then the harmonic force needed is given by:

$$F_{hrm}(\omega) = F_{EO+1}(\omega)$$

Because the first element in the transformed vector stands for the mean value of the starting function $f(t)$ multiplied for its length n (so it doesn't identify a fluctuating component). Actually also the higher order harmonics should be taken in account for a certain engine order (the ones defined by $EO = n \cdot z \pm ND$ where $n = 1,2,\dots,+\infty$), but it is noticed that their contribution to the total harmonic component is far significantly smaller than the first order's: these harmonics are so neglected. It is important to remember that the Parker model is applied using the tangential component of the static transmission error, due to its bigger weight; the dynamic force computed and subsequently the harmonic component will be directed in the tangential direction. It is then necessary to determine the excitation in the radial and axial directions, by using the geometric relations:

$$\begin{cases} F_{hrm,rad} = F_{hrm} \cdot r_{rad} \quad , \quad r_{rad} = \dfrac{\tan\alpha \cdot \cos\gamma}{\cos\beta} \mp \sin\beta \cdot \sin\gamma \\ F_{hrm,ax} = F_{hrm} \cdot r_{ax} \quad , \quad r_{ax} = \dfrac{\tan\alpha \cdot \sin\gamma}{\cos\beta} \pm \sin\beta \cdot \cos\gamma \end{cases}$$

Where:

- α is the pressure angle;
- β is the helical angle;
- γ is the half primitive cone angle;
- The signs $+$ and $-$ take in account whether the loaded profile is the concave or the convex one (only for bevel gears, otherwise the previous expressions are simplified).

Since the force signal is periodic over the time required for a pitch, the resulting Fourier transform usually has a very low value for the harmonic indices given by:

$$i_0 = n \cdot z \quad , \quad n = 1,2, \dots, +\infty$$

Figure 3-4 shows an example of fast Fourier transform in the orders domain. The graphic is realized by filtering a constant force with a rectangular ($CR = 1$) window, in order to highlight the expected bounces.

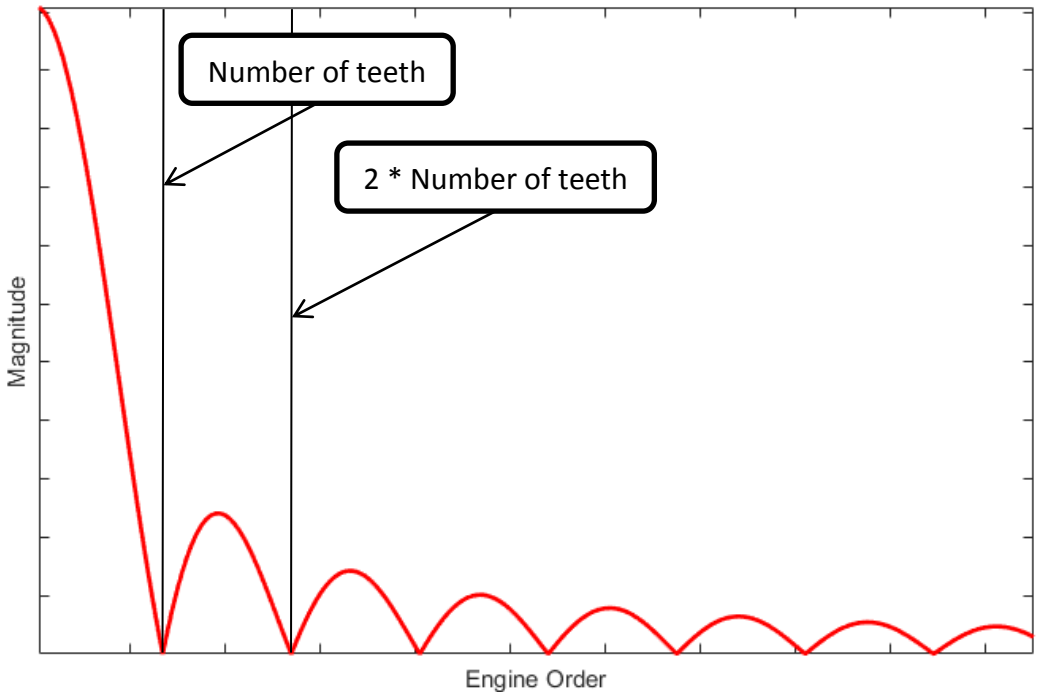

Figure 3-4: Fourier transform, rectangular window

3.4 Model sensitivity

During the tool validation, it has been found that the fast Fourier transform trend is sometimes completely different from the theoretical one. Since the first order harmonic is the one used to excite the structure, it is essential to know the effect of each main parameters on the force estimation. The filtered signal is built from the dynamic force and the window function; three main parameters have been thus identified:

1. Dynamic force fluctuation amplitude, that's directly influenced by the static transmission error fluctuation (by the Parker model); this is the most important parameter which the response is sensible to;
2. Contact ratio, which effect is to increase or decrease the load experimented by the single tooth during the pitch; this parameter has been taken in account due to the difficulty in estimating it, which makes its choice not univocal;
3. Filtering window shift over one pitch time. This parameter determines the trend of the dynamic force during the single mesh cycle by establishing the starting point of the period.

3.4.1 Dynamic force fluctuation

As explained previously, the static transmission error is computed taking in account several gear's properties, ranging from the surface imperfections to the material elasticity. It is therefore clear that different meshing gears will always have different transmission errors, either in appearance and in values, and a low STE will produce far smaller vibrating amplitudes. In Figure 3-5 is shown a comparison of the transmission errors referred to the same reduction stage of different engines. As it's possible to see, values can meaningfully change by simulating one engine or another, and the percentage fluctuation can increase by an order of magnitude.

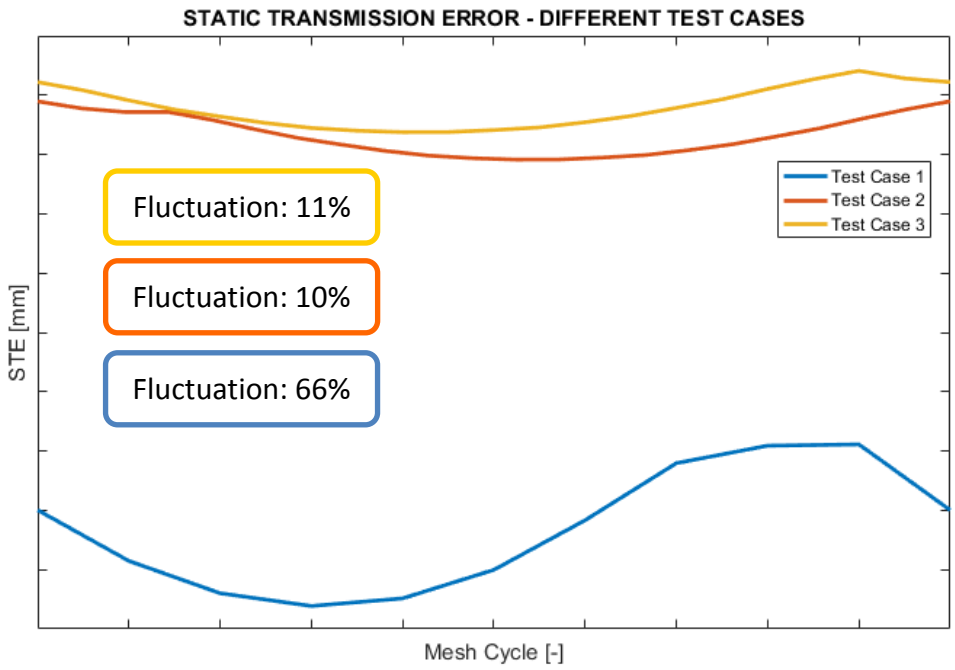

Figure 3-5: STE amplitude comparison

The dynamic force produced by the Parker's model asymmetrically fluctuates around the static force value (which is its integral mean) and its amplitude is strictly related to the STE. Analysis has been performed by defining a parameter that contains information about the dynamic force percentage variation. With reference to Figure 3-6 the parameter is defined as:

$$\Psi = \frac{A_0}{F_s} \quad , \quad A_0 = \frac{A_+ - A_-}{2}$$

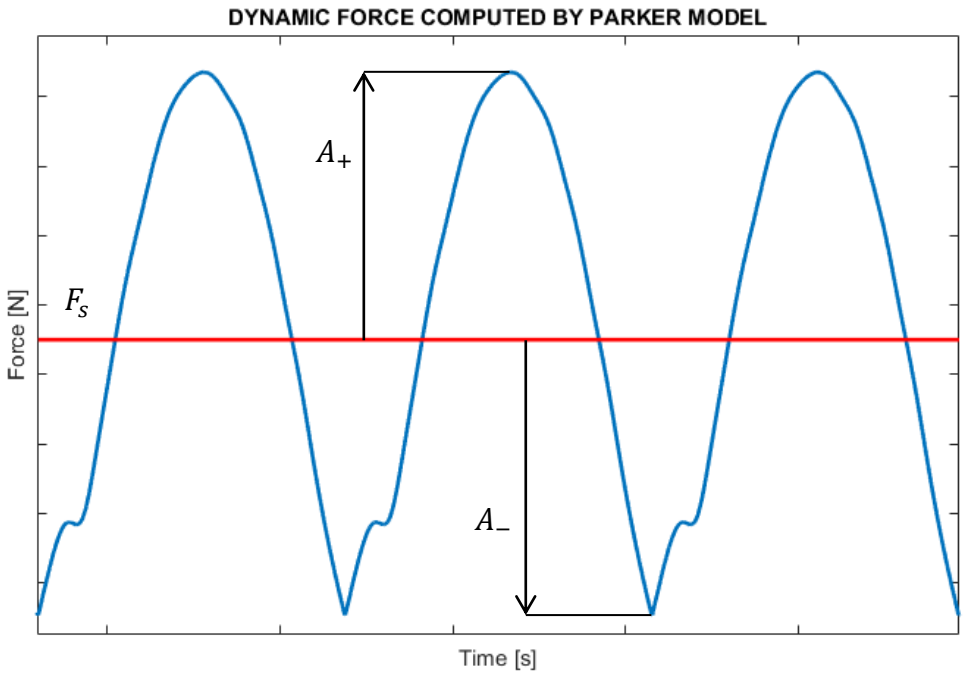

Figure 3-6: Dynamic force fluctuation ratio

The parameter just defined can be correctly used to characterize the real dynamic force of meshing gears; in fact, knowing it and the static load in the mechanical transmission, it is possible to define an equivalent sinusoidal dynamic as:

$$f_{DYN,eq} = F_s - \Psi \cdot F_s \cdot \sin(z \cdot t)$$

This function is shown in Figure 3-7 (in the angle domain, equivalent to the time one), compared to the real dynamic force computed by the Parker model:

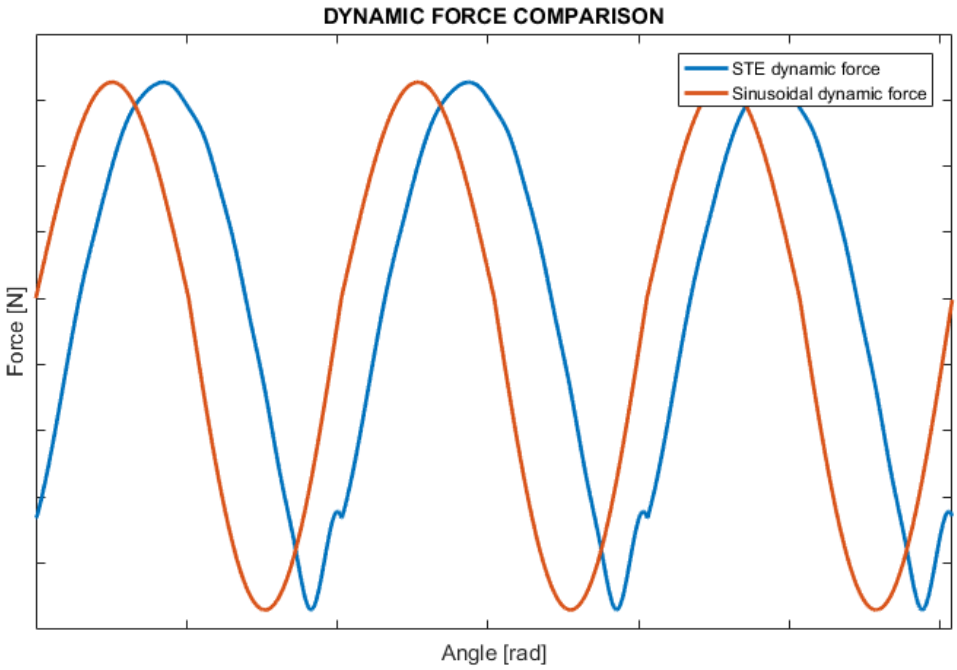

Figure 3-7: Dynamic force - sinusoidal vs tool computed

A few considerations can be made:

1. The equivalent function, being a sinusoid, symmetrically fluctuates around the static force value; since the real dynamic force does not show this symmetry, approximation could be made by an asymmetric function that assumes the same values of the force at the beginning and at the end of the period. This approach is not taken into account because the asymmetric function provides almost identical results as the symmetric one. Furthermore this approach is analytically less correct, because the equivalent function doesn't have the same integral mean as the real dynamic force, so the energetic content of the force is not preserved;
2. The equivalent function is time (or angle) shifted compared to the dynamic force; this could lead to phase differences in the frequency domain. Since the interest is on the Fourier transform amplitude, the shift does not cause errors.

By applying a filtering window with a certain contact ratio to the dynamic force and to the equivalent one, it is possible to perform the orders decomposition. As shown in Figure 3-8, harmonic components are pretty similar in the two cases.

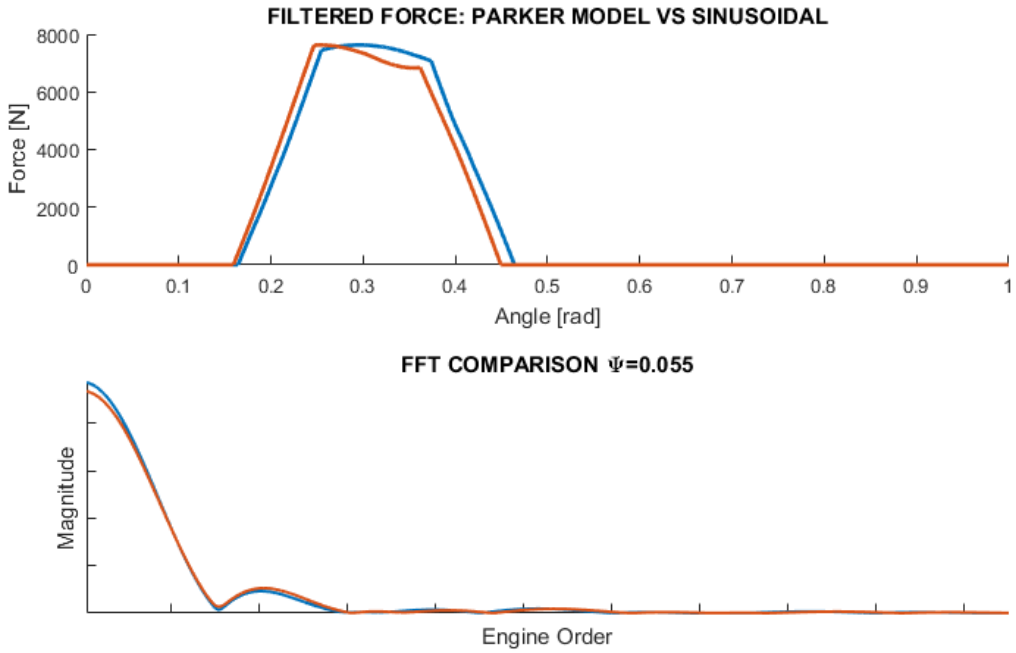

Figure 3-8: Harmonic component - sinusoidal vs tool computed

Once explained the Ψ parameter meaning and proved its effectiveness, a sensitivity analysis has been performed using the equivalent sinusoid function instead of the dynamic force, due to its mathematical manageability. This analysis has been computed only for one engine, the one which had the most fluctuating static transmission error (and thus the most oscillating dynamic force). In the following tests, so, the static force, the number of teeth and the contact ratio always keep the same values. In particular a unitary contact ratio has been chosen, because this makes the window function a rectangle, and so each deviation from the theoretical behavior is due to the dynamic force swings. In Figure 3-9 a) the input functions are shown before and after the window application.

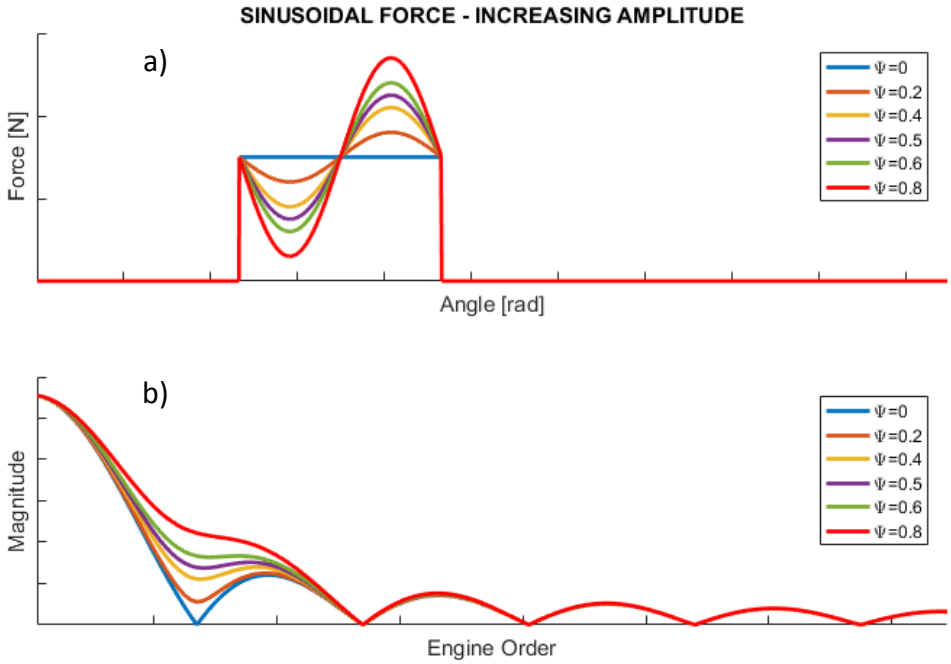

Figure 3-9: Dynamic force amplitude sweep

The Fourier transform of the time domain signals are displayed in Figure 3-9 b). For $\Psi = 0$ the dynamic force is identical to the static one; this is obviously a theoretical case only, because such a condition would be true if the static transmission error was equal to zero, as if the meshing gears had an infinite stiffness. In this case the resulting fft exactly has the expected trend, with zero values for harmonic orders equal to multiple of the number of teeth.

One important thing to notice is that the trend of the Fourier transform is a direct cause of the dynamic force fluctuation magnitude: the same analysis already described has been repeated for several static force values, the harmonic decomposition has been reduced to its dimensionless form and the resulting diagram is exactly the same for the different cases (Figure 3-10).

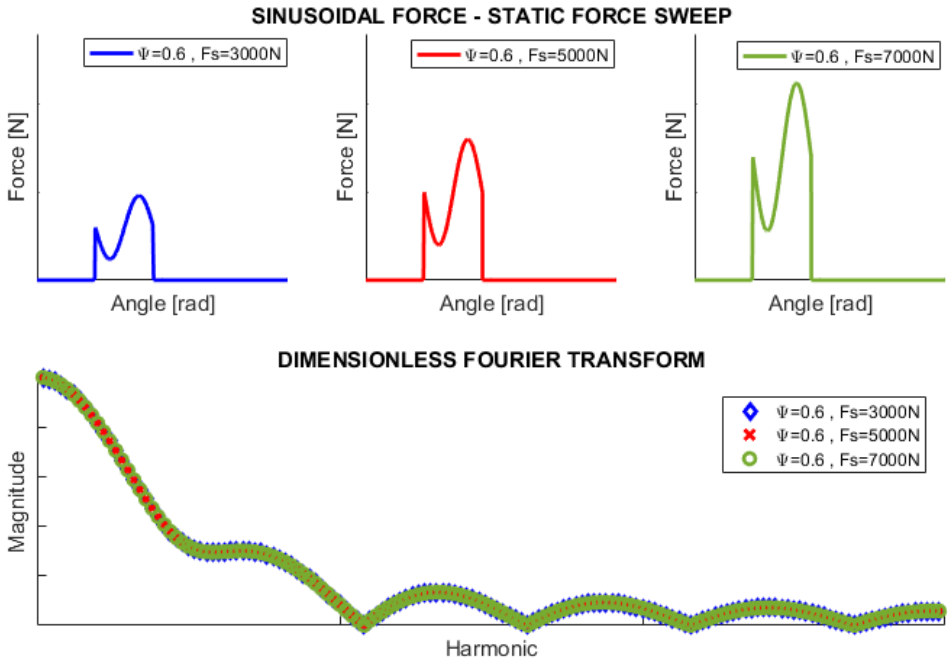

Figure 3-10: Dimensionless Fourier transform

3.4.2 Contact ratio

The contact ratio is one of the most difficult parameters to estimate in the entire analysis. This is because of several considerations, partially explained previously:

- The Parker model is related to spur gears, whereas the great majority of the simulated gears are bevel ones. The main reason for which bevel gears are used is that more than one couple of teeth is in contact at each time instant. This is mathematically equivalent to a greater contact ratio; in order to not underestimate the harmonic component of the force, an equivalent contact ratio is used. This parameter will be completely different from the real one, and so its value could not always be the correct one;
- The simplified expression shows no dependence of the contact ratio from the load transmitted by the meshing gears, while it's well known that there is a non-linear correlation between the two.

Analysis has been performed for a contact ratio between one and two, because this is the variation range for the parameter in the case of spur gears. In order to insulate the contact ratio effect on the Fourier expansion of the force, the static transmission error effect has been neglected, assuming a coincidence between the static and the dynamic forces. The static force value has been arbitrarily chosen equal to 3000 N (a reasonable value for the simulated test cases). It is important by the way to point that this static force value only aims to produce sensible harmonic forces. Using a unitary force would have led to the same results for what concerns the qualitative contact ratio effect on the response. The force signal transformed into the frequency domain has so a rectangular, trapezoidal or

triangular shape, whereas the real rotating force will have a strongly irregular trend, strictly related to the STE one. In Figure 3-11 it is possible to see the starting signals in the angle domain (equivalent to time domain through the rotational speed) and the respective Fourier expansions.

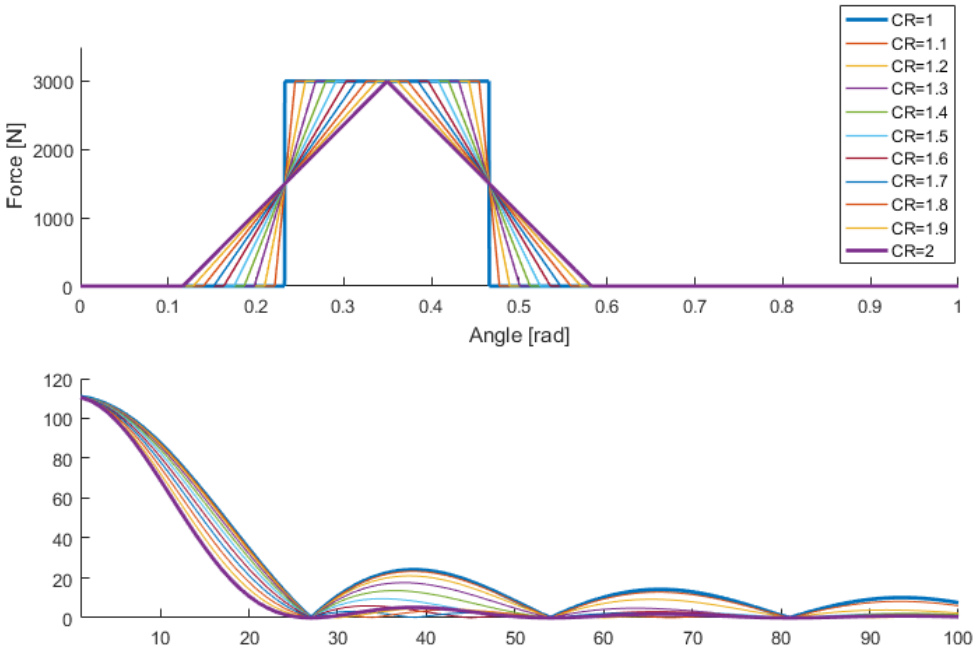

Figure 3-11: Contact ratio sweep

In the figure it is possible to see the window shape gradually changing from a rectangle ($CR = 1$, blue line) to an isosceles triangle ($CR = 2$, violet line). It is immediately clear that when the CR grows, the harmonic component for each mode decreases, as it is legit to expect, because a high contact ratio means that the total exchanged load is well distributed over more than one tooth. Contact ratio also has one additional effect: as a matter of fact it does affect the ratio between the forward and the backward harmonic components for a given mode. In Figure 3-12 this ratio is plotted against the contact ratio values for various modes.

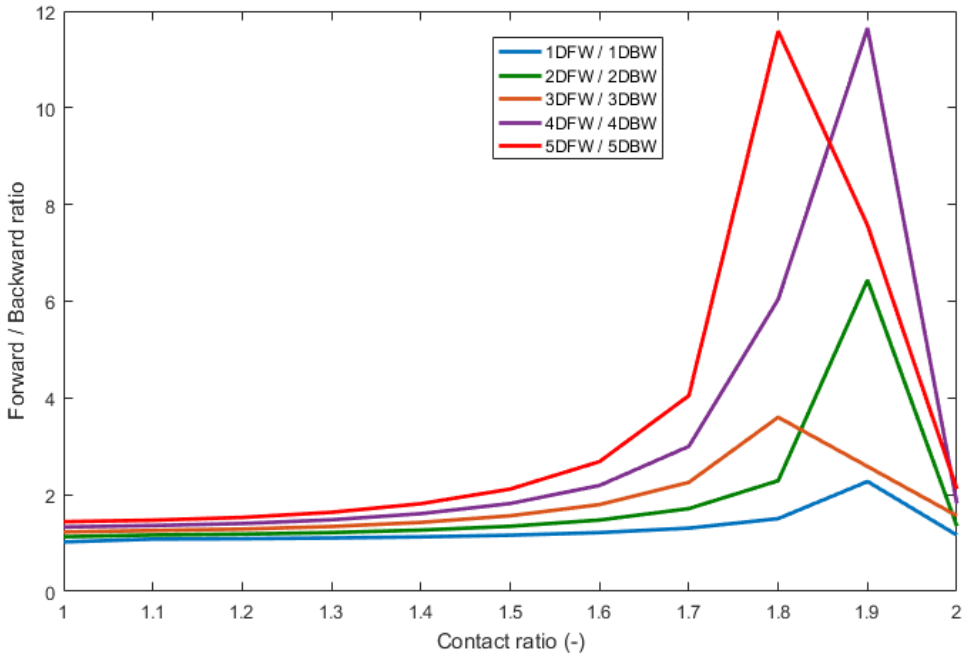

Figure 3-12: Forward / Backward harmonics ratio

It is clear that when the contact ratio is slightly smaller than an integer value (2 in this case), the forward harmonic component is several times greater than the backward one. Since the non-damped solution process is linear, this means, if a mean Q-factor value is assumed, that the forward response will be even one magnitude greater than the backward one. This behavior has been proved by considering a contact ratio between 1 and 3 (Figure 3-13). In this case there always are more than two teeth meshing at each given instant, so the window will be a trapezoid which maximum will be given by:

$$W_{MAX} = \frac{1}{CR - 1}$$

The Fourier expansion has the same trend previously explained for contact ratio immediately smaller than integer values. The only additional consideration that can be done is about contact ratios between 2 and 2.4-2.5. It is possible to notice that in this range the backward harmonic is greater than the forward one, behavior not observed in the previous analysis. The reason of this trend is given by the Fourier series shape for $CR > 2$: in this range the function presents a bounce even for $EO < z$, which lead to a substantial decrease of the forward harmonic component. As the contact ratio grows again, then, the frequency where the bounce is experimented decreases and the softening effect on the forward harmonic wanes ($2.5 < CR < 3$).

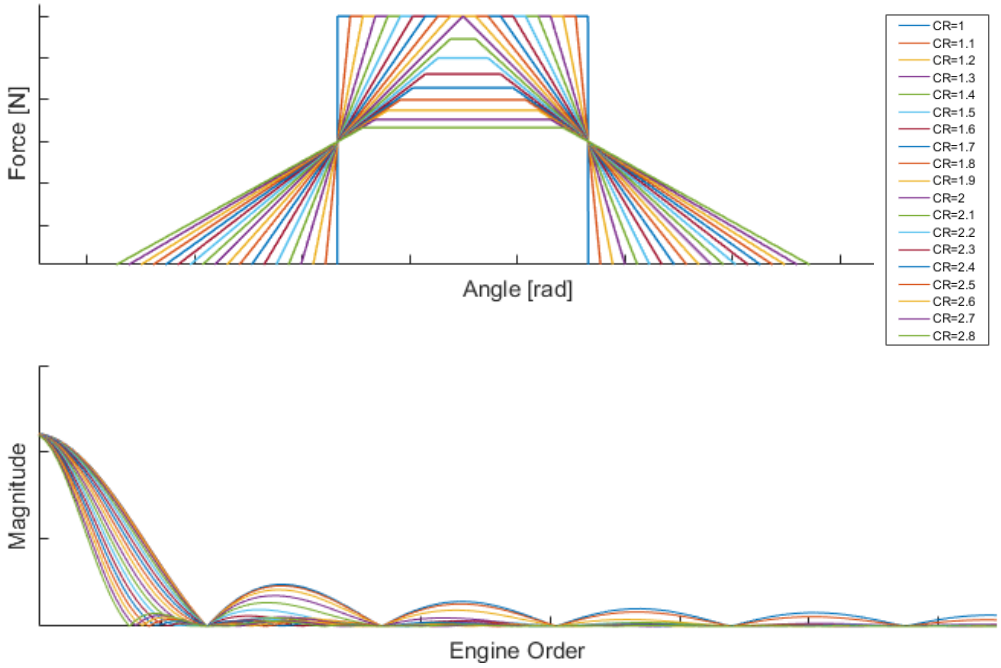

Figure 3-13: Contact ratio sweep - CR>2

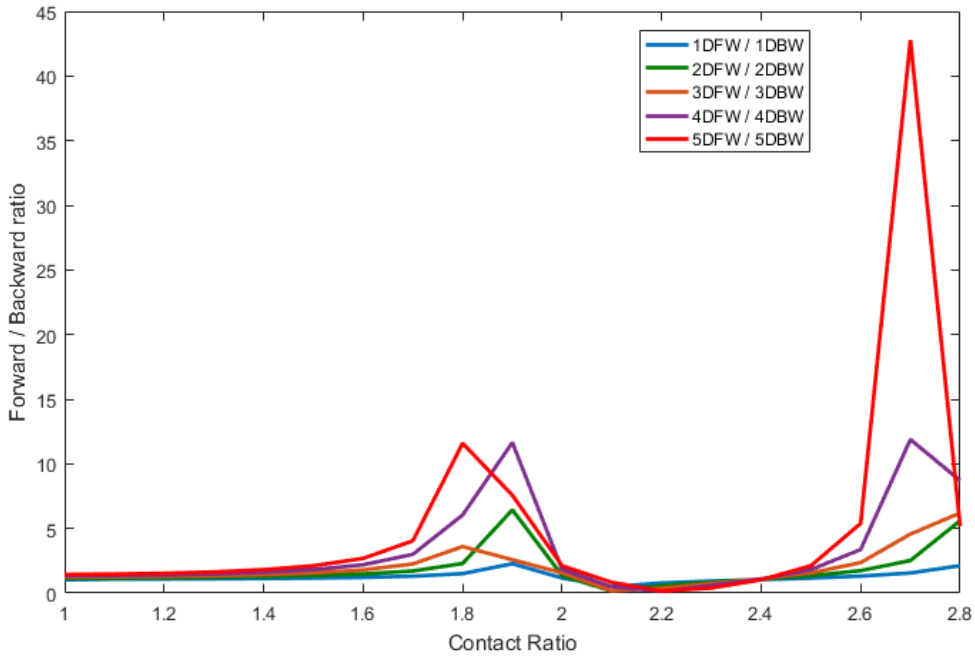

Figure 3-14: Forward / Backward harmonics ratio - CR>2

3.4.3 Window shift

The last parameter sensitivity analysis on the Parker model has been performed by changing the position of the trapezoidal window over one pitch period. If a static force had been used, the signal would always remain the same after the application of the window, wherever it is located. In the case of fluctuating dynamic force and a rectangular window ($CR = 1$), instead, the filtered force changes in

the time domain, but its frequency content remains the same, with the introduction of a phase (which is not a variable of interest in the present analysis). The window positioning has therefore meaning only if a fluctuating force and a contact ratio not equal to 1 are both assumed. Under these hypothesis, it is possible to obtain different configurations for the rotating force, which limits are displayed in Figure 3-15.

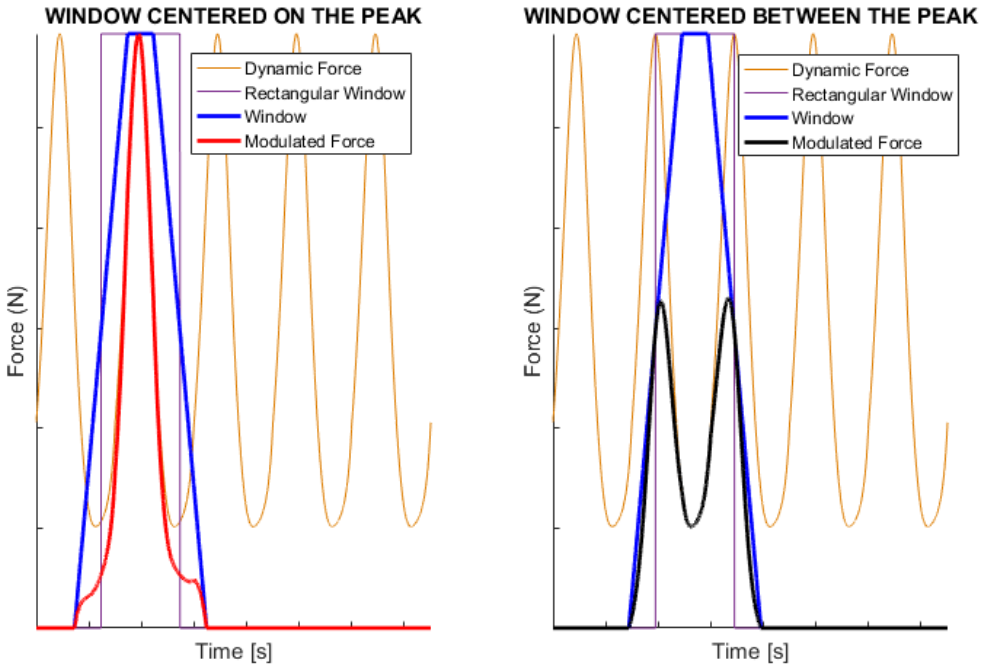

Figure 3-15: Window position sweep

As it is possible to notice in the previous figure, the two resulting forces have completely different shapes, even if their integral means, which are representative of the static force transmitted in the meshing process (weighed by the window frequency content), remain equal, according to the cyclic symmetry hypothesis. A complete sweep of the window positioning over a pitch can be observed in Figure 3-16.

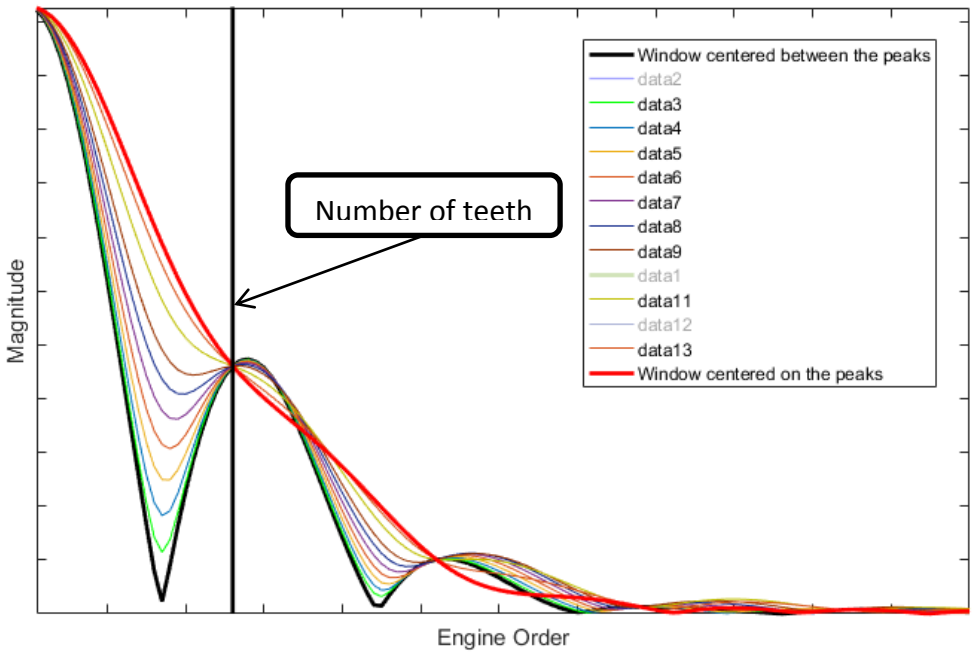

Figure 3-16: Window position - Fourier transform

The analysis plotted in the previous image is performed using geometry, contact ratio and STE of a specific test case. A superimposition of multiple effects can thus be observed: the STE is extremely variable and this feature causes the Fourier expansion not to bounce for $EO = z$; the equivalent spur gear contact ratio based on the specific gear is implemented, conditioning the ratio between forward and backward responses. In the previous figure, the red and black lines are related to the window positioning in Figure 3-15, which represent the limits of the sweep. By observing the Fourier transform comparison, the two main effects of the positioning:

- A new bounce, for $EO < z$, appears when the dynamic force values at the limits of the rectangular window are near to the static force exchanged (which is numerically equal to the dynamic force mean);
- As for the contact ratio, the ratio between the backward and forward harmonic forces changes with the window positioning. In this case, anyway, the effect is far less significant, since the ratio doesn't even reach 1.5 (in the case of the contact ratio sensitivity analysis one magnitude greater results have been obtained). In Figure 3-17 the ratio between forward and backward harmonic forces are plotted against the different window positioning.

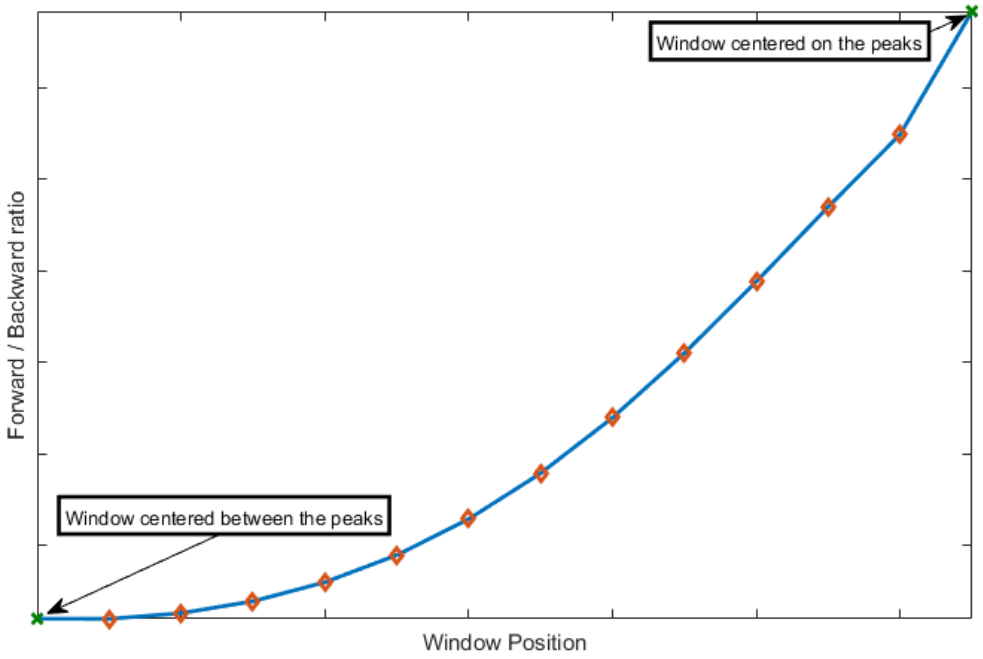

Figure 3-17: Window position - Forward / Backward ratio

In the tool it is supposed that the static transmission error provided is synchronized with the single pitch; in other words, the first value of the STE vector should be the error in the instant when the tooth comes into contact. If the user has provided a correct STE, the application of the window follows the procedure graphically described in Figure 3-18.

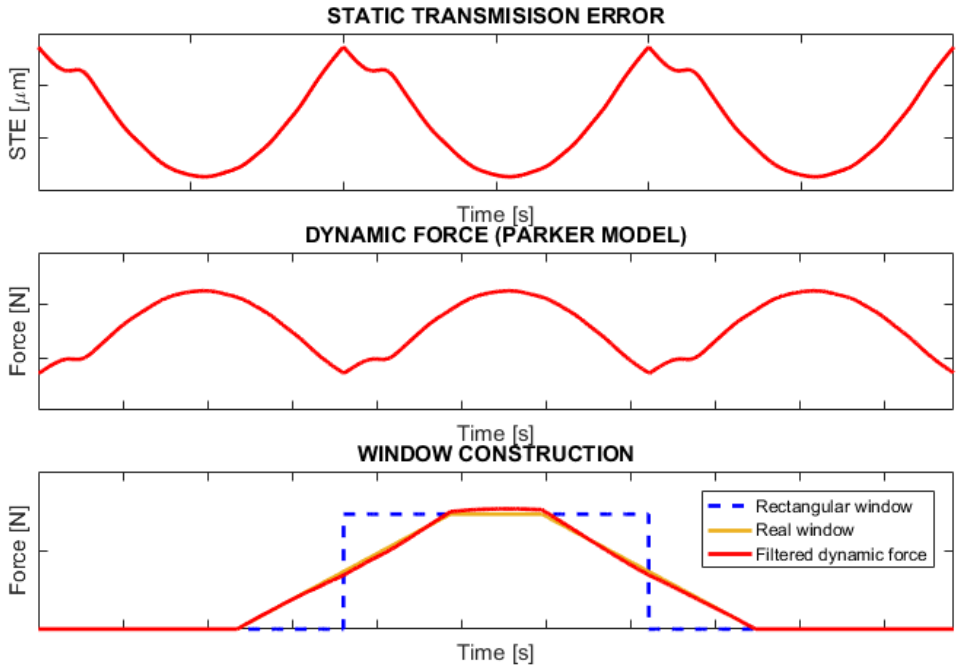

Figure 3-18: Filtering window construction

3.4.4 Parker model simplification

As a last thing about the model for the dynamic mesh force computation, a simplified version of the Parker model has been implemented, and its results (in terms of linear response) have been compared with those produced by the whole model. The new version of the model has been built from the former one by supposing infinite inertias; under this hypothesis the tooth dynamics is completely separated from the gear's body. The Parker model simulates the interaction between two teeth by connecting them with a variable-stiffness spring and a damper. Since the body inertias are infinite, the connection elements don't experiment any elongation or compression, and the dynamic force is only a function of the time history of the mesh stiffness, determined by the STE. In mathematical terms, considering two time instants t_1 and t_2, it is possible to write:

$$\begin{cases} k_m(t_1) \cdot x_0 = F_{DYN}(t_1) \\ k_m(t_2) \cdot x_0 = F_{DYN}(t_2) \end{cases}$$

Where:

- k_m is the mesh stiffness, inversely proportional to the STE;
- F_{DYN} is the dynamic force.

By dividing the first equation for the second, the following expression is obtained:

$$\frac{F_{DYN}(t_1)}{k_m(t_1)} = \frac{F_{DYN}(t_2)}{k_m(t_2)} = \frac{\Delta F_{DYN}}{\Delta k_m} = \frac{F_s}{\bar{k}_m}$$

It is finally possible to determine the dynamic fluctuation of the mesh force as:

$$F_{FLU} = F_s \cdot \frac{\Delta k_m}{\bar{k}_m} = F_s \cdot \left(\frac{k_m(t) - \bar{k}_m}{\bar{k}_m} \right)$$

Since the mesh stiffness is defined by:

$$k_m(t) = \frac{F_s}{STE(t)}$$

It is possible to determine the direct relation between the STE and the dynamic force by operating a substitution in the previous expressions:

$$F_{FLU} = F_s \cdot \left(\frac{\overline{STE}}{STE(t)} - 1 \right) = \frac{T}{R_b} \cdot \left(\frac{\overline{STE}}{STE(t)} - 1 \right)$$

Where:

- T is the torque;
- R_b is the base radius, since the model is entirely referred to the contact line.

The final dynamic force is then expressed by:

$$F_{DYN} = F_s + F_{FLU}$$

The previous approach leads to dynamic force trend like the one displayed in Figure 3-19. As can be easily noticed, the transient part of the resulting force disappears (since the differential equation has been replaced with an algebraic one). The resulting Fourier expansion presents only minimal deviations from the one computed by using the model without simplifications. The same analysis has been performed for several gears in different engines, and the goodness of the model simplification has been validated by comparing the dynamic forces, the Fourier series and finally the resonance amplitudes computed by the two methods. Results are shown below.

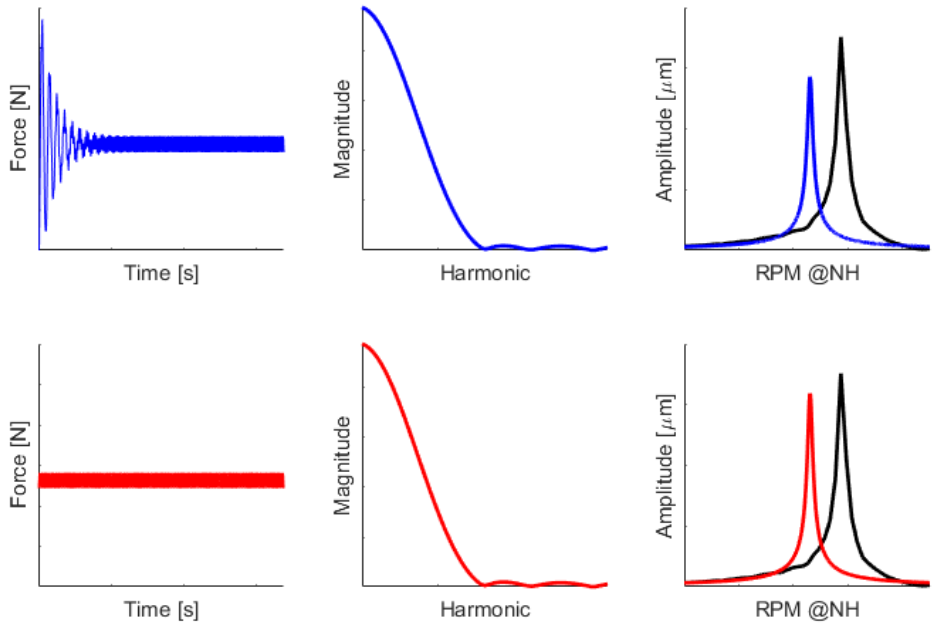

Figure 3-19: Parker model - complete vs simplified

The mismatch between the two responses is always very contained (10%), proving that the dynamic behavior of the teeth is almost completely independent from the body of the gear, treated as an infinite inertia. The two approaches don't produce exactly the same results because of the gears inertia influence on the response. The main difference between the two models is in the fact that the complete one takes into account the contact loss between teeth. Even if in the simulated test cases the contact loss weight in the final response is not very relevant, it is not excluded that it is not in some other case (for example for very high magnitude vibrations). Moreover the differential model only requires three more parameters to be applied:

- The two gears polar inertias, easily measurable from the CAD model of the sector;
- The mesh damping ratio, which is assumed equal to 0.08, from literature.

Since the model is referred to an equivalent single degree of freedom system, the right inertias to use should be equivalent ones too, while the real gears inertias have always been used. A sensitivity analysis has been performed by applying inertias varying between the 50% and the 200% of the ones measured for the real gear. As displayed in the following (Figure 3-20) the model is not sensitive to the parameter; in fact the dynamic force amplitude shows a maximum percentage variation of 3%, obtained by doubling one of the inertias, which is far beyond the realistic variation range of the parameter (even a 50% variation of the inertia is not very likely). This low dependence of the harmonic force from the gear mass is perfectly coherent with the previous assumptions: the dynamic behavior of the tooth is almost independent from the gear body.

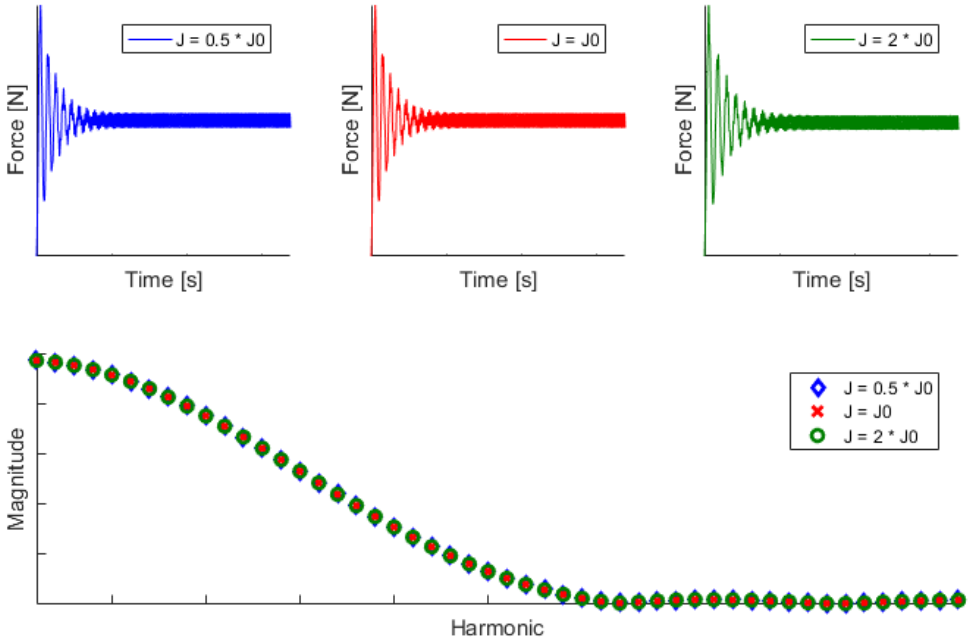

Figure 3-20: Polar inertia sweep

Given the previous considerations, the whole Parker model has been implemented in the final version of the tool, since the computation time gain provided by the simplified one is not significant and the contact loss is considered, covering therefore a wider range of applications. The strongest approximation in the harmonic force computation is the equivalent spur gear contact ratio, but its application is in the filtering window construction, downstream the dynamic force computation. For this reason the approximation does not present real practical advantages. It is important to be aware of the presence of the simplified model, because it allows to compute a first approximation response even without full knowledge of the gear geometry.

4 Contact force estimation

The ultimate purpose of the simulations run using the POLIGear tool is the estimation of the effect produced by the installation of damper rings on gears. In order to estimate the damper ring performance, therefore, it is useful to determine the energy dissipated and the damped response Q-factor. As explained previously, the frequency response of the system is the solution of the differential system:

$$[M_G] \cdot \{\ddot{q}_G\} + [C_G] \cdot \{\dot{q}_G\} + [K_G] \cdot \{q_G\} = \{F_{G,TOT}\}$$

$$[M_D] \cdot \{\ddot{q}_D\} + [C_D] \cdot \{\dot{q}_D\} + [K_D] \cdot \{q_D\} = \{F_{D,TOT}\}$$

Where:

$$\{F_{G,TOT}\} = \{F_G\} + \{F_{CF,G}\} + \{F_{NL}\}$$

$$\{F_{D,TOT}\} = \{F_{CF,D}\} - \{F_{NL}\}$$

It is therefore essential to develop and implement a model to simulate the interaction between the gear and the damper ring.

4.1 Contact model

The model will involve strong non-linearity, because it tries to reproduce the relative motion between the two component, also involving all the friction phenomena generated by the rotation. The contact model, however formulated, is then mathematically expressed as a non-linear operator that takes as input the displacements of the interfaces between the two components and gives as output the contact forces exchanged in the process. Since the simulated bodies are in rotating motion, it is legit to suppose that the displacements will be a periodic function of time (or rotational speed). The contact model will therefore describe a hysteresis cycle (precisely due to its non-linearity), that will be swept clockwise delimiting an area, which has the meaning of the energy dissipated over one complete period. In Figure 4-1 the logical scheme for the contact model is shown.

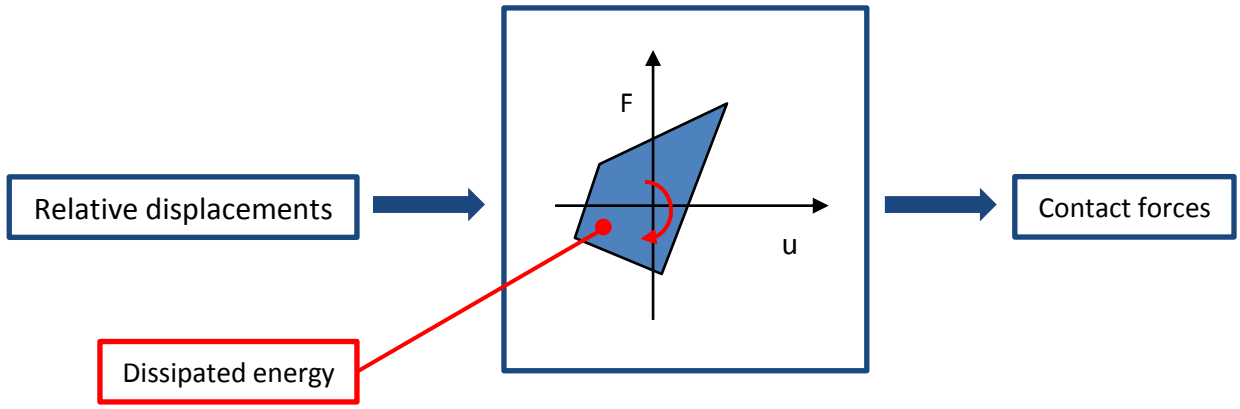

Figure 4-1: Contact model block diagram

Because of the non-linear friction effects, it is clear that for each relative displacement value there are more than one contact force value: to determine the right one it is then necessary to know the previous force value:

$$F_{NL}(t_i) = f[u(t_i), F_{NL}(t_{i-1})]$$

Since the simulations have been run for finite element models, the easiest way to implement a contact model is to define a contact element, which will be interposed between nodes belonging to the gear contact interface and the corresponding ones on the damper ring surface. This kind of implementation requires therefore the interfaces of the two components to have exactly the same number of nodes, precisely placed on the same coordinates (an example is given in Figure 4-2).

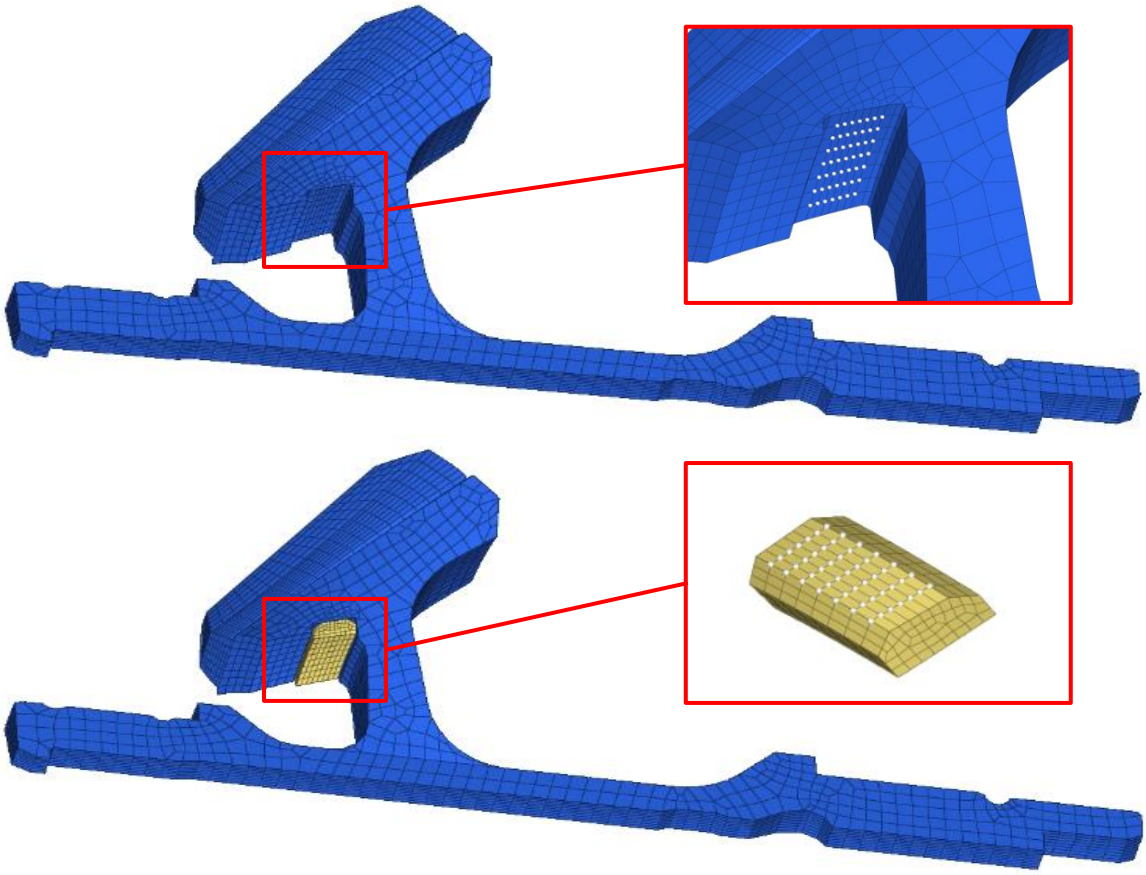

Figure 4-2: Contact nodes

As it is possible to see in the previous figure, the number of contact nodes for each component is completely arbitrary and left to the user; it would be theoretically possible to choose only one contact node, even if the resulting frequency response would probably result insufficiently accurate. There are only two restrictions, and breaking them leads to real errors in the simulation. First of all, each node on the gear contact interface must be exactly paired with a node on the damper interface, and the two nodes must have the same coordinates: if nodes without the same location are chosen, the contact element is incorrectly positioned, producing then senseless contact forces. It is then important to notice that some of the nodes on the groove borders in the previous figure belong to the left and right interfaces as well as to the contact one. These nodes can be arbitrarily assigned to one or the other group, but not both, because the information about the displacement of the cyclic sector interface nodes is concentrated into a certain number of modes after the Tran reduction, explained previously. To apply the contact model to a set of nodes, anyway, it is necessary to save the information about its physical displacement, and it's therefore required to keep the whole set as master along the entire reduction process.

4.2 Contact element

In literature several contact models can be found. Each of those uses a different set of parameters in order to simulate the surfaces interaction, build the hysteresis cycle and finally determine the contact forces; as explained in the previous paragraphs, the finite element modeling used in the present work naturally leads to a formulation in which the single interface nodes are linked one by one by means of a contact element. The one currently implemented in the code is graphically shown in Figure 4-3.

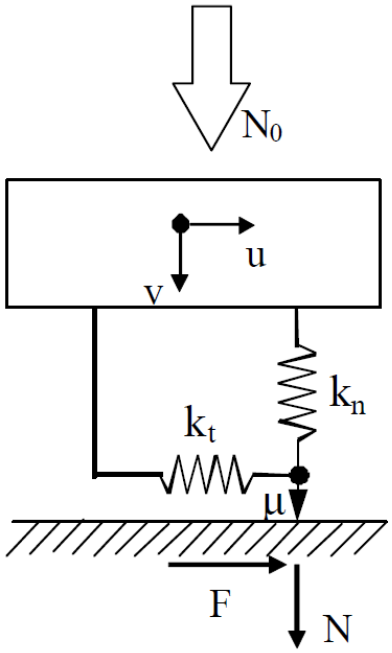

Figure 4-3: Contact element – Source

In the previous figure all the parameters and the variables involved in the problem are displayed. The contact element has two degree of freedom, each of those is related to the contact force in a specific direction. According to the typical system configuration, $v(t)$ is the difference between the radial displacements of corresponding nodes on the gear and on the damper ring, and can be computed as:

$$v(t) = -\left(q_{rad,G}(t) - q_{rad,D}(t)\right)$$

Where the minus sign is due to the opposite conventions chosen in the definition of the global cylindrical system (centered on the rotation axis), which has an outgoing radial axis, and the local reference system displayed in the contact model figure. At any given moment the $v(t)$ determines the normal force exchanged, and therefore the motion state between the contact surfaces (a more detailed walkthrough is presented in the following paragraphs). The most important feature is that the contact surfaces can't exchange traction force, because these wouldn't have physical meaning: if the normal contact force becomes equal to zero, in fact, contact loss is experimented and there's no

force exchange until the centrifugal load pushes back the ring on the groove surface. The state just described is called "*lift off*".

The displacement $u(t)$ is the tangential one in the local reference system. In the global cylindrical system it will be a linear combination of the tangential and the axial relative displacements. The linear coefficients are determined by defining an angle α between the u direction and the rotation axis. The tangential displacement can thus be expressed as:

$$u(t) = \left(q_{ax,G}(t) - q_{ax,D}(t)\right) \cdot \cos\alpha + \left(q_{tg,G}(t) - q_{tg,D}(t)\right) \cdot \sin\alpha$$

The previous expression is often considered in the case $\alpha = 0$, since the tangential direction is the same in the two reference systems. The complete formulation is implemented anyway, to take in account the prospect of an inclined damper.

4.3 Contact parameters

When the relative displacements are known, the last step for the contact force estimation is the hysteresis cycle building. Doing so requires a set of parameters, depending on the contact model chosen. In the implemented one, each relative motion direction has one stiffness, which physical meaning is explained in the following; the information about friction regroups all the dissipative phenomena and determines the area magnitude of the cycle and is given in the form of a friction coefficient, which is freely changeable by the user. The last characteristic parameter is the centrifugal load due to the rotation itself, and provides the operative conditions (while the other parameters are defined with the system)

4.3.1 Centrifugal load

The first parameter required is the operating centrifugal load. It is important to notice that the hysteresis cycle is built for each contact element, that is for each pair of contact nodes on the gear and the damper surfaces. In the present case a simplifying hypothesis has been made: the complete centrifugal load experimented by the damper ring is equally divided among the contact nodes; this will not be the real behavior of course, but it's not far from reality either, so the assumption doesn't significantly change the result of the simulations. The total centrifugal load can be expressed as:

$$N = m_D \cdot \omega^2 \cdot r$$

Where:

- m_D is the damper ring mass;
- ω is the rotational speed of the system;
- r is the radial position of the damper ring barycenter.

According to the hypothesis explained previously, the centrifugal load on the single contact element is computable by:

$$N_0 = \frac{N}{z \cdot n_C}$$

Where:

- z is the number of cyclic sectors;
- n_C is the number of contact nodes on a single damper ring cyclic sector.

The centrifugal load produced by the gear rotation is supposed to be entirely let off on the interface with the damper ring. This is another simplification, but it is coherent with the real geometry of the damper ring, which is provided with a lateral cut (Figure 4-4); this cut has two purposes:

1. Allows the damper ring to be assembled in the gear groove;
2. During the run, the centrifugal load "opens" the damper ring and pushes it against the contact interface of the groove; this is only possible because of the cut presence. The radial stiffness of the damper ring is therefore very low, and this feature allows the expected behavior of the component, because the damping of the resonances originates from the slithering between the two contact interfaces.

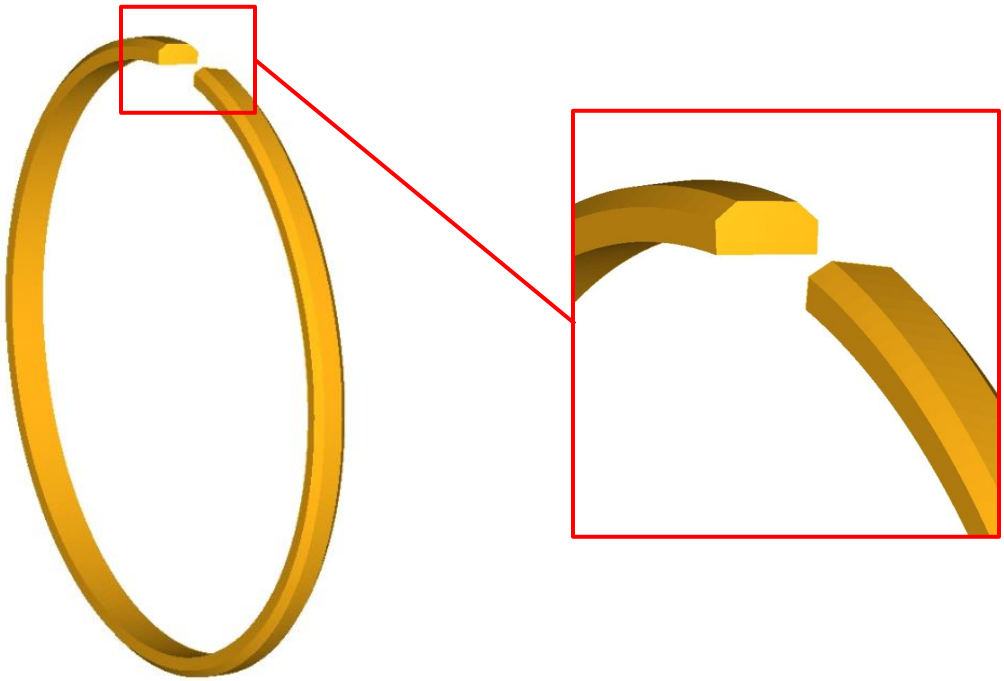

Figure 4-4: Damper ring lateral cut

Given the presence of the lateral cut, the damper ring structure is not properly cyclic symmetric. By the application of the symmetry hypothesis, anyway, only cyclic displacements are allowed. Since the non-linearity of the system considered, this assumption can lead to frequency shift between the real and the simulated structures. A detailed analysis of the two approaches would be required to fully

investigate the validity of the simplification implemented, but frequency shift introduced by the lateral cut presence are not relevant, according to experimental data. Although there's not a perfect match, the implementation of the real damper ring geometry would require a full change of the reduction process for the specific component, too an onerous code modification compared with the advantage brought.

4.3.2 Friction coefficient

The friction coefficient takes into account the fact that the motion between two rotating rigid bodies involves non-linear dissipative effects due to the slithering between the surfaces. The estimation of this coefficient is extremely difficult, as always when simulating all the friction effects (which are scarcely repeatable even in experimental tests) regrouping them in one single parameter; in fact the friction between gear and damper ring is strongly influenced by several factors, including:

- Operating temperature;
- Lubrication between the rotating components;
- Load conditions.

All the listed factors can have a large impact on the friction and then to the final damper ring performance, which is related to the hysteresis cycle area.

Due to all the previous considerations, the friction coefficient is left to the user as a free to choose parameter. In order to perform the validation of the damped responses against experimental data, anyway, a single friction coefficient value has been selected for all the different test cases, realistically assuming that the various experimental tests undergo to similar operating conditions. This is a pretty strong approximation of course, but has been believed to be the correct way to proceed in the absence of more accurate data.

The effect of the friction coefficient in the mathematical model is of crucial importance, because it determines if and when dissipative phenomena take place. In fact the contact nodes will always show relative displacements (defined by $u(t)$ and $v(t)$ in the previous paragraph); at the beginning these displacements will only produce elastic deformations, which determine no dissipations (the hysteresis cycle has a null area and degenerates therefore into a line). This motion condition is called "*stick*". When the tangential force $F(t)$, determined by the displacements $u(t)$, becomes greater than $\mu \cdot N(t)$, determined by the friction coefficient and by the normal displacements $v(t)$, the contact between the two surfaces changes, and the "*slip*" state takes place. In this state, according to the Coulomb law, the tangential force is equal to $\mu \cdot N(t)$ and the contact surfaces slither.

4.3.3 Contact stiffness

The contact stiffness in the two motion directions are the last parameters required in order to build the hysteresis cycle and to calculate then the contact force. Stiffness is estimated as the ratio between the local loads experimented on the contact surface and the relative displacements. The

surface load is determined from the centrifugal load exchanged on the interface. Several models are available for the computation of the relative displacements; almost all of these are based on detailed contact mechanics. The specific implemented model is the one proposed by Cerruti and Boussinnesq [13] and it simulates two-dimensional elastic contact displacements by using an energetic approach; contact surfaces are outlined as a semi-infinite plane pressed against a finite dimension rigid body (which represents the damper ring, so its shape is defined). In Figure 4-5 an example of surface modeling is shown.

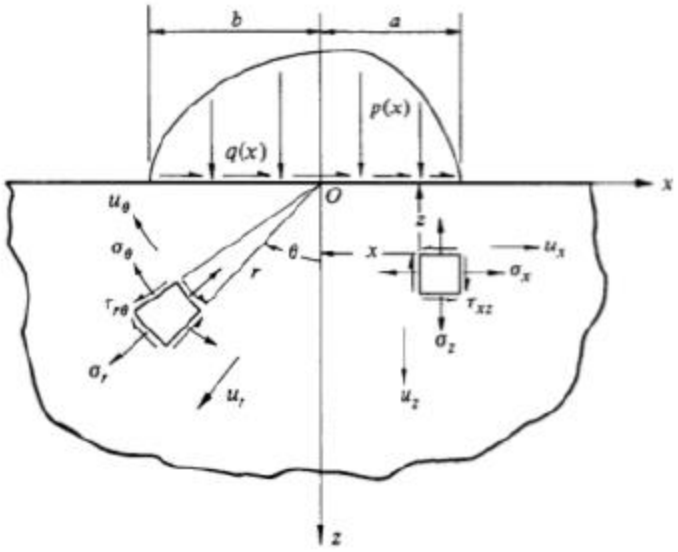

Figure 4-5: Contact surface modeling

The analytical derivation of the expressions used in the contact model is not reported in this work, but synthetically geometrical data and load operating conditions are used to determine the contact forces and displacements, then simply divided to compute the stiffness. The implemented routine determines the global normal and tangential stiffness on the basis of the contact loads. The result of the calculation is then equally split among the contact nodes. In Figure 4-6 it is possible to see a typical normal stiffness trend: it is a non-linear monotonic growing function, because an increasing centrifugal load (which is the primal contact cause) determines a global stiffening of the system, determining contact between the two components.

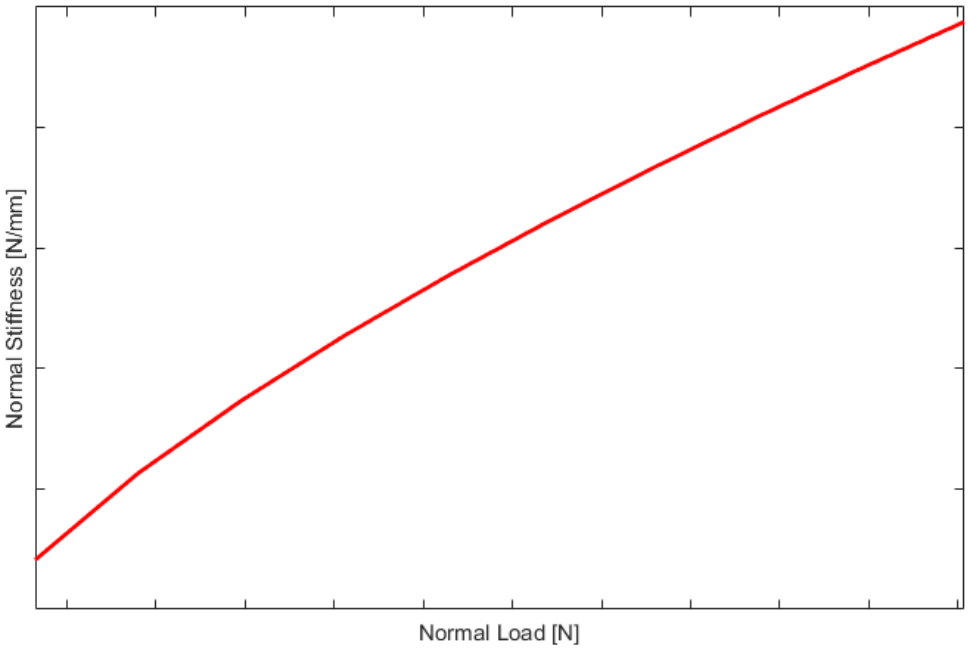

Figure 4-6: Contact normal stiffness POLIGear computation

The normal and tangential contact stiffness influence the slope of the lines forming the hysteresis cycle and establish the transition between stick and slip states (along with the friction coefficient value). More detailed walkthrough is reported in the following paragraph.

4.4 Hysteresis cycle

When all the contact parameters have been computed, it is possible to build the hysteresis cycle and determine the forces required to solve the non-linear differential system and obtain the damped frequency response. The starting point is a displacement range, delimited by u_{min} and u_{max}. As explained previously, if the contact always were in stick state, there's no hysteresis cycle, the relation between the displacements and the contact force is linear (with slope equal to the tangential stiffness) and there aren't dissipative effects. In this case the only effect of the damper ring is a stiffening of the whole structure. The concepts just illustrated are shown in Figure 4-7.

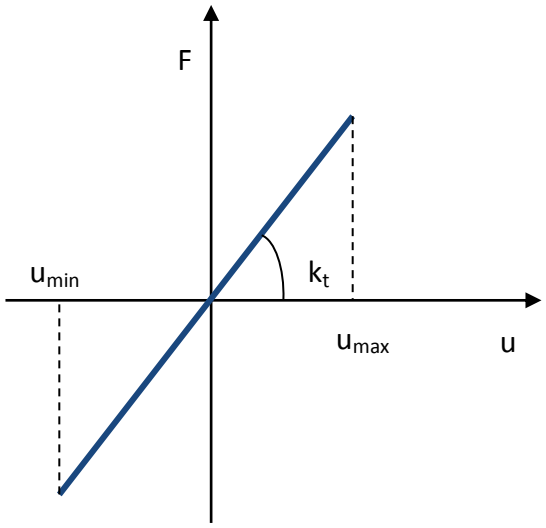

Figure 4-7: Hysteresis cycle - stick state

If the limit imposed by the Coulomb condition isn't ever crossed, the ring reduces the frequency response maximum amplitude without introducing any damping effect. In this case the purpose of the component is not properly served, because the stiffening effect can only slightly lower the peaks. In order to produce massive damping, it is necessary to produce non-linear friction phenomena on the contact interface. This is the part in which the normal stiffness k_n, the centrifugal load N_0 and the friction coefficient μ come into play. In Figure 4-8 it is possible to see the $u - F$ correlation after the application of the Coulomb condition.

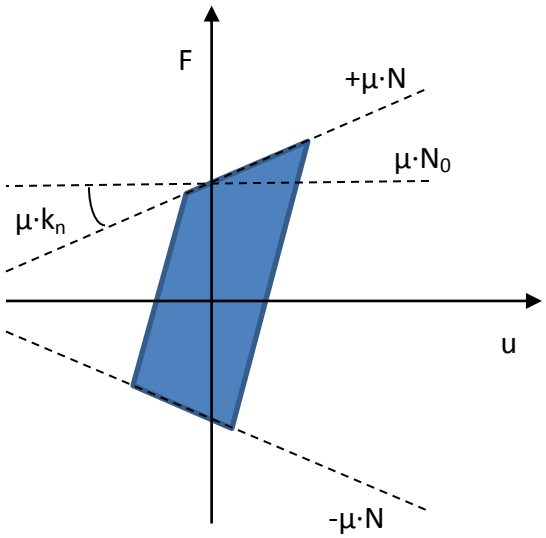

Figure 4-8: Hysteresis cycle - stick + slip states

By observing the previous figure it is possible to recognize the influence of each contact parameter listed. The contact force has a linear trend until it is minor than $\mu \cdot N(t)$. At this point it is possible to see a sudden change in the force value, which becomes equal, at any given moment, to the dynamic friction force. It is important to notice that the one displayed is only a theoretical cycle, because the real ones produced by the simulations will not show any discontinuity on the first derivative, gradually changing trend from the stick state to the slip one.

The last operation required in the construction of the cycle is the implementation of the lift-off state. This is done by considering that if the normal contact force becomes minor than zero, its value must be imposed equal to zero. In this condition, the tangential force is null too. In this condition, the damper ring is only subject to the centrifugal load, that provides to push it back in contact with the groove interface. This is not a desired configuration of course, because the damper ring doesn't produce any effect (it doesn't stiffen the structure either); the contact loss is periodic because of the rotation of the components, so the potential contact loss is repeated over time. The result of this behavior is that a periodic impact between the two components occurs, compromising not only the damping effect, but also the integrity of the structure. Looking at the hysteresis cycle, the system experiments the lift-off state if the displacement range (represented on the abscissa axis) has inside itself the origin of the divergent lines given by $\pm\mu \cdot N(t)$, that form the upper and lower cycle limits and determine the energy dissipation. In these conditions, the hysteresis assumes a triangular shape, like the qualitative one shown in Figure 4-9.

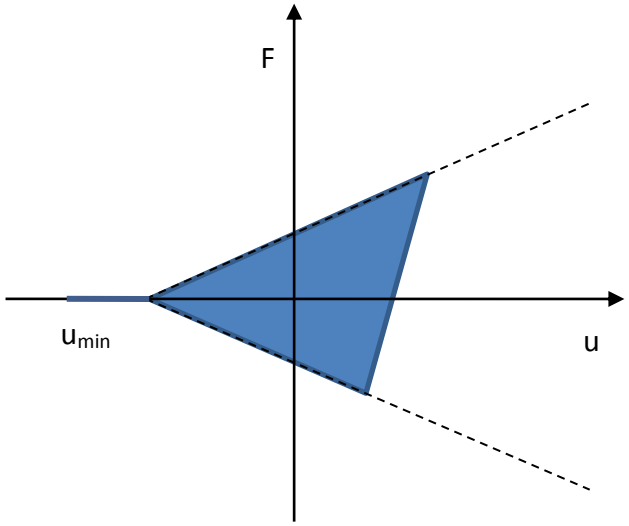

Figure 4-9: Hysteresis cycle - lift-off state

It is possible to notice that the extreme left side part of the diagram is completely useless for the system correct operation, since there's no force exchange on the contact interface. As a last observation about the non-linear contact model, it is once more remarked that the contact stiffness

are computed considering the whole bodies; the obtained values are then equally distributed among the contact nodes. It is then clear, since the friction coefficient is taken as a global parameter, that the hysteresis cycle always has the same input parameters, no matter which specific contact node is observed. The difference between the nodes resides in the displacement range, that could be completely different, considering the material continuity constraint of course. The physical meaning of the previous considerations is that contact state at a given moment is not uniquely defined for the whole contact surface, but is determined by the interaction between the single nodes couples. The natural consequence is that there could be energy dissipation even if the greater part of the contact surface is in stick state; this condition is called micro-slip state. It is finally possible to write the basic expressions required for the hysteresis cycle construction:

$$\begin{cases} F(t) = {F_0}^* + k_t \cdot (u(t) - {u_0}^*) \\ N(t) = N_0 + k_n \cdot v(t) \end{cases}, \quad Stick\ state$$

$$\begin{cases} F(t) = sign(\dot{u}) \cdot \mu \cdot N(t) \\ N(t) = N_0 + k_n \cdot v(t) \end{cases}, \quad Slip\ state$$

$$\begin{cases} F(t) = 0 \\ N(t) = 0 \end{cases}, \quad Lift - off\ state$$

5 Tool validation

One of the main purposes of this work is the validation of the results produced by the POLIGear tool, compared with experimental data or other finite elements simulations, according to the tool aspect to validate. In order to make clearer the procedure undertook in the following paragraphs, it is good practice to recall which the most significant components of the tool are, and which are therefore the results subject of validation.

As detailed previously, the starting point for any simulation are the finite element models of the main rotating component (gear, seal, turbine disk, etc.) and of the damper ring. Only one sector models are provided, since the analysis is performed using cyclic symmetry hypothesis. Mass and stiffness matrices are subject to a dynamic reduction process, in order to have a reasonable computation time. Within this process the cyclic symmetry constraint is applied, and the resulting matrices should be dynamically equivalent to the full $360°$ ones. This equivalence is the first step of the validation, performed by comparing the linear response resonance frequencies with those foreseen by a modal analysis (performed using ANSYS apdl) and at last with the natural frequencies of the experimental data.

Once the reduction is performed, only the accessory, contact and external load nodes are kept as master; all the other degrees of freedom are replaced by an arbitrary number of modes, since their displacement is not of particular interest for the analysis. By using these reduced matrices, the linear solution is computed; its amplitude is then compared with the information provided by experimental data, in order to assess the accuracy of the Parker model in estimating the dynamic force exchanged in the mechanical transmission.

The reduced matrices of the gear and damper ring sectors and the meshing dynamic force are the starting point for the non-linear frequency response computation. The next step in the simulation is the computation of the contact stiffness, used then to determine the hysteresis cycle and finally the contact force. An intermediate validation step could be the comparison between the analytically computed stiffness and the experimental ones; this check has not been performed because of the specific systems simulated: usually the contact stiffness is indirectly measured by detecting the frequency shift in the response of the gear alone and equipped with the damper ring. This shift is proportional to the additional stiffness introduced by the damper ring presence to the rotating system and could in principle be used in estimating the tangential contact stiffness. This procedure has nonetheless two main problems:

- For a bevel gear system, the frequency shift is very low, mainly because of the difference between the two involved components size difference (in fact the shift is more evident for pinion than for gears). A discretely appreciable shift is obtained only by using a parametric

stretch of the damper, in order to increase the ring mass. The mass increased damper rings are only simulation products anyway, so the experimental comparison is not possible for them;

- Any experimental test can measure the global stiffness effect at most. This means that it is not possible to distinguish between the tangential and normal stiffness. It would be therefore very difficult to have a realistic visualization of the hysteresis cycle.

In the last part of the simulation, a non-linear solver is implemented in order to compute the response. The non-linear frequency response is the main object of the tool, and several considerations are made about it. For what concerns the validation aspect, the simulated response is compared with the experimental one in terms of resonance frequency and amplitude. The damper ring performances are then examined. In Figure 5-1 a complete overview of the simulation process is shown, in order to have a clear idea of the results reported in the following. In the figure, the results subject to validation are explicitly marked.

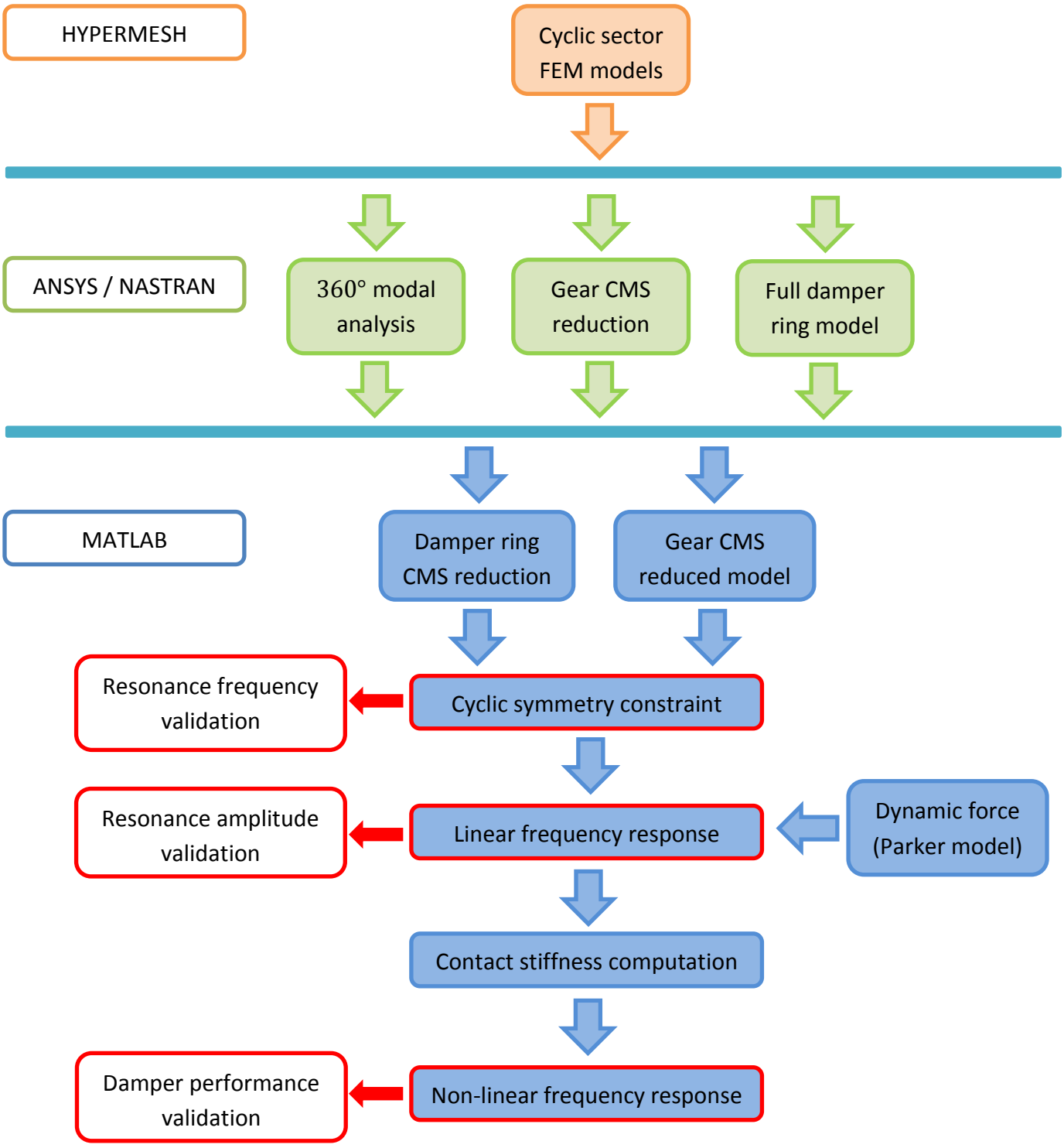

Figure 5-1: Tool workflow

5.1 Resonance frequency validation

The first part in the validation process is the comparison between the resonance frequencies of the simulations and those obtained from more reliable sources, in this specific case:

- Experimental data;
- Modal analysis results.

The comparison is used to validate the whole reduction process. This takes in account the CMS and Tran reductions and most of all the cyclic symmetry hypothesis (because, as explained previously, this is an approximation, given the asymmetrical nature of the meshing force). The target of the validation is to prove that, at a given engine order, the dynamic behavior of a single cyclic sector with symmetric boundaries is almost the same as the one obtained from the full $360°$. In mathematical terms this is expressed by computing the eigenvalues of the reduced matrices:

$$[K]_r - {\omega_0}^2 \cdot [M]_r = 0$$

The obtained values are then matched with the natural frequencies computed by the modal analysis. This analysis is performed on a full $360°$ model obtained in ANSYS from the sector model. The resonance frequencies extracted from the analysis are related to the respective rotating speed values through the Campbell diagram. In order to simplify the problem, the gyroscopic effects have been neglected; this is an approximation of course, but a pretty fair one considering that the simulated cases show relatively low frequencies. Under this hypothesis, the curves on the Campbell diagram reduce to straight lines. Assuming that the forward and the backward modes open symmetrically (another assumption, made because further data are extremely related to the specific case and because of its wisdom, assessed by observing experimental data). In this case, considering the inertial reference system, the frequency line split in two component; the excitation line is given by:

$$f = \frac{z \cdot \Omega}{60}$$

Where z is the number of teeth and the rotational speed Ω is expressed in rpm. The desired resonance speeds are the intersections between this line (which is the one related to the first harmonic) and the opened frequency lines, given by:

$$f = f_0 \pm \frac{\Omega \cdot k}{60}$$

Where the k factor determines the slope of the lines and its value is computed by taking in account the predominant direction of the considered mode:

$$k = \begin{cases} ND & , \ axial\ direction \\ ND \cdot \dfrac{ND^2 - 1}{ND^2 + 1} & , \ radial\ direction \end{cases}$$

Where ND is the number of nodal diameters and is related to the specific engine order.

If the prevalent direction of the mode of interest is not clearly defined, the k factor can be assumed equal to an average mass of the two listed. In the simulated cases, anyway, the expression related to the axial direction has almost always been more than enough to locate the experimental resonance with very good accuracy. All the previous analytical expressions are graphically shown in Figure 5-2.

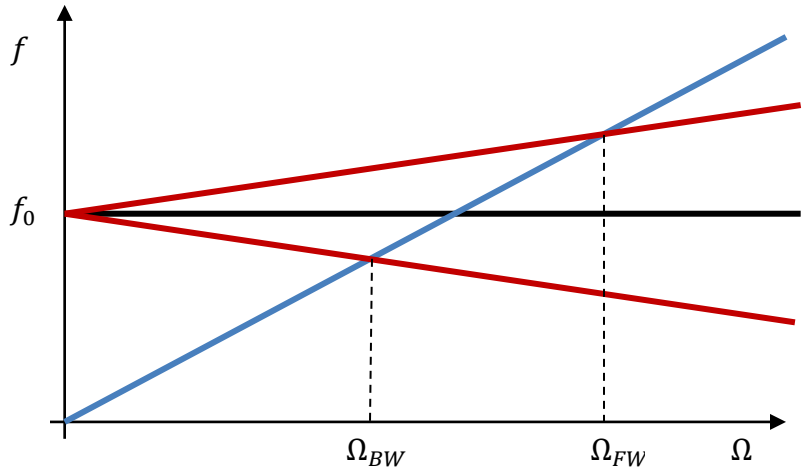

Figure 5-2: Campbell diagram - inertial reference system

Actually the tool does not work in an inertial reference system, but computes the harmonic excitation force in a rotating cylindrical system, which has the same speed of the shaft. The concept is the same, but in this case the excitation line opens and the frequency one remains constant, giving rise to the Campbell diagram in Figure 5-3.

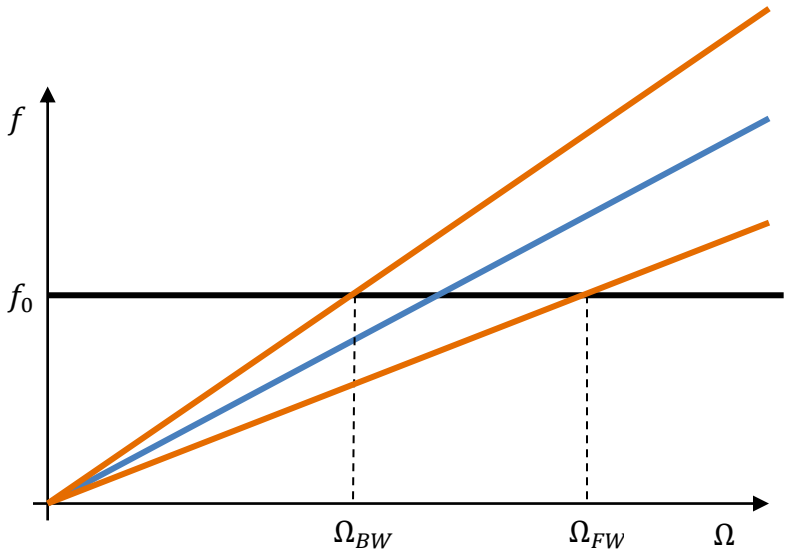

Figure 5-3: Campbell diagram - rotating reference system

The match between the natural frequencies is essentially determined by two parameters, both connected to the reduction process:

- The number of modes selected for the CMS reduction;
- The number of modes selected for the Tran reduction.

These modes are used to replace a certain number of slave physical degrees of freedom, in order to reduce the computation time and preserving the dynamic behavior at the same time. If the number of modes is increased, then the dynamics will be ever more equivalent to the not reduced system's. It is nonetheless clear that if the number of modes is too high the time reduction effect will not be appreciable; a right balance must therefore be reached. For what concerns the Tran reduction, the influence of the number of modes is slightly softened, because this is a reduction that operates on the interface nodes only, so the slave nodes number is significantly lower than the CMS reduction one.

The validation procedure has been led for several gearboxes of different engines. In order to avoid an heavy dissertation, anyway, only one case results are reported in the present thesis, since the other cases are equivalent at the most. The reduction validation is proved by displaying the natural frequencies produced by the modal analysis with those of the final matrices (passed through the CMS reduction, the cyclic symmetry boundary and Tran reduction). A comparison between natural frequencies computed by ANSYS and by POLIGear is reported below.

Mode shape	Error between ANSYS and POLIGear (%)
2DBW	-0.0014
2DFW	-0.0004
3DBW	-0.0005
3DFW	-0.0017

As it is possible to observe for the specific case, the maximum frequency shift is 0.0014%, a very low value, so the reduction process can be considered validated. A further proof is given by a comparison between the resonance rotational speeds computed by POLIGear and experimental ones. This is only a partial check, because for a specific gear no more than four-five mode shapes can be observed (and therefore simulated) in the operating speed range. In Figure 5-4 it is possible to see the simulated linear response versus the experimental one.

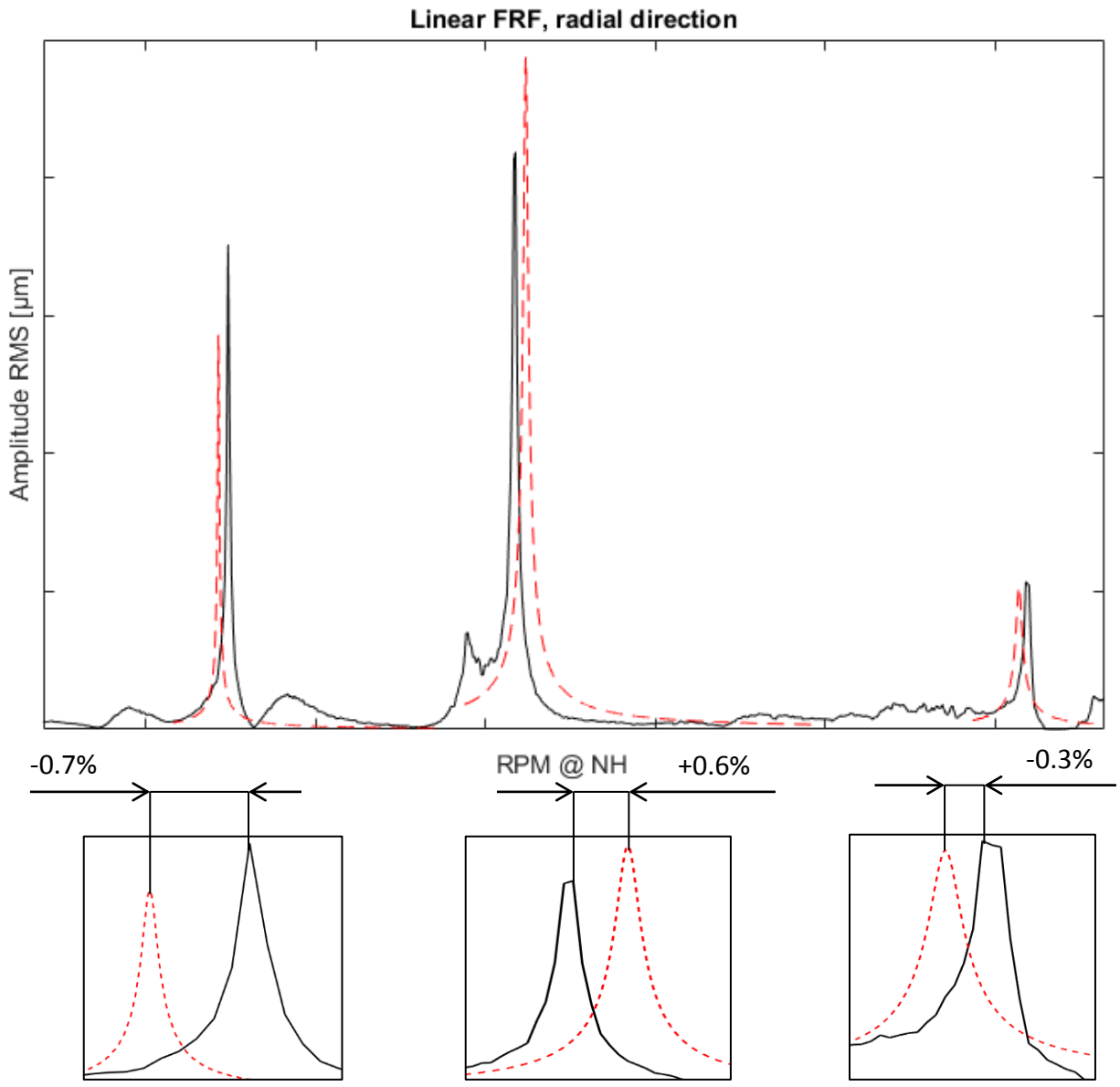

Figure 5-4: Non-damped FRF – frequency validation

The results are very accurate, with a maximum shift of 0.7%. In other cases it is possible to observe slightly greater differences (always lower than 5% nonetheless); the mismatch cause is that all the simulations have been run using the same material properties. This because the model is not really sensitive to the material (unless a completely different material is used). Minor changes can be possible especially for what concerns the Young modulus E. It is also important to notice that POLIGear doesn't take in account the dynamic of the cinematic chain in which the simulated gear is installed, while the experimental data do of course. Due to these considerations, the computed results have been found to be more than satisfying.

The frequency validation is performed only for the main component because this contains far more nodes and elements. The damper ring modes have always been chosen equal to one third of the respective gear modes (both for the CMS and for the Tran reductions), and this has been found to be more than enough to reproduce the ring dynamics.

5.2 Linear response amplitude validation

The POLIGear tool has been designed to simulate the performance of a gear after the installation of a damper ring. The main excitation force is nonetheless due to the mesh process, that produces harmonic forces at different engine orders. It is very important therefore to have a good estimation of the dynamic overload given to the gears imperfections. The purpose of the Parker model is to allow the user to easily compute the dynamic force and extract the proper harmonic without recurring to dedicated software. It is anyway possible to run a simulation by using the first POLIGear version; in this case, the user must autonomously compute the dynamic force (using Transmission3D for example), filter it by using a contact window, extract the harmonic component and determine the three dimensional components.

When experimental data are available, it is also possible to auto tune the simulated response by scaling it in order to obtain the same resonance amplitudes and determine, by the scaling factor, the harmonic excitation. In design phase, experimental data are not available, and it is therefore very important to dispose of a tool to have a preliminary estimation of the force.

The validation of the linear response amplitude allows to focus the attention on the most sensitive parameters of the simulation and to identify the main approximations and limits in the model. The validation is displayed for the most significant cases only.

The amplitude of the response is strictly related to the torque transmitted. The correlation is linear, unless the contact loss between the meshing gears introduces non-linearity in the system. The main input of the Parker model is the static transmission error over one mesh cycle, torque dependent too. It is then fundamental to know the conditions in which experimental tests have been run. In particular the torque can be kept constant during the speed sweep or not.

The first case is the most simple to simulate, because only one transmission error file is required. In and Figure 5-5 are shown the static transmission error and the linear response for a specific case.

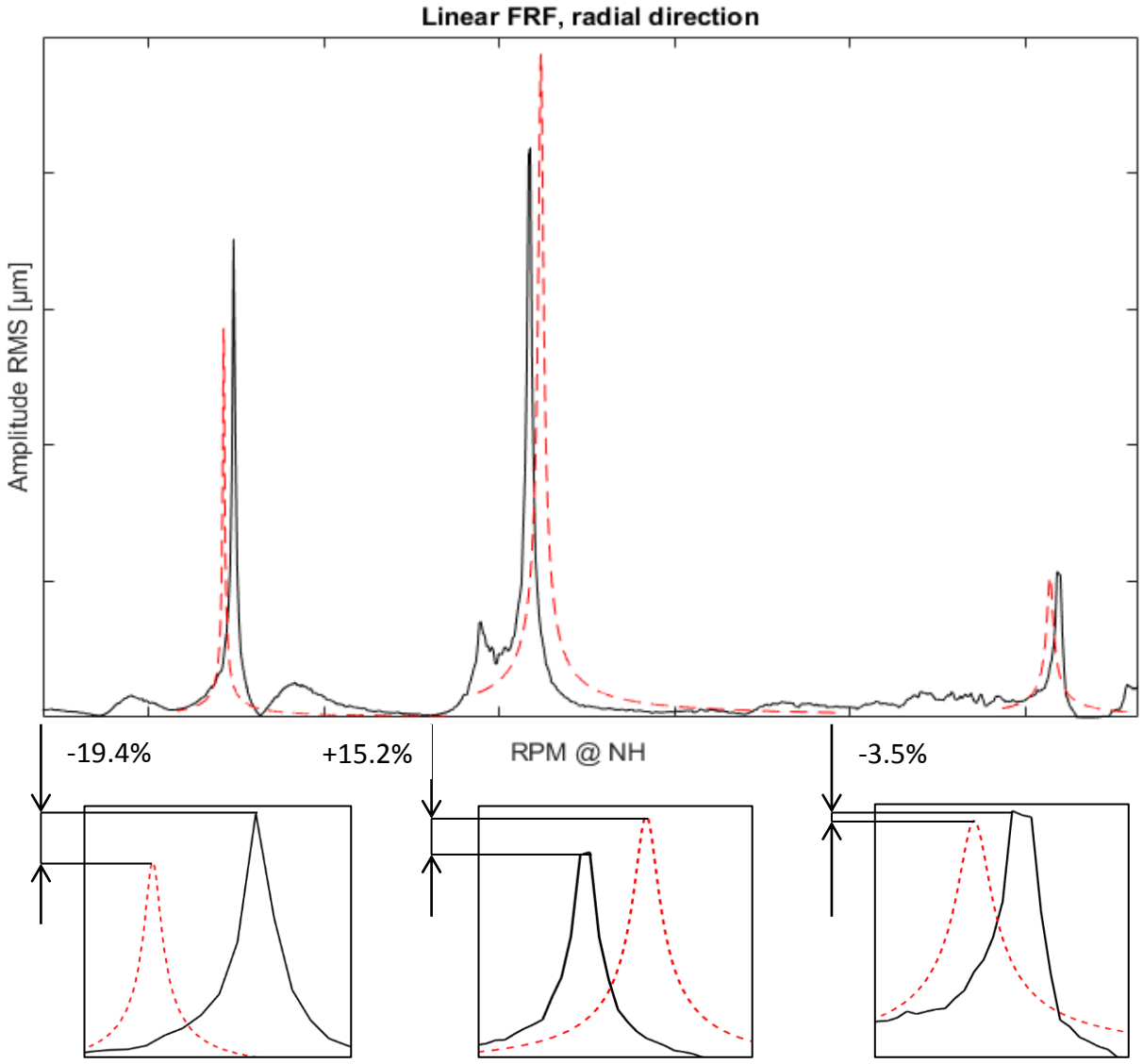

Figure 5-5: Linear FRF - amplitude validation

As it is possible to see, the results produced by the tool are pretty accurate, being the maximum mismatch equal to the 19.4%. Unfortunately in this case only the experimental validation is possible, and this comparison doesn't allow to insulate single parameters effects. The resonance amplitude is strongly influenced by three parameters:

- Torque;
- Q-factor;
- Contact ratio.

In addition to these, other parameters have a minor influence. One is the information about the gear geometry used to apply the Parker model. Since simulated components usually are bevel or at least conical gears, they have to be reduced to an equivalent spur gear system, on which the Parker model can be applied. The parameters required for the definition of such a system are the polar inertias and the base radii of the rotating bodies. As proved in the dynamic force estimation section, the model perceives only magnitude changes in the equivalent mass, determined by huge changes on the polar inertias, so it is legit to say that minor inertia variations don't produce any appreciable effect on the linear response. For what concerns the base radius determination, if the gear is not a bevel one, the choice is obvious because the base circle has the same dimension anywhere along the face width; otherwise the mean section has been selected as reference. The influence of this choice on the final response amplitude is related to the fact that both the static force and the dimensional version of the STE (expressed in length unit) are computed by the base radius:

$$\begin{cases} F_s = \dfrac{T}{R_b} \\ STE_m = STE_{rad} \cdot R_b \end{cases}$$

The variation of the base radius over the face width can be approximately equal to 30%, a value that only allows minor amplitude variations. Anyway the mid-face radius has believed to be the most natural choice.

In the case of constant torque experimental tests, like the one displayed in the figure, the simulation tends to match with experimental data for each engine order simulated. This is explained by considering that in the analysis the dependence of the contact ratio from the torque has been neglected, due to the extreme difficulty in its determination. If the torque is constant, anyway, this dependence is not relevant and the same value of contact ratio can be effectively used to estimate the amplitude of each mode shape resonance. In this case, therefore, the amplitude of the linear response is only determined by knowing each peak Q-factor.

Some mismatch can occur if experimental tests have been run without imposing constraints on the load. In this case the torque value is different according to the instantaneous rotational speed. It is possible to know the exact value of the torque near the resonance peaks, and consequently the respective transmission error. In Figure 5-6 it is possible to see how the STE trend changes with torque.

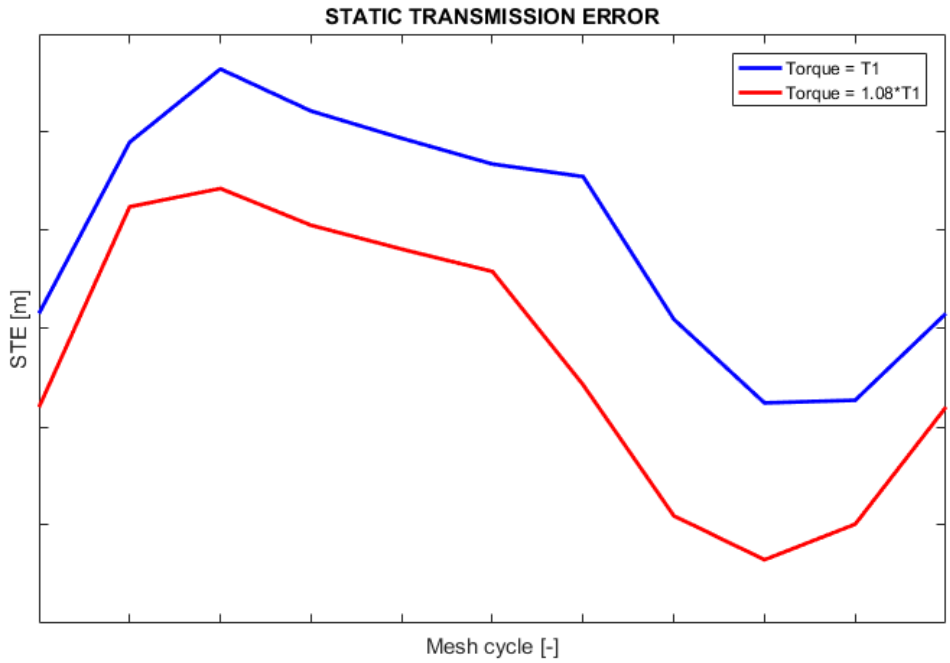

Figure 5-6: Static transmission error - variation with torque

The correct estimation of the contact ratio at that torque requires the use of dedicated software and should be adapted to the equivalent spur gear anyway. It is accepted that contact ratio increases with the torque, because the load is better distributed on the meshing gears. The comparison between simulations and experimental data for the case which the previous STE are related to is reported in Figure 5-7.

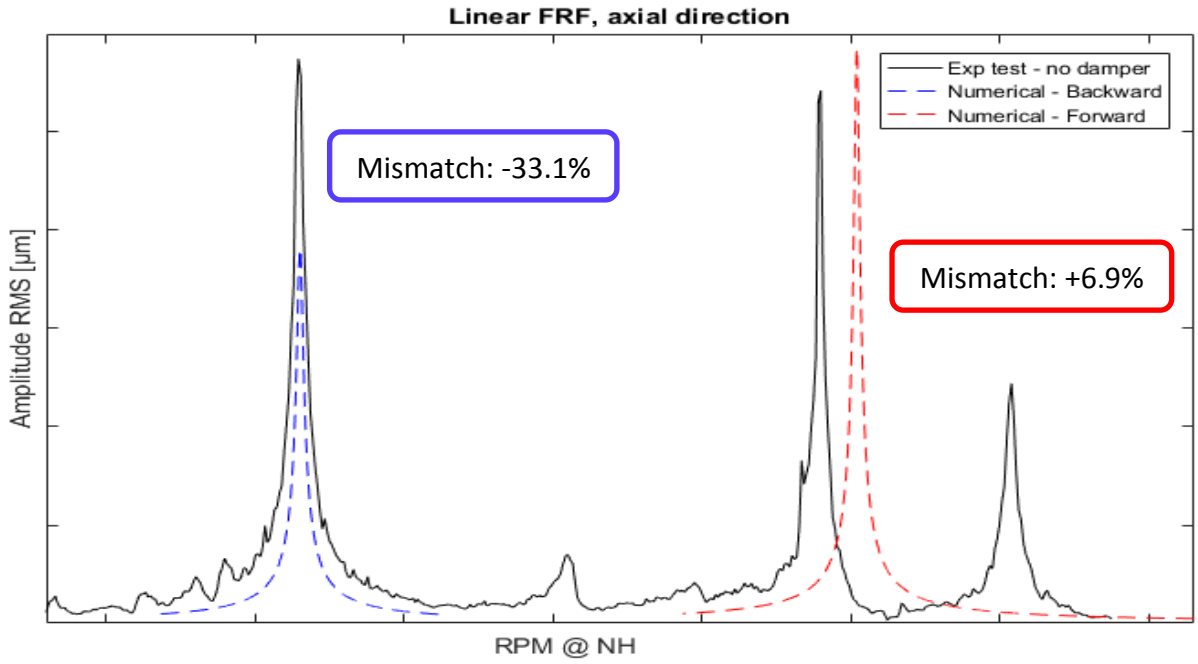

Figure 5-7: Linear FRF - peaks at different torques

The only two simulated resonance peaks are the forward and backward shapes of one single mode. The same contact ratio value has been used for the two simulations, and in fact the backward response results slightly underestimated, coherently with the considerations listed previously. The contact ratio is therefore identified as the main approximation introduced in the model.

One particular to consider about the linear response is related to the simulation of higher ND modes ($7D$ or $8D$ mode shapes for example): in this case the slope of the opening modes on the Campbell diagram is significant and an interaction with other modes in the operating speed range is more likely. It is therefore possible to have two resonance speed very near to each other; since POLIGear simulates the response for a given engine order, it doesn't take in account the possible interaction between modes (called mode superposition). In this case the real solution is obtained by manually adding the two computed solution. A possible solution for this problem could be the implementation of a multi-harmonics analysis, in which the responses at different engine orders are sequentially computed and then automatically added to build the complete linear response for a given gear.

As a last consideration about the linear response it should be noted that the response computation doesn't consider the presence of two gears, but simulates the second one with the dynamic force exchanged. In the experimental data associated with a specific gear, therefore, there will be track of the resonances of the other gear, that cause vibrations in the whole system. Sometimes these induced motion can interact with a resonance of interest; an example is given in Figure 5-8, in which experimental data for two mating gears are reported, with rotational speed axes reduced to the engine shaft, for comparability.

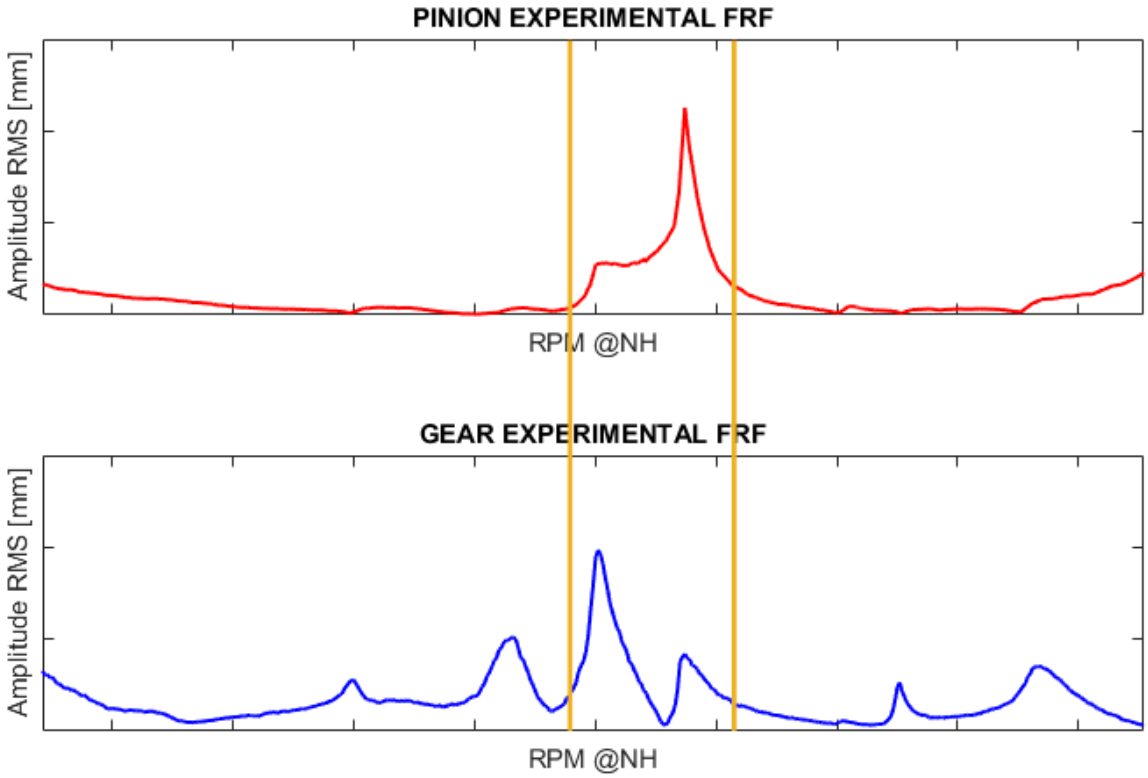

Figure 5-8: Meshing gears resonance interaction

In this case the experimental peak can assume a significantly asymmetrical shape, and its maximum value could not be representative for the comparison. This is a very complex matter to solve, because it requires an extremely detailed knowledge of the interaction between two meshing components. Since the target of the tool is the simulation of the interaction between the gear and the damper ring, anyway, the obtained results are more than enough to consider the methodology validated.

5.3 Damper ring performance validation

The last step in the validation process is the evaluation of the effectiveness of the damper ring. This is done by considering three major parameters that define the final damped response:

- Resonance frequency;
- Resonance amplitude;
- Q-factor.

The first two points are directly used for the validation of the contact model implemented. The followed procedure is exactly the same as that used to validate the linear model: for each test case, simulations with different engine orders have been run, comparing the results with experimental tests. An example is given in Figure 5-9 for a specific mode shape.

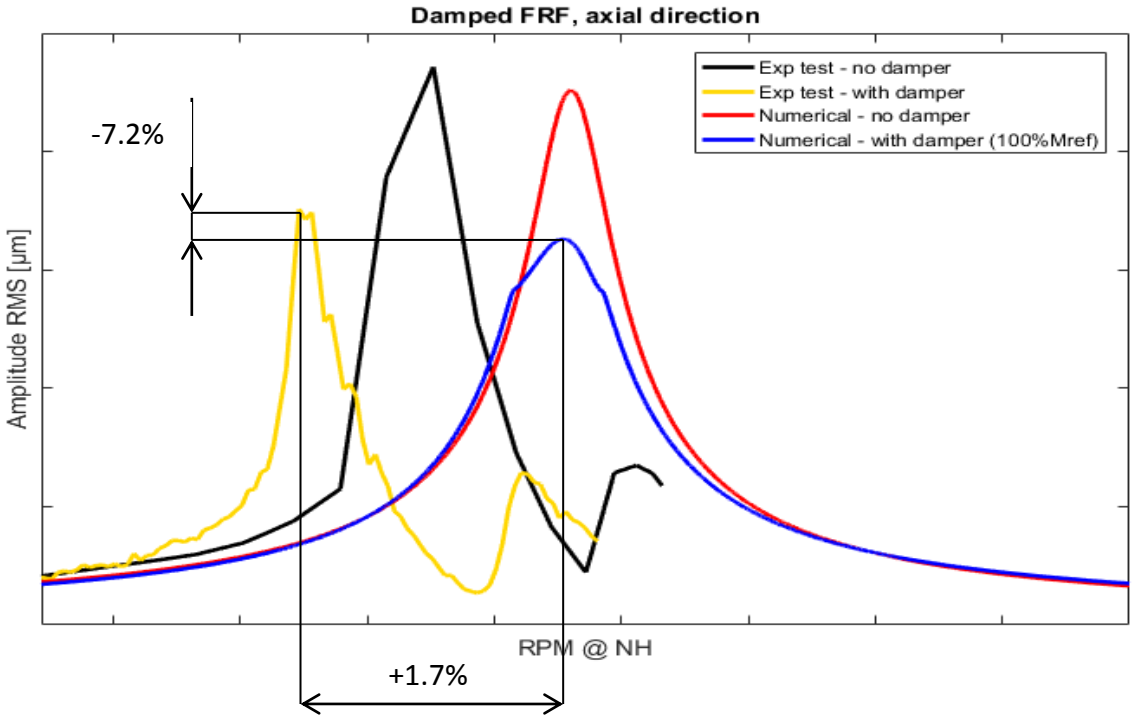

Figure 5-9: Damped FRF - Frequency and amplitude validation

As it is possible to observe, there is a slight frequency shift between the experimental and the simulated damped responses. As a matter of fact the simulated system appears to be more stiff than the real one. This is coherent with what has been explained in the FEM model processing performed by the tool: the damper ring is assumed to be cyclic symmetric, considering the presence of the lateral cut only in the mass and volume computation. It is neglected the effect of the cut on the axial stiffness. This hypothesis finds now its defense, because even making the simplification the frequency shift with the experimental evidence remains lower than 2%, definitely a satisfying result.

It is important to notice that the results reported in this thesis work are the ones related to the complete tool validation: simulations have been run without any sort of auto-tuning. Since the basis for the determination of the damped response is the linear one, contingent errors on the latter are obviously propagated to the first. In order to validate the non-linear model only, it is possible to run each case by manually imposing the value of the mesh harmonic force so that there's perfect match with experiments.

The damped response has been furthermore computed for different values of the damper ring mass. The different geometries of the ring have been computed by using a parametric mesh stretching approach. This method allows to modify the real sector provided to the tool without changing the number of nodes or elements. An example of parametric stretch is shown in Figure 5-10. It's clear that this approach is efficient if the mass variation is not extreme, because the newly produced elements could be bad conditioned.

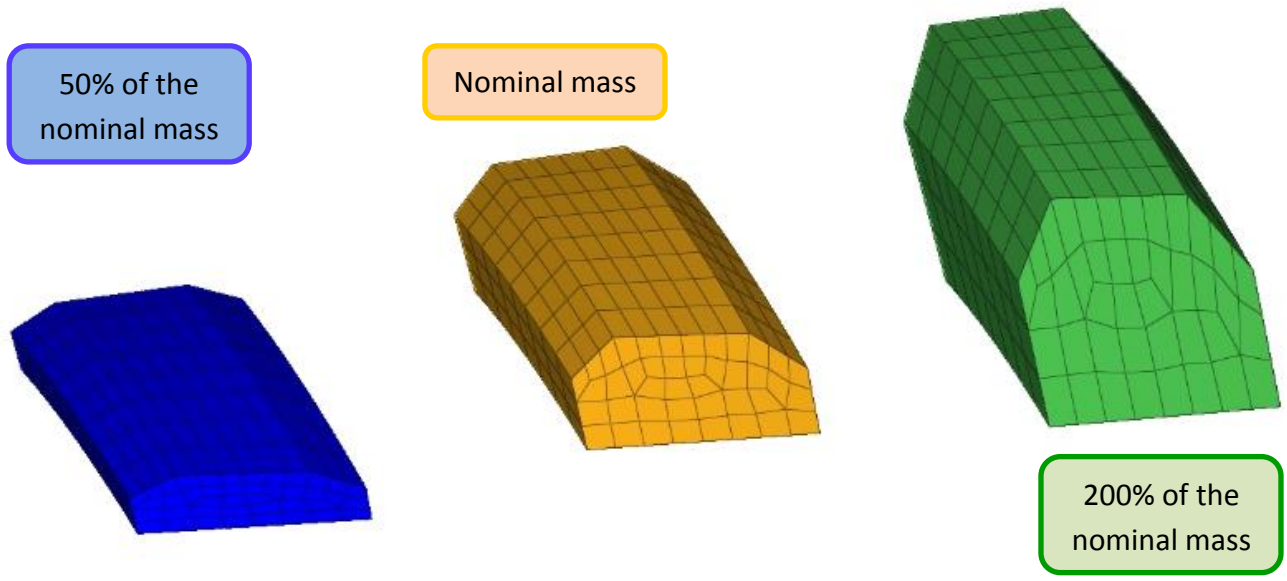

Figure 5-10: Damper ring mesh parametric stretch

In the case of the damped response, unfortunately, there is lack of experimental data, because, as said previously, the damper ring is equipped only if there's extreme need of damping dangerous vibrations. The best practice is therefore to follow as much as possible a design procedure that takes in account and prevents the vibratory phenomena. Experimental test with the damper ring are so led only for engine components that show real operating problems. The available data are not enough to fully validate the contact model, but since the damper configuration is planned for many gears, the non-linear simulation have been run anyway, in order to identify a common behavior in the different test cases. As explained previously, the variable of interest is the absolute value of the damper ring mass. A sweep of its value over a wide range allows to get trends like the one reported in the following (Figure 5-11).

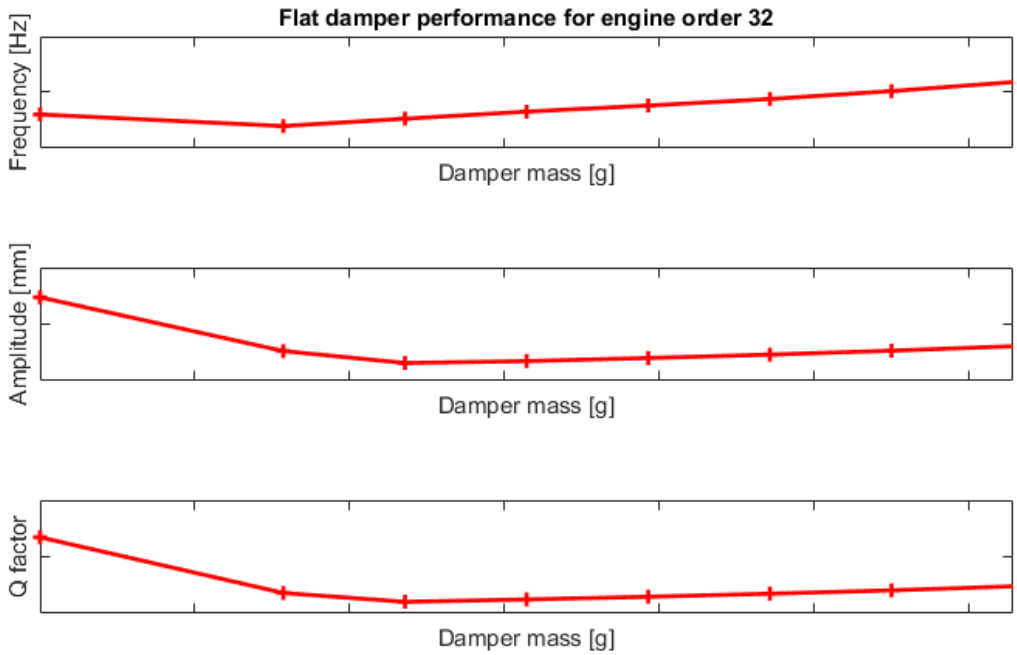

Figure 5-11: Damper ring performance plot

As it is possible to observe, increasing the damper percentage mass with respect to the nominal value, there is a first phase in which the resonance frequency decreases, indicating that the damper ring presence reduces the system stiffness. After reaching a minimum, the frequency curve starts to monotonically increase with the damper mass. This is coherent with the problem physics: in fact, the more the ring is massive, the greater will be the centrifugal load to which is subject to. This force pushes the damper ring against the groove wall and the system becomes equivalent to a rigid body with an increased stiffness, due to the damper presence.

The amplitude curve trend is coherent with the previous considerations: in the first part the resonance amplitude decreases as the damper mass increases, indicating that the contact is mainly in slip state, which is the desired one for the correct operation of the system. In this state there's a significant amount of energy dissipation, a qualitative reference is given by the Q-factor curve. As the damper ring mass increases and the damper sticks to the gear, there is far less relative displacement, leading to lower contact forces and damping effect. The minimum points for the frequency and the amplitude curves are not necessarily reached for the same mass values. This is not a problem, because the optimal damper mass is the one that minimize the amplitude and the Q-factor.

The performance curves are qualitatively the same for each test case and engine order. The damper behavior diverges from the expected one only for one case. The results for this specific gear are shown in Figure 5-12.

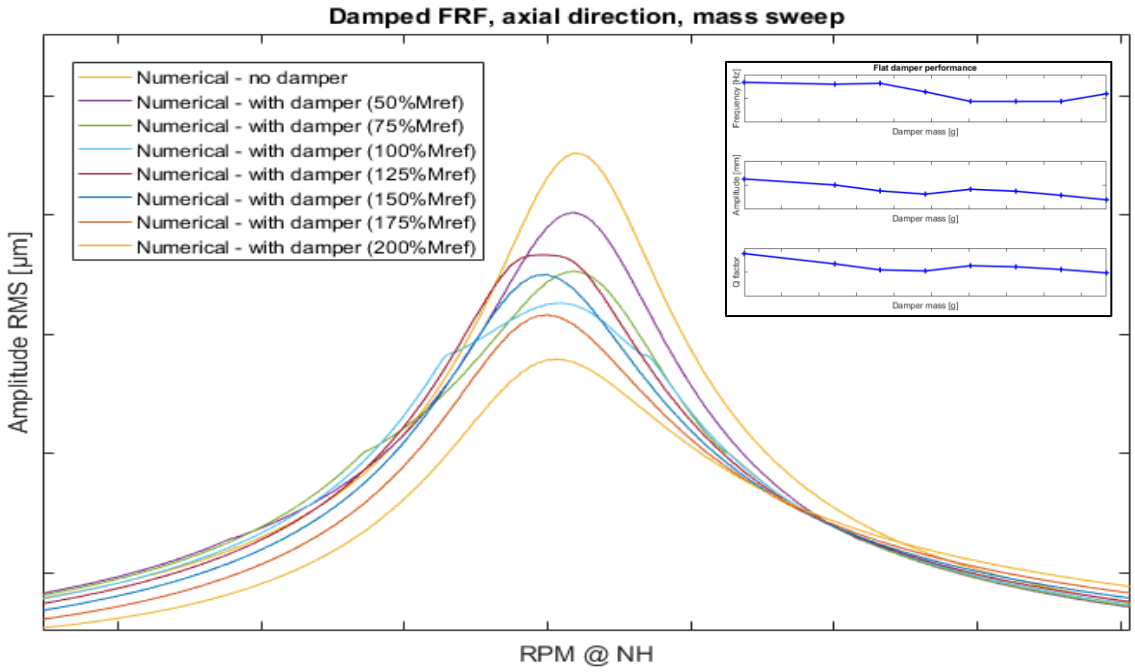

Figure 5-12: Damped FRF mass sweep

It is immediately clear the abnormal trend, together with the fact that the damper ring doesn't have a significant effect on the final response (even in experimental data the damping produces an amplitude decrease of 25% only). The irregular trend is due to two main factors:

- The bad positioning of the groove on the gear. It is important to notice that the damper is positioned so that the damping is optimized for a single mode. The location of the groove is therefore chosen looking at the modal deformed shape of the gear and determining where the modal displacements are larger;
- The inadequate damping provided by the positioning causes a continuous change in the prevalent state of the contact, which is stick or slip alternately, without any predominance.

In order to bypass the damper bad positioning, the only possible choice would be a huge increase of the ring mass. In fact, for the same test case examined previously, simulation has been run by using a mass equal to four times the nominal one. The resulting frequency response is shown in Figure 5-13. In this case a slight more pronounced damping effect is observed, but it is reached by a not realistic mass value.

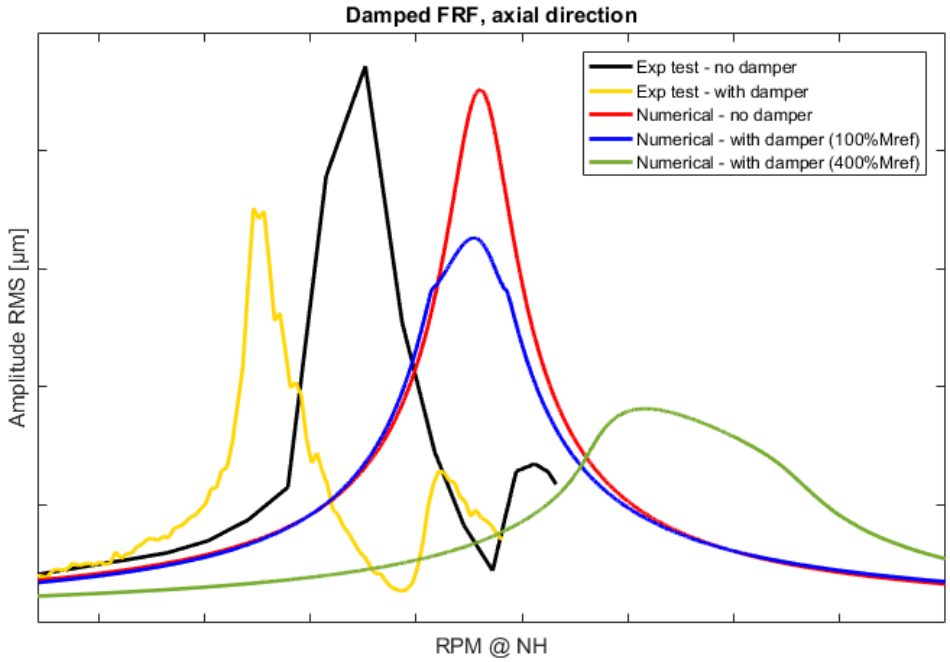

Figure 5-13: Damper mass effect on FRF

It is therefore concluded that the maximum result in terms of damping is not necessarily reached for ring masses equal to the nominal ones, but a performance analysis is required to correctly choose the value (and geometry consequently). It is also remarked that any possible consideration on model parameters must be made after the position of the damper ring, because the choice could completely upset the operation of the system and even its likelihood of failure. Unfortunately the groove positioning on the gear is a really difficult process to automatize, because many aspects of various kind must be taken in account. For example, beside the vibratory aspect, the groove presence should be studied considering it as a possible crack source in the gear structure.

Always considering the previous test case, a first attempt repositioning analysis has been performed. Following the classic procedure, a modal analysis has been performed on the full $360°$ gear model. The modal deformed shape for the mode of interest, that is the one with $ND = 3$, is shown in Figure 5-14.

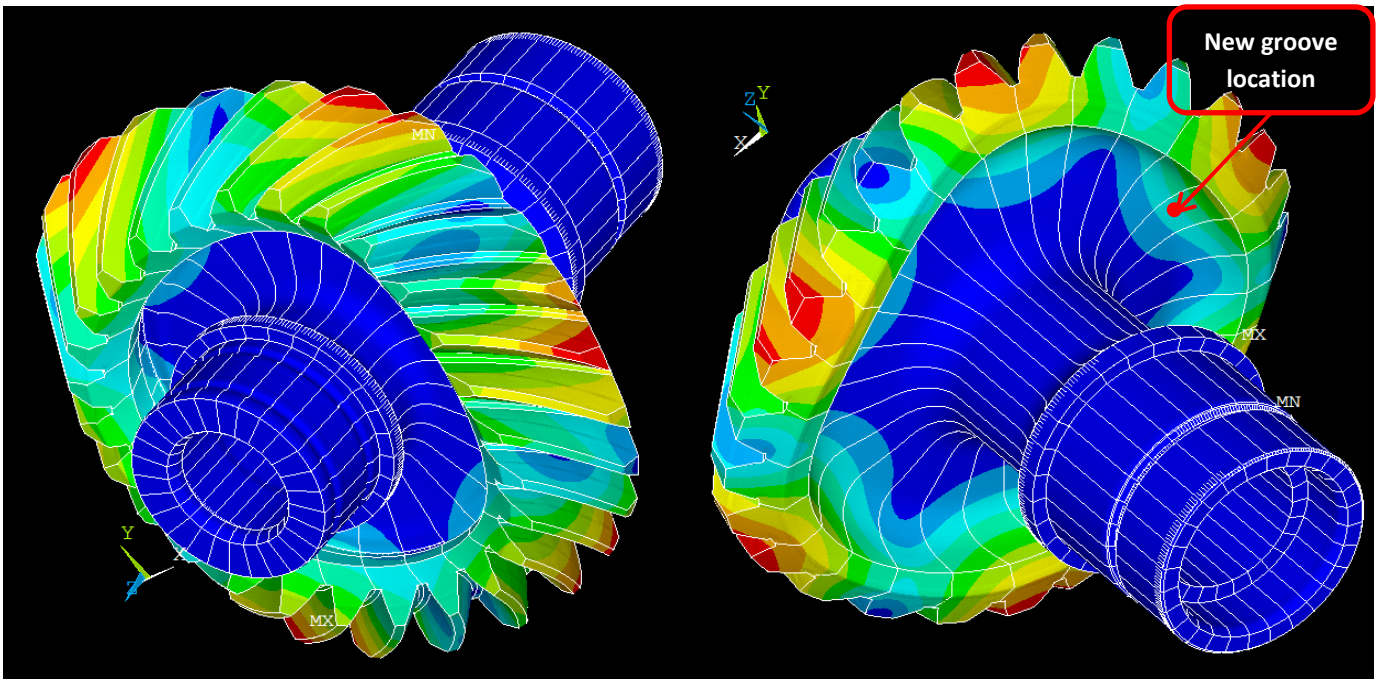

Figure 5-14: Damper repositioning - Modal results

Since the highest displacements are located near the tooth border (and not near the connection between the tooth and the web, where the damper ring has been positioned), the system geometry has been modified moving the groove. The gear sectors before and after the intervention is reported in Figure 5-15. It is important to notice that the present repositioning has been performed without considering possible

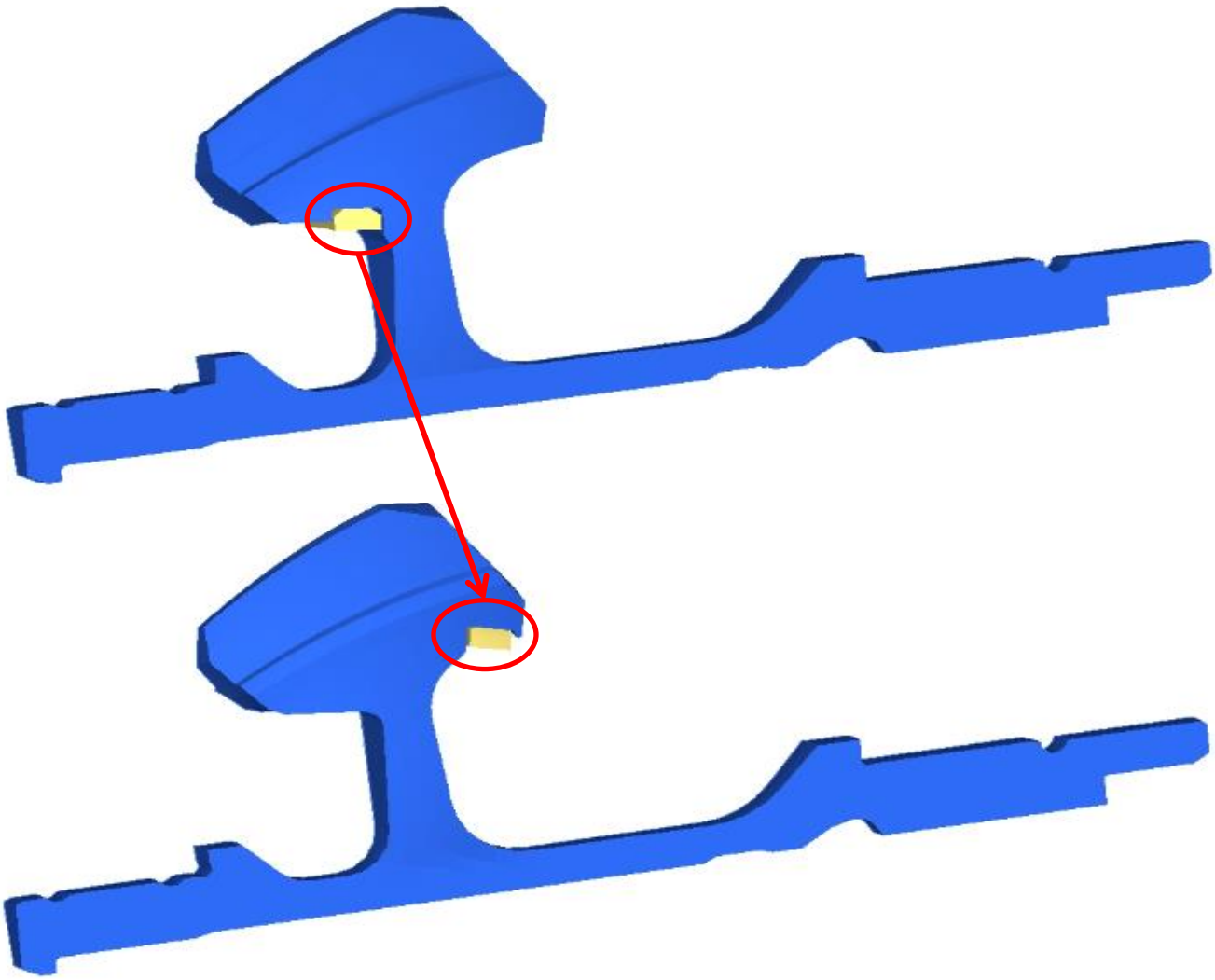

Figure 5-15: Damper repositioning - Geometry

The linear frequency response has been computed first of all. The results are reported in the following (Figure 5-16), compared with those obtained by the real geometry. In the figure it is immediate to note a slight difference between the two response curves in terms of frequency and amplitude. This shift is not a concern and it is actually expected, because the proximity sensor which displacements have been measured is very near to the new position of the groove. Since the groove is obtained by removing material, the local stiffness in the surrounding volume will obviously decrease. Given this consideration, the difference between the two curves is minimal, and this allows a comparison between the two configurations.

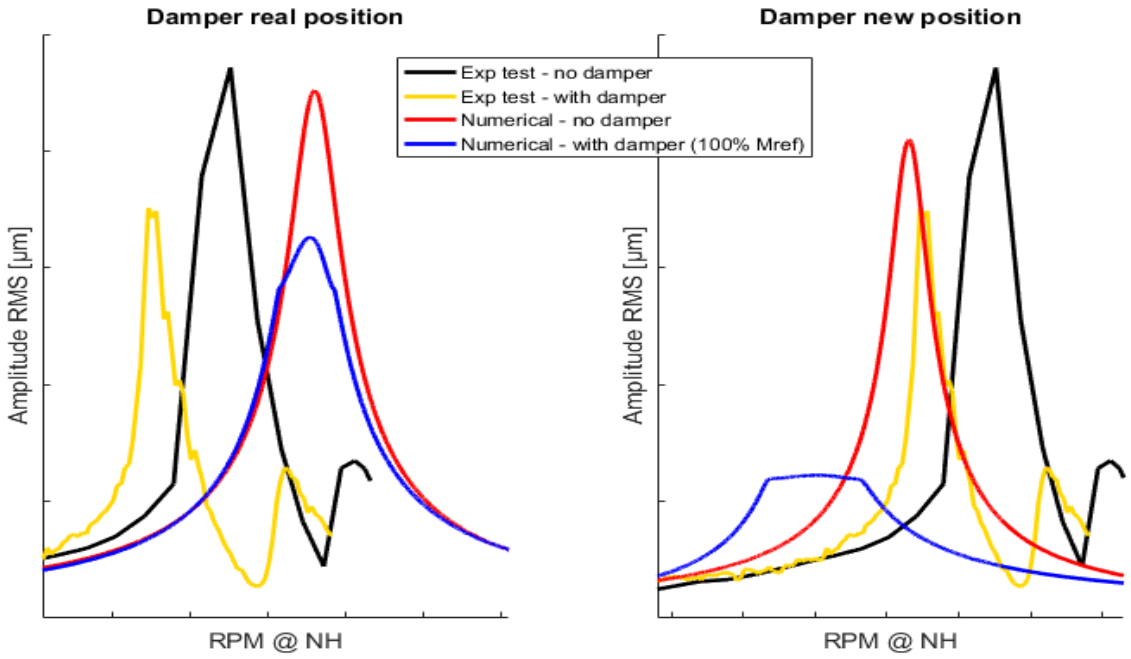

Figure 5-16: Damped FRF before and after repositioning

In this case the damper behavior is the one expected: the damped response shows a resonance frequency lower than the linear one (about 1%); the peak is heavily damped and even losses the typical Gaussian shape, showing a sort of plateau near the resonance; this is index of transition between the stick and the slip states. The most important information about the energy dissipation is given by the response Q-factor, which is almost halved, the same trend of the amplitude.

6 Code development

During the thesis work, POLIGear code has been improved by the addition of several features. At the beginning some basic functions have been developed, in order to automatically perform or speed up some pre-simulation operation, such as:

- Q-factor determination. As explained in the previous chapters, the Q-factor is used to determine the damping ratio which the gear is subject to. Its value is a free parameter for the analysis and the user can arbitrarily choose it. If experimental data are available, anyway, it is possible to estimate their Q-factor and then impose its value to the non-damped response. Estimation is performed using the half power method, linearly interpolating the resonance peak. This approach is very accurate if the experimental FRF has a shape similar to a Gaussian curve and if the sampling frequency is sufficiently high.
- Determination of the rotational speed range to simulate. Each resonance peak of the experimental FRF is excited by a specific engine order. Fixed the latter, it is therefore important to have at least a preliminary idea about the location of the related peak, in order to not perform time consuming, useless calculations. The first estimation of the resonance speed by determining the natural frequency of the gear launching a modal analysis on the full $360°$ model. By these frequencies it is possible to build the Campbell diagram of the structure and determine thus the resonances. The extraction of the modal analysis results and the approximate Campbell diagram construction have been automated. In the final code, modal analysis automatic launch has become an integrating part of the analysis preparation.

In order to understand the importance of the process automation, it is remembered that the whole POLIGear software is developed in MATLAB environment. Launching a simulation doesn't require any specific programming knowledge, but it is essential to provide precisely formatted files. These files are:

- Text files, containing information about simulation parameters and finite element model properties;
- MATLAB files, containing data in fixed, defined format;
- Other files, containing mass and stiffness reduced matrices. These files are required because, as explained previously, the first reduction stage, the CMS one, is performed using dedicated software, because its implementation in MATLAB would involve inefficiency, due to matrices dimensions.

In Figure 6-1 it is possible to have a global overview of the previous tool operation.

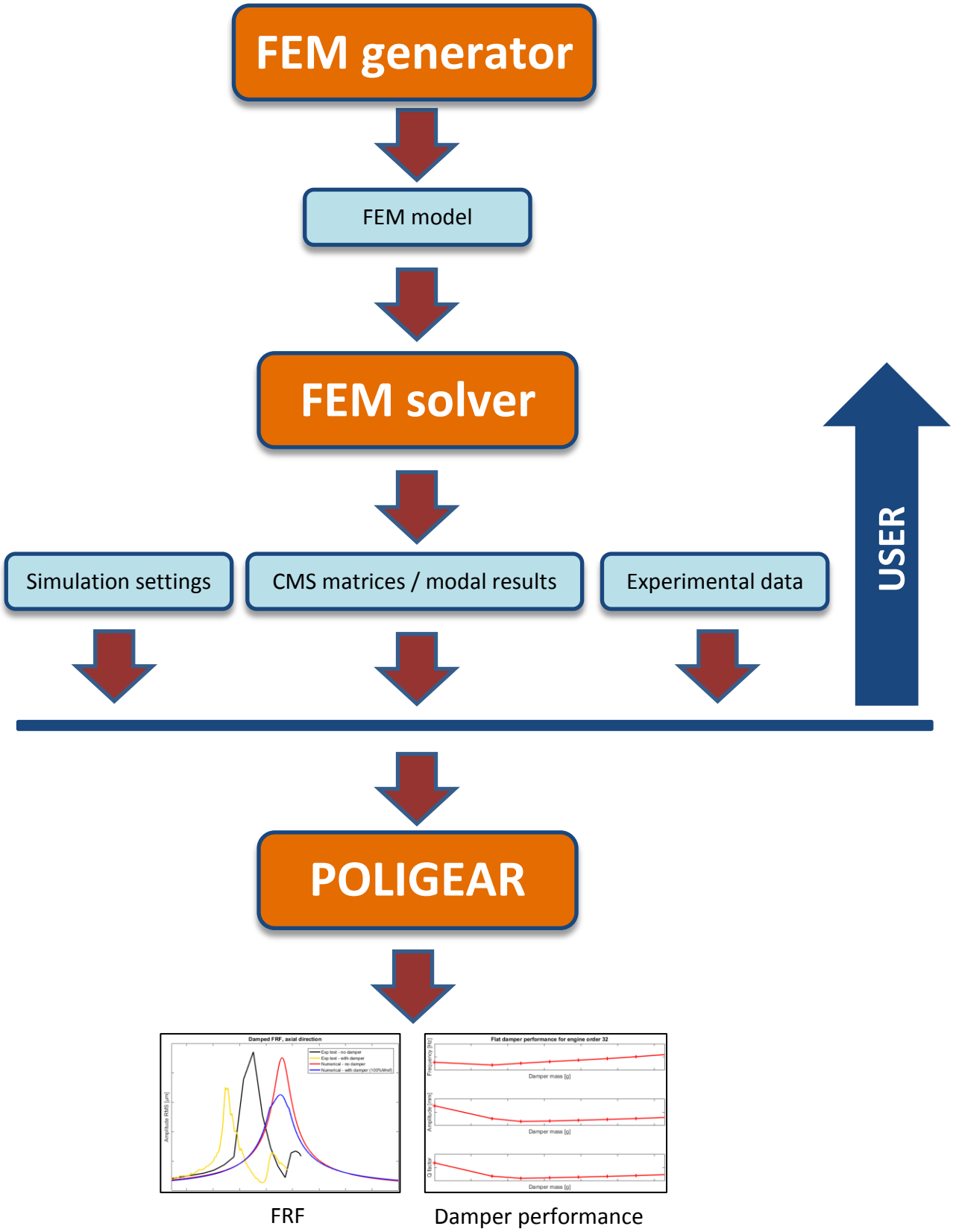

Figure 6-1: POLIGear previous version structure

Files in the first two points of the previous list have been made completely transparent to the user by the development of a graphic user interface (GUI) for the tool, that allows an interactive selection of the various required settings, without any overabundant input.

Since the CMS reduction is not performed inside the tool, user must know how to use a FEM solver. This problem is once again solved passing the required parameters to the GUI and launching a solver (ANSYS apdl in this case) in batch mode. A specific macro is automatically written in ANSYS compatible language (it basically is a text file); this list of instructions is then passed to the operating system, that launches the solver and produces results, consequently imported in suitable MATLAB structures. This way a simulation can be launched without any sort of coding knowledge.

The only part left to the user is the extraction of a cyclic sector geometry from the CAD model of the complete system and the following finite element modeling. This operation could be automatized in the next future too, by developing a parametric mesh generator directly inside MATLAB environment.

The final structure of the tool is shown in Figure 6-2. By using the graphic user interface, the amount of time required for the launch of a single test case has been drastically reduced, making possible all the validation work and the sensitivity analysis of the tool methodology.

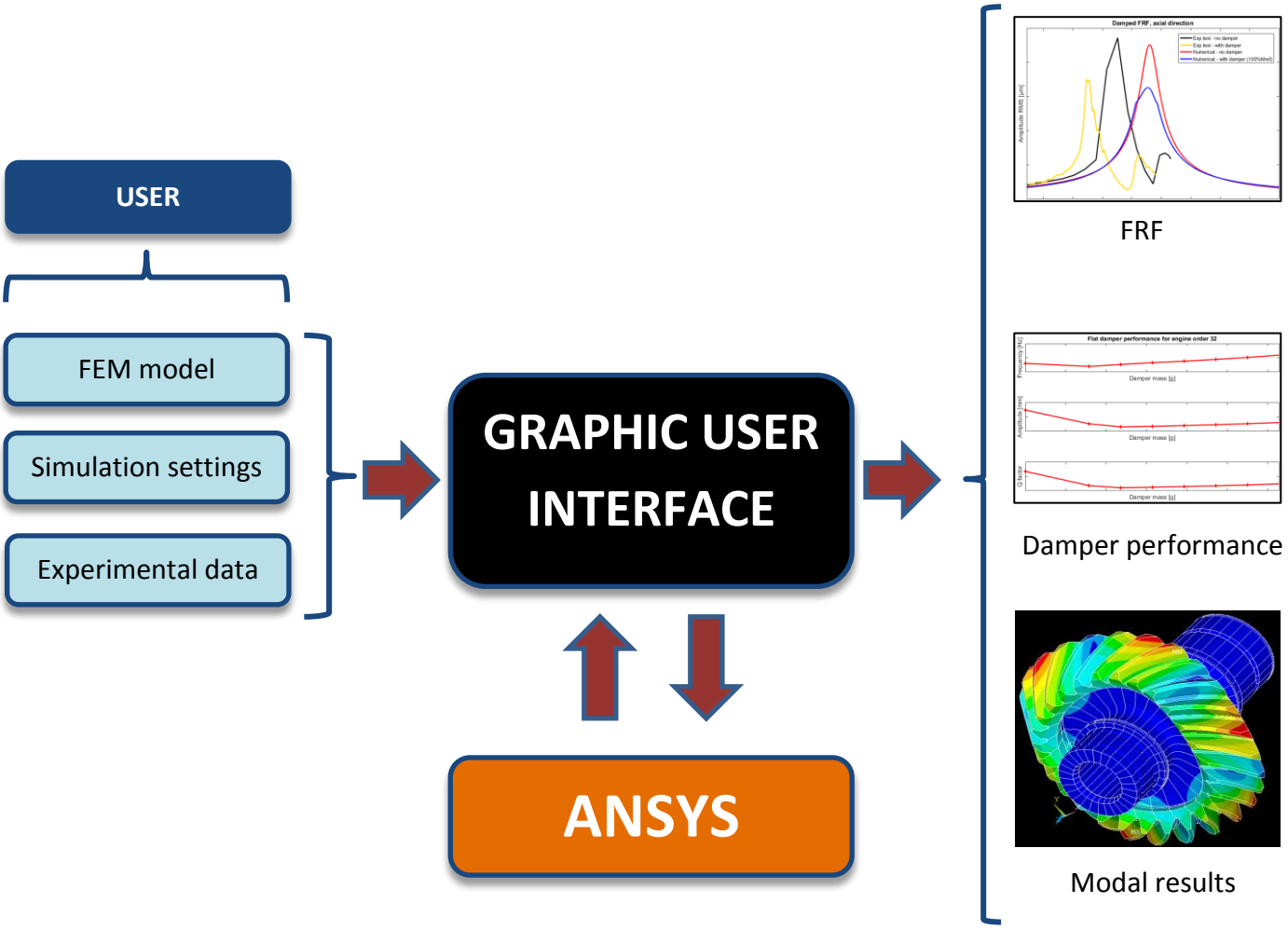

Figure 6-2: POLIGear actual version structure

7 Conclusions

In the present work, the final step of a tool development has been performed. The process includes three main aspects:

- Code finalization;
- Validation of results;
- Determination of the analysis critic parameters.

The tool software has been improved in order to make a test case launch as easy as possible, even for a non-experienced user. This feature has been found to be essential before internal release of the tool. Therefore the final version of the tool interfaces itself with the user by a GUI, transparently performing all pre-processing operation and extracting results, without requiring any other action from the user.

The most relevant part of the thesis work has been the whole tool response validation. This task has been performed by comparing experimental test data with the results produced by the software. Comparison has been performed on the frequency responses, with particular attention to the following characteristics:

- Resonance peaks frequency;
- Resonance peaks amplitude;
- Damping entity according to ring mass.

The match between experimental and simulated frequencies has found to be very good; this validates the supporting assumption taken, the cyclic symmetry, and the whole reduction process between the sector FEM model and the final matrices effectively used for the computation. The comparison between non-damped experimental and simulated responses has the purpose to validate the effectiveness of the model proposed by Parker for the determination of the dynamic overload produced during the mesh process. The model provides a sufficiently good accuracy, even if some improvements are still possible and will be discussed in the following. The non-linear response has been validated in the same way described for the non-damped one, and results have found to correctly estimate the damper ring installation on the system, determining a strong dependence of the response behavior from the damper ring mass and positioning on the gear.

Once performed the results validation, the most influential simulation parameters have been identified and their effect has been insulated by performing sensitivity analyses in order to determine qualitatively and quantitatively their effect on the final response, in order to determine some general criteria to effectively perform simulations without disposing of experimental comparison.

Bibliography

[1] Craig R. and Bampton M., "*Coupling of Substructures for Dynamic Analyses*", *AIAA Journal,* vol. 6, n. 7, July 1968

[2] Fasana A., Marchesiello S., "*Meccanica delle Vibrazioni*", Clut, 2006

[3] Genta G., "*Vibration Dynamics and Control*", Springer, 2009

[4] Guyan R. J., "*Reduction of Stiffness and Mass Matrices*", *AIAA Journal,* vol. 3, n. 2, 1965

[5] Jacazio G., Pastorelli S., "*Meccanica applicata alle Macchine*", Levrotto & Bella, 2001

[6] Panning L., Sextro W. and Popp K., "*Spatial Dynamics of Tuned and Mistuned Bladed Disks With Cylindrical and Wedge-Shaped Friction Dampers*", *International Journal of Rotating Machinery,* vol. 9, n. 3, 2003

[7] Parker R. G., Vijayakar S. M., and Imajo T., "*Non-linear dynamic response of a spur gear pair: Modelling and experimental comparisons*", *Journal of Sound and Vibration*, 2000

[8] Petrov E. P., "*Explicit Finite Element Models of Friction Dampers in Forced Response Analysis of Bladed Disks*", *Proceedings of the ASME Turbo Expo*, Montreal, Canada, 2007

[9] Pyttel B., Schwerdt D., Berger C., "*Very high cycle fatigue - Is there a fatigue limit?*", *International Journal of Fatigue*, vol. 33, 2011

[10] Thomas D. L., "*Dynamic of Rotationally Periodic Structures*", *International Journal for Numerical Methods in Engineering,* vol. 14, 1979

[11] Tran D.-M., "*Component mode synthesis method using interface modes. Application to structure with cyclic symmetry*", *Computers and Structure*, 2001

[12] Zucca S., Firrone C. M. and Faccini M., "*A Method for the Design of Ring Dampers for Gears in Aeronautical Applications*", *Journal of Mechanical Design,* vol*. 134,* 2012

[13] Dell'Olio g., "*Analisi dinamica del comportamento di ruote dentate dotate di anelli di smorzamento*", 2016